STRUCTURAL AND FUNCTIONAL ANALYSIS OF CYCLOOXYGENASE-2 INHIBITION BY NON-STEROIDAL ANTI-INFLAMMATORY DRUGS

By

Kelsey Constance Duggan

Dissertation

Submitted to the Faculty of the

Graduate School of Vanderbilt University

in partial fulfillment of the requirements

for the degree of

DOCTOR OF PHILOSOPHY

in

Biochemistry

May, 2011

Nashville, Tennessee

Approved:

Professor Lawrence J. Marnett

Professor John A. Oates

Professor Alan R. Brash

Professor Richard N. Armstrong

Professor F. Peter Guengerich

In memory of my grandfather, John Jackson,

a lifelong learner

ACKNOWLEDGEMENTS

My time at Vanderbilt would not have been nearly as successful or enjoyable without the contributions of many fellow researchers and friends. First, I have to thank my advisor, Professor Larry Marnett, for providing a tremendous amount of encouragement and guidance in both my research and in attempts to conquer my fears of public speaking. He is constantly developing new research ideas and programs, and has created a laboratory environment where trying something new is encouraged and making a mistake is not something to be ashamed of. As someone who was an inexperienced researcher upon beginning graduate school, it was this environment that allowed me to become an enthusiastic scientist.

Through the Integrative Training in Therapeutic Discovery program, I had the unique experience of being dual-mentored. I was very honored to work with John Oates and his laboratory. The members of Oates laboratory are a kind and welcoming group with a common love of baked goods. I have truly enjoyed my time spent on the 5th floor. It has been extremely rewarding to receive this additional perspective on my work, and from Dr. Oates I learned the importance of staying focused and performing research in a logical and ordered fashion. I am also appreciative of the guidance from committee members Richard Armstrong, Alan Brash and F.P. Guengerich. I was fortunate to have the opportunity to work with an exceptionally knowledgeable and inspiring committee.

I am thankful to Annie Blobaum and Melissa Turman for introducing me to the cyclooxygenase program and for their patience in teaching me assays and helping to plan my initial experiments. Phil Kingsley answered countless questions regarding HPLC and mass-spectrometry experiments. I also must thank Matt Walters for his hard work in the

synthesis of the naproxen analogs reported in this work. I am indebted to Jeff Prusakiewicz, a former lemming, who made many interesting observations that I had the privilege of investigating further. Carol Rouzer has been a careful and enthusiastic editor of much of my writing, and I have appreciated her advice throughout graduate school. Finally, I would like to thank Brenda Crews for keeping us all in line, and all of the lemmings for their positive attitudes and willingness to share knowledge.

COX crystallography has certainly been a challenging, but rewarding adventure. First, I am very grateful to Joel Musee for his willingness to try something new and agreeing to go on this journey with me; we definitely figured things out as a team. Joel Harp was generous with his time in everything from scooping crystals to taking us on our first trip to the synchroton. We could not have asked for a more knowledgeable and enthusiastic collaborator than Jim Kiefer. His expertise was a key factor in our crystallography successes and it has been a pleasure working with him. We are also indebted to Karen Seibert for providing the protocols that made this work possible.

Celeste Riley, Anne Lara, Mary Veazey and Stephen Doster have provided valuable administrative support. Because of their hard work, I was able to focus solely on science. I have enjoyed many conversations over afternoon diet coke breaks in the VICB office, and am thankful for their constant encouragement.

My friends and family have undoubtedly saved my sanity during the last four years. I am so thankful to my friends, from South Carolina to Nashville, for their love and support during graduate school. Each one helped remind me that there is life beyond science, and I know for certain that a bad science day never seems as bad after a cocktail or two with friends. I also must thank my brother, John, who is truly my opposite, but

because of this, he is always able to put things into perspective and remind me that there is no single route to happiness and fulfillment; this has been much needed throughout life and especially graduate school. I have been blessed with the most amazing and proud grandparents anyone could hope for, and am grateful for their unwavering support throughout all of life's endeavors. Finally, I am most grateful for my mother. Thank you for the many hours of listening to me talk about my science woes and triumphs, and for never allowing me to settle for anything less than my absolute best.

TABLE OF CONTENTS

Page

LIST OF TABLES

LIST OF FIGURES

LIST OF ABBREVIATIONS

2-AG	2-arachidonoylglycerol
AA	arachidonic acid
ACN	acetonitrile
AEA	arachidonoylethanolamide; anandamide
ASA	acetylsalicylic acid
CB	cannabinoid
COX	cyclooxygenase
DHA	docosahexaenoic acid
DMSO	dimethyl sulfoxide
DM-INDO	2′-*des*-methyl indomethacin
-EA	ethanolamide
EGF	epidermal growth factor
EPA	eicosapentaenoic acid
ERAD	endoplasmic reticulum-associated degradation
FAAH	fatty acid amide hydrolase
-G	glyceryl ester
GI	gastrointestinal
GPCR	G-protein coupled receptor
HETE	hydroxyeicosatetraenoic acid
HpETE	hydroperoxyeicostetraenoic acid
IC_{50}	inhibitory concentration 50%
INDO	indomethacin

IL	interleukin
LC	liquid chromatography
LOX	lipoxygenase
LPS	lipopolysaccharide
MAGL	monacylglycerol lipase
MBD	membrane binding domain
MeOH	methanol
MS	mass spectrometry
MS/MS	tandem mass spectrometry
NSAID	non-steroidal anti-inflammatory drug
PG	prostaglandin
PGI_2	prostacyclin
PPA	5-phenyl-4-pentenyl-1-alcohol
PPARδ	peroxisome proliferator-activated receptor δ
PPHP	5-phenyl-4-pentenyl-1-hydroperoxide
PPIX	protoporphyrin IX
POX	peroxidase
RMSD	root mean square deviation
SRM	selected reaction monitoring
TXA_2	thromboxane A_2
WT	wild-type

CHAPTER I

INTRODUCTION

Biology and Biochemistry of COX enzymes

Prostaglandins. Prostaglandins are important signaling molecules that mediate a diverse array of physiological and pathophysiological events throughout the body. The synthesis of these bioactive lipids is regulated by three distinct enzymatic reactions (Figure 1). First, upon activation, phospholipase A_2 (cytosolic or secretory) can release arachidonic acid (AA) from the phospholipid bilayer, which allows AA to then bind in the active site of cyclooxygenase (COX) enzymes. COX, also known as prostaglandin endoperoxide H synthase, catalyzes the conversion of AA to prostaglandin H_2 (PGH_2). Finally, tissue specific synthase enzymes convert PGH_2 to the prostaglandins (PGE_2, PGD_2, $PGF_{2\alpha}$), prostacyclin (PGI_2) and thromboxane (TXA_2) (1). Prostanoids then exert their effects by signaling through separate G-protein coupled receptors (GPCRs) (2).

As mentioned above, prostaglandin signaling is involved in a variety of biological functions. For example, prostanoids play a major role in the maintenance of vascular homeostasis. Vascular endothelium-derived PGI_2, a vasodilator and anti-thrombotic agent, are thought to counterbalance the effects of TXA_2, which induces vasoconstriction and thrombosis (3-6). PGE_2 and PGI_2 are also important regulators of kidney function and gastric cytoprotection (7,8). Pathophysiological responses mediated by prostanoid signaling include pain, fever, inflammation, and tumorigenesis (4,9,10), reviewed in (11,12).

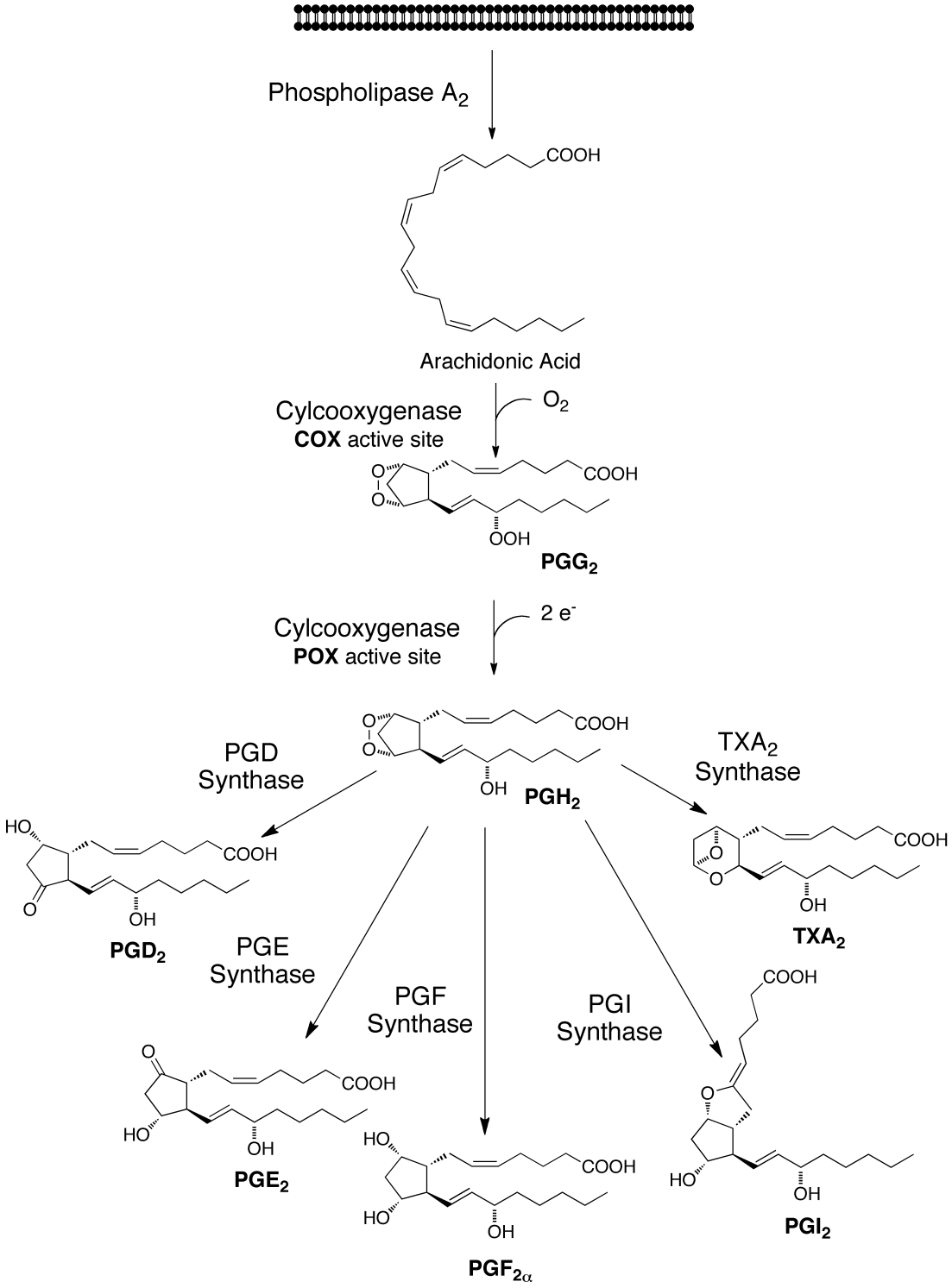

Figure 1. Biosynthesis of prostanoids.

COX, which catalyzes the committed step in prostaglandin biosynthesis, was first characterized in 1967 from preparations of sheep vesicular gland (13). COX enzymes are membrane-bound homodimers localized to the lumen of the endoplasmic reticulum and the inner and outer membranes of the nuclear envelope (14). One molecule of heme (Fe^{3+}-protoporphyrin IX) is non-covalently associated with each 70 kDa COX monomer. The heme moiety is required for catalysis but can be removed and reconstituted with minimal effects on enzyme activity (15,16).

The COX reaction. The conversion of AA to the parental prostaglandin, PGH_2, occurs at two spatially distinct but functionally coupled active sites within the COX enzymes. The *bis*-dioxygenation of AA takes place in the L-shaped cavity of the COX active site, resulting in the formation of the hydroperoxy endoperoxide, prostaglandin G_2 (PGG_2) (17). PGG_2 then diffuses out of the COX site to the peroxidase (POX) active site, where it undergoes a rapid two-electron reduction to form the hydroxy endoperoxide, PGH_2 (18). Hydroperoxides other than PGG_2 can be reduced in the POX active site, and initiation of the COX reaction is dependent upon a two-electron oxidation of the heme moiety at the POX site. The necessity for heme oxidation at the POX active site to initiate COX catalysis is best explained by a branched-chain mechanism as shown in Figure 2 (19). The two-electron oxidation of heme occurs in conjunction with the two-electron reduction of a hydroperoxide substrate, and results in the formation of a ferryloxo protoporphyrin radical cation ($(PPIX^{\bullet})^{+}Fe^{4+}O$) termed Compound I (20,21). In the presence of a reducing co-substrate, two subsequent one-electron reductions return the heme moiety to its resting state (22) (23). Alternatively, Compound I can abstract a

hydrogen from Tyr-385 in the COX active site leading to the formation of a tyrosyl radical, thereby initiating the oxygenase reaction.

Hamberg and Samuelsson first proposed that COX catalysis was mediated by a free radical mechanism in 1967 (13,24,25). Their hypothesis was later supported by electron spin resonance spin-trapping experiments to detect carbon-centered radicals, and is the basis for the putative mechanism of the COX reaction described herein (26). When a fatty acid substrate, namely AA, is bound within the COX active site, the tyrosyl radical at position 385 can abstract the 13-pro-(*S*) hydrogen forming a carbon-centered arachidonyl radical. As shown in Figure 2, this radical is trapped at C11 by molecular oxygen producing an 11-(*R*)-peroxyl radical, which undergoes two subsequent cyclizations to form a bicyclic endoperoxide and an allylic radical with electron density at C13 and C15. A second molecule of molecular oxygen traps the radical at C15, and reduction of this newly formed peroxyl radical by Tyr-385 generates PGG_2. This final step also serves to regenerate the tyrosyl radical, which allows for additional rounds of COX catalysis independent of POX activity. In addition to prostaglandins, the COX enzymes produce a variety of minor products. For example, 11-hydroperoxyeicosatetraenoic acid (11-HpETE) is formed if the 11-(*R*)-peroxyl radical does not undergo cyclization to form the endoperoxide ring at C9, while 15-hydroperoxyeicosatetraenoic acid (15-HpETE) is formed when molecular oxygen traps the initial arachidonyl radical at C15 rather than C11.

The number of turnovers of each COX molecule is limited by reaction-catalyzed self-inactivation of the COX enzymes *in vitro*; this is a first-order, irreversible process. The precise mechanism of auto-inactivation remains unclear, but there is evidence for the

loss of both POX and COX activities. Furthermore, the self-inactivation of both activities appears to be hydroperoxide-dependent, but the concentration and structure of the hydroperoxide involved does not significantly affect the rate of inactivation (27). It has been hypothesized that active radical intermediates, formed after the radical is transferred from Compound I to Tyr-385, react with the protein leading to modification of the heme or protein and loss of activity. It appears that the oxoferryl heme, rather than the tyrosyl radical, is the source of the damaging species (28). Interestingly, various reducing co-substrates protect COX enzymes from self-inactivation (29). The physiological relevance of COX suicide inactivation is unknown, as *in vitro* reaction conditions do not exactly mimic the cellular environment of the enzyme. However, it has been shown that low levels of fatty acid hydroperoxides irreversibly inactivate COX derived from intact platelets (30,31). Additionally, in intact vascular tissue, there is evidence that AA metabolism, and subsequent hydroperoxide generation, leads to self-catalyzed COX inactivation; this is thought to be the limiting factor in endothelial PGI_2 biosynthesis (32). Therefore, the self-inactivation of COX may act as a mechanism of autoregulation *in vivo*.

Two COX isoforms. The mechanistic studies described above were largely performed with COX-1, which was first purified from bull seminal vesicles in 1976 (15). A second COX isoform, dubbed COX-2, was discovered in the early 1990's and found to share approximately 60% sequence identity with COX-1 (33). The mechanism of catalysis is fundamentally the same for COX-1 and COX-2, but there are key structural and functional differences between the two isoforms. The COX-1 gene, *Ptgs-1*, is

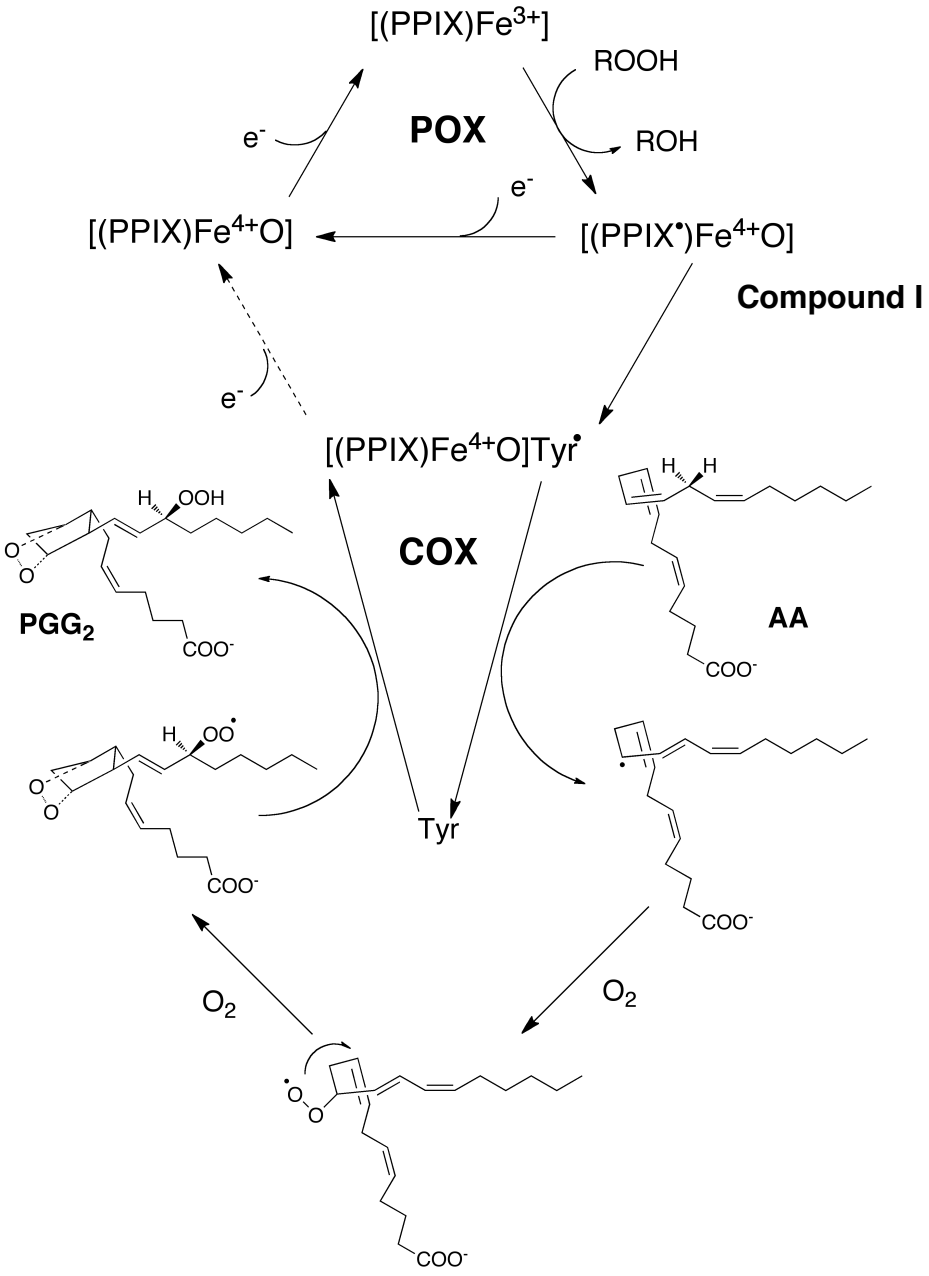

Figure 2. Branched chain mechanism for COX catalysis. In the POX active site, the heme moiety, $(PPIX)Fe^{3+}$, undergoes a two-electron oxidation to form Compound I, $(PPIX•)Fe^{4+}O$, while the hydroperoxide substrate (ROOH) undergoes a two-electron reduction. The enzyme can be brought back to its resting state by two subsequent one-electron reductions or the radical can be transferred to a tyrosine residue in the COX active site. When AA is bound within the COX active site, the newly formed tyrosyl radical can abstract the 13-pro-(*S*) hydrogen from the fatty acid substrate. AA undergoes several radical rearrangements in addition to two oxygenation reactions to allow the formation of the hydroperoxy endoperoxide, PGG_2. The radical is then transferred back to the tyrosine residue to allow the initiation of subsequent catalytic cycles.

constitutively transcribed throughout the body and codes for a relatively stable 2.8 kb mRNA. While *Ptgs*-2, which codes for COX-2, is an immediate early gene that is activated by various stimuli including cytokines, growth factors, and tumor promoters. An instability sequence in the 3'-untranslated region leads to the rapid turnover of the 4 kb COX-2 mRNA.

The constitutive expression of COX-1 suggests that this isoform is primarily involved in the immediate release of prostaglandins following activation of phospholipase A_2 as occurs with platelet aggregation, and in " housekeeping functions" such as cytoprotection in the stomach, whereas the inducible expression of COX-2 indicates a role for this isoform in the formation of prostaglandins in pathophysiological states, namely pain and inflammation. However, this paradigm is oversimplified as COX-2 is constitutively expressed in the kidney, cardiovascular system, and specific regions of the central nervous system, and COX-1 is reportedly induced in neuroinflammation and cellular differentiation.

"Knock-in" studies, in which *Ptgs-1* is inserted under the regulatory sequence that controls *Ptgs-2* expression in mice, indicate that the two COX isoforms are not functionally interchangeable (34). In macrophages from knock-in mice, COX-1 is expressed in response to stimuli that induce COX-2 expression, but the enzyme fails to produce PGE_2 at low concentrations of AA. Analysis of urinary prostaglandin metabolite profiles revealed that COX-1 knock-in can effectively restore PGE_2 levels, which are markedly reduced in COX-2 null mice, but only partially compensates for the decrease in PGI_2 biosynthesis. COX-2 deletion also results in significant defects in reproductive and renal function, which are only partially rescued or delayed in COX-1 knock-in mice.

The inability of COX-1 to completely compensate for COX-2 *in vivo* may be related to differences in sensitivity to hydroperoxide activation, as the concentration of hydroperoxide required to activate COX-2 is approximately one order of magnitude lower than the hydroperoxide concentration necessary for COX-1 activation *in vitro* (35). These findings suggest that COX-2 may be able to function in cells with low hydroperoxide or substrate concentrations, while COX-1 remains inactive. The basis for the differential hydroperoxide requirement is unknown, but appears to be related to the identity of the side chain at position 383 as mutation of Thr-383 in COX-2 to the corresponding COX-1 residue, histidine, leads to a reduction in COX activation efficiency (36). Selective coupling of COX-1 and COX-2 with specific downstream synthase enzymes may also play a role in the differences in isoform function observed in the knock-in studies (37).

COX-1 and COX-2 also exhibit differences in protein turnover. In both murine NIH/3T3 fibroblasts and HEK293 cells, COX-2 is preferentially and rapidly degraded under conditions in which COX-1 is quite stable (38). Interestingly, degradation of COX-2 is slowed by the addition of proteosome inhibitors. This is in agreement with studies indicating that, in addition to degradation associated with suicide inactivation, COX-2 is a target of the ER-associated degradation (ERAD) pathway, a quality control system in which *N*-glycosylated proteins residing in the ER lumen are transported across the ER membrane and subsequently ubiquitinated, then degraded by the 26 S proteosome. COX-2 contains an additional 19 amino acids at the C-terminus (594-612) that are not present in COX-1, and there is evidence that this region of the enzyme is responsible for targeting COX-2 to the ERAD system (38). Three *N*-glycosylation sites are conserved between the

two COX isoforms, but the cassette of 19 amino acids unique to COX-2 contains a fourth *N*-glycosylation site, Asn-594. Mutation of Asn-594 stabilizes COX-2, suggesting that glycosylation of this residue is critical for entry into the ERAD pathway.

COX Enzymes and the Endocannabinoid System

Endocannabinoid biochemistry and physiology. A critical difference between COX-1 and COX-2 lies in their ability to oxygenate neutral derivatives of AA, particularly the endocannabinoids arachidonoylethanolamide (AEA) and 2-arachidonoylglycerol (2-AG). Endocannabinoids target the same GPCRs that are engaged by the active component of marijuana (*Cannabis*), Δ^9-tetrahydrocannabinol. To date, two cannabinoid receptors have been identified, termed CB_1 and CB_2 (39,40). AEA is a partial agonist of CB1, whereas 2-AG is full agonist at the CB_1 and CB_2 receptors. CB_1 is expressed throughout the central nervous system with the highest expression in the basal ganglia, hippocampus, and cerebellum, whereas CB_2 is predominantly expressed in the immune system (41) (40). Both CB_1 and CB_2 can modulate adenylate cyclase and mitogen-activated protein kinase activity, but CB_1 appears to couple to ion channels while CB_2 does not. Cannabinoid signaling is thought to play a role in a variety of biological processes including cognition, motor function, food intake, body temperature, pain, and inflammation.

AEA was identified in 1992 through a screen for endogenous ligands for cannabinoid receptors (42). The synthesis of AEA is a two-step process. First, *N*-acyltransferase catalyzes the transfer of AA from phosphatidylcholine to the head group of phosphatidylethanolamine leading to the formation of N-arachidonoyl

phosphatidylethanolamine (NAPE). AEA can then be generated upon cleaveage of NAPE, which can occur through three distinct enzymatic pathways: hydrolysis of NAPE by a NAPE-selective phospholipase D, deacylation of NAPE by α/β hydrolase 4 and subsequent cleavage of the glycerophosphate, or phospholipase C-mediated hydrolysis of NAPE to generate phosphoanadamide, which can then be dephosphorylated (43,44).

2-AG was identified and isolated from mammalian intestinal tissue in 1995 (45,46). The concentration of 2-AG in the brain is 170 times greater than that of anadamide (47), but like AEA, multiple pathways may lead to the generation of 2-AG. The best-characterized pathway begins with the hydrolysis of AA-containing phosphatidylinositol-4,5-bisphosphate by phospholipase C-β to form the corresponding 1-acyl-2-arachidonoyl-diacylglycerol (DAG) (44). This intermediate is then hydrolyzed by DAG lipase to generate 2-AG.

Termination of endocannabinoid signaling can occur via hydrolysis by serine hydrolases or oxidative metabolism by COX, lipoxygenase (LOX), or cytochrome P450 (CYP) enzymes. Fatty acid amide hydrolase (FAAH) hydrolyzes AEA to form AA and ethanolamine. Although not specific for AEA, FAAH appears to tightly regulate its levels. FAAH can also mediate 2-AG hydrolysis, but the major metabolizing enzyme for 2-AG has been identified as monacylglycerol lipase (MAGL), which metabolizes 2-AG to yield AA and glycerol. Cravatt and colleagues developed a selective inhibitor of MAGL, dubbed JZL-184, and investigated its ability to block 2-AG hydrolysis *in vivo* (48). In mice, administration of JZL-184 led to an 8-10 fold increase in 2-AG levels and a broad array of cannabinoid behavioral effects, including analgesia, hypothermia, and

hypomotility. These studies suggest that inhibitors of MAGL, and possibly FAAH, can be useful probes in the examination of the endocannabinoid sysem (48).

COX-dependent endocannabinoid oxygenation. As mentioned above, endocannabinoids also serve as substrates for oxygenase enzymes. Of particular interest to this work is the oxygenation of endocannabinoids by the COX enzymes (Figure 3). Yu *et al*. reported the first evidence of COX-mediated endocannabinoid metabolism in 1997 (49). In their studies, partially purified hCOX-2, but not hCOX-1, metabolized AEA at rates approaching those observed with AA. Further analysis utilizing lysates and intact cells confirmed the selective metabolism of AEA, as only those cells or extracts expressing COX-2 were able to oxygenate the endocannabinoid. In contrast with initial reports, kinetic evaluation of COX-2-mediated AEA metabolism indicated that, to the extent that K_m reflects K_d, the enzyme had a significantly lower affinity for AEA than AA (K_m > 60 μM for AEA versus approximately 10 μM for AA) (50,51). The products of AEA oxygenation by COX-2 parallel those of AA with the major products being PGH_2-ethanolamide (PGH_2-EA) and to a lesser extent HETE-ethanolamides (HETE-EA). It remains to be seen whether or not this reaction is physiologically relevant as the low concentrations of AEA found *in vivo*, combined with the limited activity of COX-2 against the endocannabinoid, may impede product formation.

Similar to AEA, 2-AG is selectively oxygenated by COX-2 to form PGH_2-glycerol ester (PGH_2-G) and HETE-glycerol esters (HETE-G) (52). Notably, the oxygenation of 2-AG by COX-2 is as efficient as that of AA as evidenced by steady-state kinetic analysis indicating that AA and 2-AG have comparable k_{cat}/K_m values. *In vitro*,

the prostaglandin-like product of 2-AG oxygenation, PGH_2-G, undergoes non-enzymatic isomerization to form PGD_2-G and PGE_2-G. Conversion of 2-AG to PGH_2-G has also been examined in RAW 264.7 murine macrophages, where exogenous 2-AG is rapidly converted to PGH_2-G. PGD synthase expressed by the macrophages then acts on the endoperoxide intermediate to form PGD_2-G (52). This finding prompted the investigation of the ability of PGH_2-G, as well as PGH_2-EA, to serve as substrates for additional prostaglandin synthases in cellular and subcellular systems (53). Kozak *et al.* reported that both PGH_2-G and PGH_2-EA are efficiently converted to D-, E- and I- series prostaglandin glycerol esters and ethanolamides, respectively, by the appropriate synthase enzymes (53). Although thromboxane synthase is able to catalyze the isomerization of PGH_2-G, product formation is reduced approximately 20-fold when compared to the isomerization of the free acid, PGH_2; this suggests that PGH_2-G is a poor substrate for thromboxane synthase.

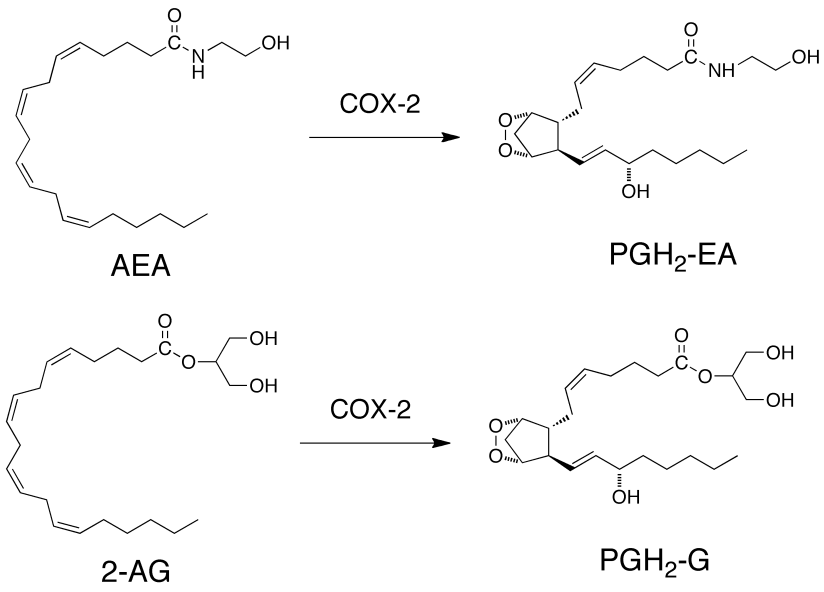

Figure 3. Oxygenation of endocannabinoids by COX-2.

Endocannabinoid oxygenation in vivo. Concentrations of 2-AG exceeding the K_m for oxygenation by COX-2 have been reported in the brain and various other tissues, suggesting that PG-G formation may occur under physiological conditions (54). Detection of endocannabinoid-derived prostanoids *in vivo* has been difficult, however, possibly due to the fact that PG-Gs can be hydrolyzed to form PGs indistinguishable from those formed by AA oxygenation. The first evidence for the formation of PG-Gs under physiologically relevant conditions came from studies in which stimulation of RAW 264.7 cells with bacterial lipopolysaccharide (LPS) plus interferon-γ followed by the calcium ionophore ionomycin led to the production and extracellular release of low-levels of PGD_2-G (52). In similar studies, mouse peritoneal macrophages treated with LPS followed by zymosan generated PGE_2-G and PGI_2-G (55). Due in part to a 10-fold difference in the levels of 2-AG and AA released upon treatment with zymosan, the total amount of PG-Gs was approximately 1000-fold lower than those of traditional PGs; additional limiting factors in PG-G production are under investigation. Recently, endogenous PGE_2-G has been isolated from a rat hind paw extract, further suggesting that 2-AG-derived prostaglandin-like products are naturally occurring *in vivo* (56).

Physiology of oxygenated endocannabinoids. Accumulating evidence suggests that PG-EAs (or “prostamides") and PG-Gs have physiologic roles distinct from those of traditional prostaglandins. For example, PGE_2-EA reduces the expression of IL-12p40 in activated macrophages and microglial cells (57). The parent endocannabinoid, AEA, also negatively regulates IL-12p40 production, thereby inhibiting the expression of the

cytokines, IL-12 and IL-23. The inhibitory effects of AEA and PGE_2-EA on IL-12p40 are partially reduced by an EP_2 receptor antagonist, but an EP_4 receptor antagonist has no effect. These results indicate that the specific activation of EP_2 may play a role in the downregulation of IL-12p40 induction by AEA and PGE_2-EA. Further, these findings suggest that the endocannabinoid system could potentially be targeted in the treatment of autoimmune or chronic inflammatory diseases.

A structural analog of $PGF_{2\alpha}$-EA, bimatoprost, is an ocular hypotensive agent marketed for the treatment of glaucoma and ocular hypertension. While neither bimatoprost nor $PGF_{2\alpha}$-EA exhibit significant activity at prostaglandin receptors, some have suggested that bimatoprost acts as a prostaglandin prodrug. However, extensive ocular distribution and metabolism studies indicate that bimatoprost exerts its effects as the intact, prostamide-like molecule (58). In fact, bimatoprost appears to signal through a heterodimer comprised of the F prostanoid (FP) receptor and a splice variant of the FP receptor with a truncated C-terminus (59).

In agreement with the bimatoprost studies described above, endocanabinoid-derived prostanoids generally have little or no affinity for traditional prostaglandin receptors, suggesting that orphan GPCRs or unknown heterodimeric complexes mediate the signaling of PG-Gs and PG-EAs. In RAW 264.7 cells, low concentrations PGE_2-G, but not PGE_2, mobilize Ca^{2+}, stimulate a transient increase in inositol 1,4,5 phosphate (IP3) levels, and activate PKC, leading to ERK phosphorylation (60). The activity of PGE_2-G in RAW 264.7 cells was shown to be independent of hydrolysis to PGE_2. Moreover, the affinity of PGE_2-G for E prostanoid receptors was at least two orders of magnitude lower than that of PGE_2, and binding to the thromboxane receptor,

prostacyclin receptor, D prostanoid receptor, or F prostanoid receptor was negligible. Together, these results imply that PGE_2-G-mediated calcium moblization in RAW 264.7 cells is not likely to occur through prostanoid receptor signaling.

PGE_2-G may also serve as a modulator of hippocampal synaptic transmission. In mouse hippocampal neurons, PGE_2-G causes a concentration-dependent increase in the frequency of miniature inhibitory post-synaptic currents (mIPSCs) (EC_{50} = 1.7 μM) (61). The frequency of mIPSCs is also increased by PGD_2-G, $PGF_{2\alpha}$-G, and PGD_2-EA, but not by PGE_2-EA and $PGF_{2\alpha}$-EA, whereas the endocannabinoids 2-AG and AEA reduce the frequency of mIPSCs. The ability of PG-Gs and PG-EAs to increase the frequency of mIPSCs is not likely related to hydrolysis to PGs or binding to PG receptors, as classical prostaglandins act to reduce the frequency of mIPSCs or have no effect. Calcium mobilization and MAPK-dependent phosphorylation are thought to be involved in the downstream signaling of this process, as treatment with an IP3 receptor agonist and a MAPK inhibitor blocks the PGE_2-G-mediated increase in the frequency of mIPSCs.

PGE_2-G has also been shown to increase the frequency of miniature excitatory postsynaptic currents (mEPSCs) in mouse hippocampal neurons in culture (62). The enhanced glutamatergic transmission appears to be mediated by MAPK and IP3 signaling pathways. In cultured rat hippocampal neurons, PGE_2-G caused a dose-dependent increase in terminal transferase dUTP nick end labeling (TUNEL) staining and time-dependent cleavage of caspase-3 indicating that PGE_2-G may be neurotoxic.

There is some evidence that COX-2 derived PGI_2-G may activate the nuclear receptor $PPAR_\delta$ in human vascular endothelial cells (63). Treatment of human umbilical vein endothelial cells expressing COX-2 with 2-AG leads to $PPAR_\delta$ activation, but this

effect does not appear to be mediated by the endocannabinoid itself, as cells lacking the CB1 and CB2 receptors exhibited levels of 2-AG–induced $PPAR_{\delta}$ transcription similar to those of WT cells. However, both COX-2 and PGIS activity were required for 2-AG-induced $PPAR_{\delta}$ activation by 2-AG, suggesting that 2-AG is converted to PGI_2-G, which can then activate $PPAR_{\delta}$. Importantly, the COX-2-PGI_2-G-$PPAR_{\delta}$ pathway appears to lead to the attenuation of prothombotic tissue factor gene expression.

The structural determinants of fatty acid oxygenation and inhibition of COX enzymes will be discussed in the remainder of this chapter.

Structure of COX enzymes

General COX structure. The first three-dimensional structure of COX-1 was published in 1994, followed two years later by the crystal structure of COX-2 (64,65). To date, over 30 structures of COX enzymes complexed with either substrates or inhibitors have been deposited in the Protein Data Bank. Following cleavage of the signal sequence, mature COX-1 consists of amino acid residues 25-600, with residues 33-586 showing clear electron density during crystallographic analysis (64). Similarly, residues 33-583 were resolved in the first crystal structure of COX-2; 35 amino acids at the C-terminus could not be located (65). A 14 amino acid deletion at the N-terminus of COX-2 causes the numbers of most COX-2 amino acids to be 14 units lower than those of COX-1, but by convention, the amino acids of both isoforms are referred to by the numbering of the initial COX-1 translation product. Comparison of the crystal structures of COX-1 and COX-2 reveals that the two isoforms have virtually superimposable structures with each COX monomer comprised of three domains: an epidermal growth factor (EGF)-like

domain, a membrane binding domain, and a large globular catalytic domain, which houses the cyclooxygenase (COX) and peroxidase (POX) active sites (Figure 4) (64-66). Consistent with gel-filtration studies, the COX enzymes are present as homodimers with an extensive dimer interface created by the EGF-like and catalytic domains (67).

Domain architecture. COX does not span the lipid bilayer and is therefore termed a monotopic membrane protein. However, because detergent is required to dissociate the enzyme from the phospholipid bilayer, COX associates with the membrane as if it was an integral membrane protein. The membrane-binding domain (residues 73-116) is composed of four short amphipathic α-helices (A-D). The helices are positioned approximately orthogonal to one another creating a hydrophobic surface ideal for insertion into a single face of the membrane bilayer. The helices of the membrane binding domain also surround a fairly large open area that has been dubbed the "lobby", as it is thought that substrates and inhibitors must travel through this region to enter the active site located within the catalytic domain.

The catalytic domain is structurally homologous to mammalian myeloperoxidase, suggesting that the COX enzymes evolved from soluble heme-dependent peroxidases (68). This principal domain of the COX monomer is largely composed of α-helical secondary structure. The POX active site is located in a solvent-accessible groove at the top of the catalytic domain while the COX active site lies at the vertex of a large, L-shaped hydrophobic channel that extends from the membrane-binding domain into the catalytic domain. Within the COX channel, the catalytic and membrane binding domains are separated by a constriction formed by three residues: Arg-120, Tyr-355 and Glu-524.

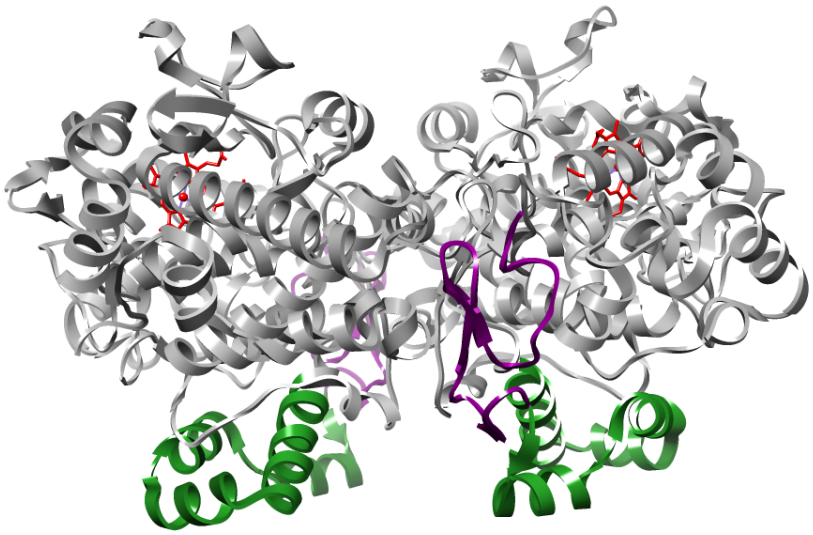

Figure 4. Three-dimensional structure of COX-2. The EGF-like domain is shown in purple, the membrane-binding domain in green and the catalytic domain is shown in grey. Heme (red sticks) is pictured bound in the peroxidase active site. PDB ID: 3PGH.

The EGF-like domain is made up of a short sequence of amino acids at the N-terminus (residues 34-72) of the protein, and its precise function remains unknown. However, it has been suggested that this domain may initiate or maintain interactions necessary for the insertion of COX into the membrane bilayer (68).

POX active site. As shown in Figure 5, the peroxidase active site is the location of heme binding where His-388 serves as the proximal heme ligand. Gln-203 and His-207 are positioned on the distal side of the heme, approximately 5 Å from the heme iron, but do not coordinate the metal (64). It is thought that these residues play a key role in the two-electron reduction of the hydroperoxide substrate (20). Mutation of His-388, Gln-203, or His-207 causes a dramatic reduction in peroxidase activity (20,69). Of note, recent

studies show that, while the k_{cat}/K_m for peroxidase activity of G203V oCOX-1 is 17% that of WT enzyme, the mutant enzyme retains full COX activity and has a specific activity similar to that of WT suggesting that this Glu-203 is not essential for the initiation of COX catalysis (70).

In contrast to the majority of peroxidases, the POX active site of COX enzymes is largely exposed to solvent and can therefore accommodate large alkyl peroxide substrates. The openness of the POX active site also allows for relatively easy dissociation of small ligands, including heme, in and out of the active site cavity. For that reason, and due to the reactivity of the heme moiety, crystallization of substrates or products bound within the peroxidase active site has been difficult. Recently, the 2.0 Å crystal structure of oCOX-1 in complex with an analog of the non-steroidal anti-inflammatory drug (NSAID) flurbiprofen provided the first view of a ligand bound in the POX active site (PDB ID: 1Q4G) (71). A detailed explanation of NSAIDs as COX inhibitors is provided below. However, in this particular structure, a glycerol molecule, used as a cyroprotectant, lies between Gln-203 and His-207 with the 1-hydroxyl group positioned roughly above the heme iron (Figure 5) (71). The 3-hydroxyl group participates in hydrogen bonding interactions with a water molecule coordinated to His-207 (71). The location of this glycerol molecule is expected to mimic the binding conformation of the peroxide moiety of alkyl hydroperoxide substrates. In fact, this structure was used as the basis for docking and molecular dynamics studies in order to predict the productive binding mode of the hydroperoxy endoperoxide intermediate, PGG_2, within the POX active site (72).

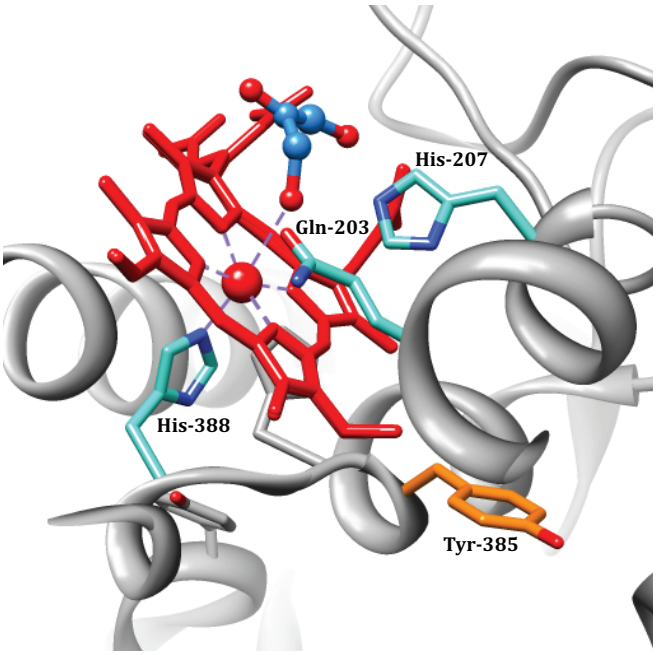

Figure 5. Glycerol molecule bound within the POX active site of COX-1. Heme (red stick structure) is shown bound in the POX active site in addition to a glycerol molecule (blue and red) shown in ball-and-stick mode. Key residues for peroxidase activity are shown in turquoise. The catalytic tyrosine is shown in orange. PDB ID: 1Q4G.

COX active site. The COX active site channel spans 25 Å from the membrane binding domain to the interior of the catalytic domain; the catalytic center is located in the upper half of the channel from Arg-120 to Tyr-385. While the COX-1 and COX-2 active sites are relatively similar, the COX-2 active site is approximately 20-30% larger than that of COX-1 (Figure 6). The size difference is partially attributed to a single amino acid change (Ile-523 in COX-1, Val in COX-2) which limits access to a pocket off the main active site channel (73). Substitution of secondary shell residues, Ile-434 and His-513, in COX-1 for Val-434 and Arg-513 in COX-2 also contributes to the difference in active site size.

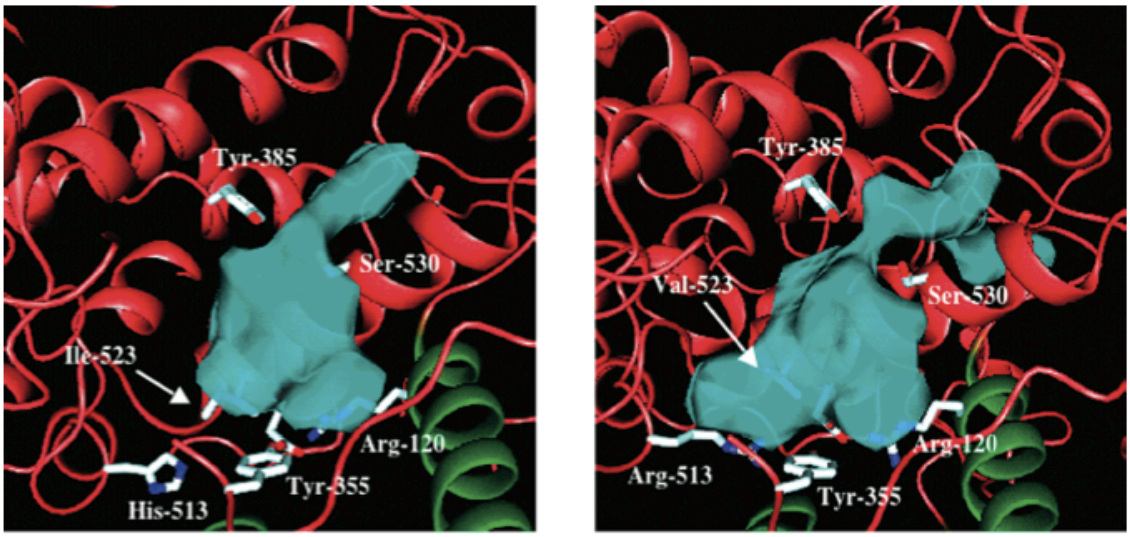

COX-1 COX-2

Figure 6. Solvent accessible surfaces in the cyclooxygenase active site of COX-1 and COX-2.

Structural basis of AA binding. Enzyme-substrate co-crystal structures in combination with mutagenesis studies provide a comprehensive understanding of the residues involved in critical COX-AA interactions. To prevent substrate consumption during crystallographic analysis, COX can be stripped of the heme cofactor and reconstituted with Co^{3+}-protoporphyrin IX to form an inactive pseudo-holoenzyme. The 3.0 Å crystal structure of AA bound to Co^{3+}-protoporphryin IX-reconstituted oCOX-1 (Co^{3+}-oCOX-1) showed that AA binds in an extended L-shaped conformation with the carboxylic acid coordinated to Arg-120 and Tyr-355 at the base of the active site (74). The aliphatic backbone extends into the catalytic site and makes a sharp bend near Tyr-385, positioning the ω-tail in a hydrophobic groove above Ser-530 and Leu-534 (74). This orientation places C-13 of AA directly beneath the phenolic oxygen of Tyr-385, allowing for the abstraction of the 13-*proS* hydrogen to initiate catalysis (Figure 7). The terminal carbon (C-20) sits directly against Gly-533, and a Gly-533 to alanine mutation renders COX-1

inactive against AA while COX-2 retains partial activity (74,75). However, mutation of Gly-533 to a larger valine or leucine residue abolishes COX-2 activity against AA. Interestingly, G533V and G533L COX-2 do have the ability to metabolize 18-carbon unsaturated fatty acids (e.g. linolenic and stearidonic acid), suggesting that binding of the ω-end of the fatty acid in this region of COX is an important determinant of substrate specificity (75).

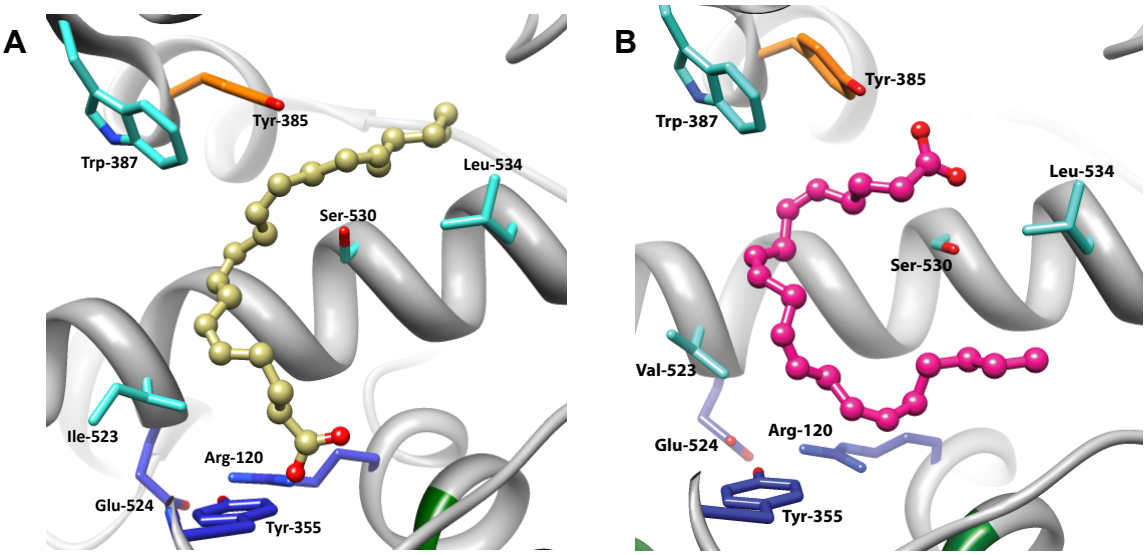

Figure 7. Crystal structures of the productive and non-productive conformations of AA within the COX active site. *A*. In the productive binding mode of AA, the carboxylate moiety of AA (yellow ball-and-stick) participates in ion-pairing interactions with Arg-120 and hydrogen-bonding interactions with Tyr-355 (blue sticks) at the base of the COX-1 active site. The aliphatic backbone participates in hydrophobic interactions with several residues (turquoise sticks and not pictured) throughout the active site. The catalytic residue, Tyr-385, is shown in orange. PDB ID: 1DIY. *B*. AA (pink ball-and-stick) is shown in the non-productive or "inverted" conformation in the active site of COX-2. The carboxylate of AA is coordinated to Tyr-385 and Ser-530 at the top of the COX active site. PDB ID: 1CVU.

Crystallographic studies of AA bound to COX-2 reveal that the fatty acid can also occupy a non-productive binding conformation within the COX active site. Kiefer and colleagues co-crystallized AA with H207A mCOX-2, a mutant enzyme lacking peroxidase activity, and observed the substrate bound in an "inverted" conformation in

which the carboxylic acid is coordinated to Tyr-385 and Ser-530 at the apex of the COX active site (2.4 Å resolution)(76). In this orientation, C-13 is located greater than 10 Å away from the catalytic tyrosine and therefore, the chemistry required to initiate the COX reaction cannot occur. Crystallization of wild-type (WT) apo-COX-2 in the presence of AA resulted in a 3.0 Å structure with a combination of AA and prostaglandin bound in the COX active site. The orientation of AA is similar to the non-productive binding mode shown in Figure 7 while the prostaglandin molecule is bound in a manner analogous to the productive conformation of AA seen in COX-1. The carboxylic acid of PGH_2 is located at the base of the active site near Arg-120 and Tyr-355 while the ω-end is positioned in the top channel of the active site; the endoperoxide ring is involved in hydrophobic interactions with Phe-381, Leu-384, Tyr-385, and Trp-387 (76). Currently, the physiological relevance of the non-productive or "inverted" binding mode of AA remains unknown.

In 2010, the Malkowski laboratory reported the 2.1 Å crystal structure of AA bound to Co^{3+}-mCOX-2 (77). In the COX-AA crystal structures described above, the substrate is bound in relatively the same position in both active sites of the COX dimer. However, in this structure, the global conformation of AA is different in each monomer of the COX-2 homodimer. Interestingly, the non-productive binding mode of AA is observed in one monomer, but the productive conformation, similar to that of AA in the COX-1 active site, is seen in the partner monomer. The major difference in the productive binding of AA in the active site of COX-2 compared to COX-1 is the lack of an interaction between the guanidinium group of Arg-120 and the carboxylic acid of the substrate (77). This finding supports previous mutagenesis studies in which mutation of

Arg-120 to Gln in COX-2 had no effect on the K_m for AA, but the same mutation in COX-1 caused the K_m for AA to increase 1000-fold compared to native enzyme (78,79). Hydrogen-bonding interactions between Tyr-355 and the carboxylic acid of AA occur in both COX-1 and COX-2.

Structural studies indicate that AA makes 49 interactions in the active site of COX-1 and participates in 54 interactions with COX-2 active site residues (74,77). Mutagenesis studies have helped to elucidate which of these interactions are critical for the proper positioning of the substrate during catalysis. Mutation of either Val-349 or Trp-387 causes a shift in the product profile of both COX-1 and COX-2, so that the enzyme forms an increased amount 11- or 15- HpETE (30-55%) while the amount of the bicyclic peroxide, PGG_2, is correspondingly decreased (80). This suggests that these residues play a key role in facilitating the cyclization of the 11-peroxyl radical leading to the formation of the 9,11-endoperoxide group.

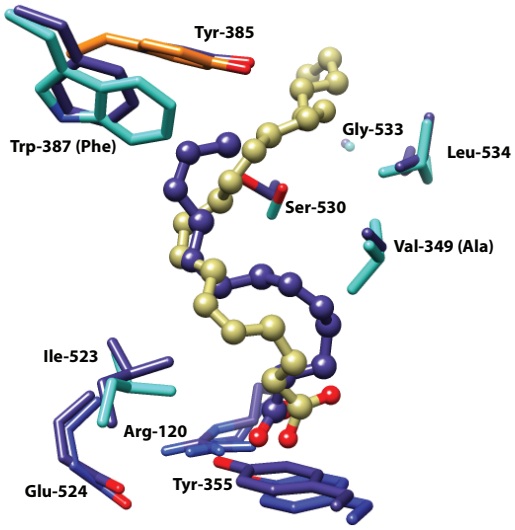

Figure 8. Overlay of AA bound in the COX active sites of WT and V349A/W387F Co^{3+}-COX-1. The structure of WT oCOX-1:AA is depicted as described in Figure 7 (PDB ID: 1DIY). The structure of the double mutant enzyme (PDB ID: 1U67) is shown in dark slate blue. C1-C-13 of AA are shown in ball-and-stick mode, and major shifts are observed at C-3 through C-6 and C-11/C-12. Mutations are noted in parentheses.

A V349A/W387F Co^{3+}-oCOX-1 double mutant produces greater than 85% 11*R*-HpETE, and a 3.1 Å crystal structure of the double mutant with AA bound in the COX active site reveals significant differences in the orientation of the substrate when compared to the WT COX-1:AA structure (Figure 8) (81). It should be noted that no electron density was observed for C-13 through C-20 of AA in the V349A/W387F COX-1:AA structure. The catalytic tyrosine is within 3 Å of C-13 of AA, indicating that the enzyme is still catalytically competent. However, interactions between Val-349 and C-3 and C-4 of AA are lost as C-3-C-6 reposition to occupy the extra space created by the V349A mutation. In addition, mutation of Trp-387 to phenylalanine eliminates interactions between C-11 and C-12, leading to greater conformational flexibility of the 11-peroxyl radical, so that the intermediate is no longer optimally aligned for endoperoxide formation (80,81).

The role of Ser-530 in promoting cyclization, as well as the control of prostaglandin stereochemistry, has also been studied by in-depth mutagenesis analyses. In oCOX-1, mutation of Ser-530 to threonine abolishes the production of PGG_2 and leads to the formation of 15*R*-HpETE almost exclusively (80). However, no detectable product formation is observed when the same mutation is made in the human COX-1 background. Substitution of Ser-530 with methionine, valine, leucine, or isoleucine in hCOX-1 also renders the enzyme inactive against AA (82). When Ser-530 is replaced with threonine in either murine or human COX-2, the ratio of prostaglandin to HpETE products is similar to that of WT, but there is a dramatic shift in the stereochemistry around C-15 toward the *R*-conformation. Mutation of Ser-530 to methionine or valine in COX-2 also results in almost complete stereochemical inversion of the oxygenation at C-15, as well as leads to increased amounts of HpETE products. Because both polar and non-polar substitutions

for Ser-530 alter the stereospecificity of the COX-2 reaction, it is likely that stereochemistry is partially controlled by steric interactions between the substrate and this region of the enzyme.

Structural basis for the binding of omega-3 fatty acids within the COX active site. Although AA is the primary COX substrate, both COX-1 and COX-2 have the ability to oxygenate a range of 18 – 22 carbon *n*-3 and *n*-6 fatty acids with varying efficiencies. Here again, a combination of mutagenesis and crystallographic analysis has helped to elucidate key enzyme-substrate interactions. Crystal structures of eicosapentaenoic acid (EPA; 20:5 *n*-3) bound in the COX active site provide insight into the basis for the low rate of EPA oxygenation (< 5% for COX-1, ~30% for COX-2 with respect to AA). In the Co^{3+}-oCOX-1:EPA structure (3.1 Å), EPA occupies an "L-shaped" conformation similar to the productive binding mode observed for AA in the oCOX-1 active site (Figure 9) (83). Like AA, the carboxylic acid of EPA forms a critical salt-bridge with Arg-120. However, the presence of an additional double bond (C17/C18) decreases the flexibility of the ω-tail of EPA in the hydrophobic groove above Ser-530, causing C-2 through C-10 to adopt a strained conformation. Consequently, C-13 is misaligned with respect to Tyr-385, precluding efficient initiation of the COX reaction. Mutation of Val-349, Ser-530, or Leu-534 further diminishes the oxygenation efficiency of EPA in a manner similar to that of AA. Interestingly, substitution of Phe-205 with leucine, at the top of the COX active site, dramatically increases the ability of COX-1 to metabolize EPA, presumably because the substrate is better accommodated in the larger active site of the mutant.

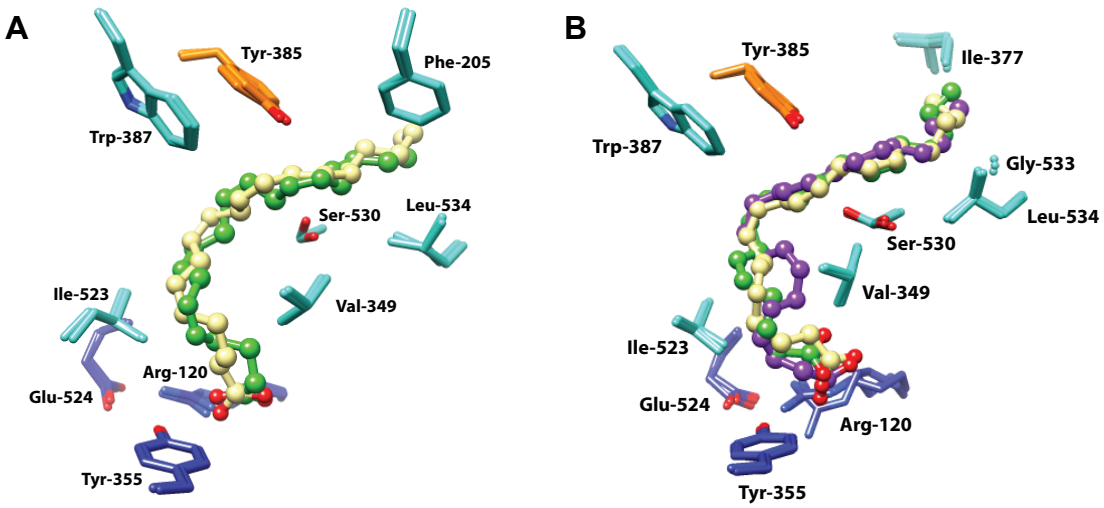

Figure 9. Binding of omega-3 fatty acids in the COX active site. *A*: AA (yellow ball-and-stick) and EPA (lime ball-and-stick) bind in an L-shaped conformation in the active site of COX-1. The ω-tail of EPA occupies a strained orientation so that C-13 is misaligned below the catalytic tyrosine (orange sticks) (PDB ID: 1DIY, 1IGX). *B*: AA (yellow), EPA (lime) and DHA (purple ball-and-stick) are shown in the productive conformation in the active site of COX-2. C-1 through C-9 of EPA are bound in a more extended conformation in COX-2 compared to COX-1 while C-1 through C-9 of DHA take on a coiled orientation like that of EPA in COX-1 (PDB ID: 3HS5, 3HS6, 3HS7). In both panels, constriction residues are shown in dark blue and additional key active site residues are shown in turquoise.

The crystal structure of EPA bound within the active site of COX-2 has also been determined (2.4 Å). Like the structure for Co^{3+}-COX-2:AA, Malkowski and colleagues observed EPA positioned in a non-productive binding conformation in the active site of one monomer and a productive conformation in the active site of the other monomer of the COX-2 dimer (77). The productive conformation of EPA in COX-2 is considerably different from the observed conformation in COX-1 (rmsd 2.28 Å). In COX-2, the orientation of EPA is similar to what is observed for AA so that there is no critical interaction with Arg-120, and C-13 is appropriately aligned below Tyr-385 for catalysis (Figure 9). The proper positioning of C-13 for hydrogen abstraction in COX-2, compared

to the misalignment in COX-1, may explain why EPA is a more effective substrate for COX-2.

In the same report, the Malkowski group described the 2.65 Å structure of docosahexaenoic acid (DHA; 22:6 *n*-3) bound to the active site of COX-2 (77). In this case, DHA occupies a productive "L-shaped" conformation in *both* monomers where the carboxylate is located near Arg-120 and Tyr-355 at the base of the COX active site and the ω-tail sits in the hydrophobic groove above Ser-530; C-20 of DHA is adjacent to Ile-377. To compensate for two extra carbons and the rigidity of two additional double bonds compared to AA, C-1 through C-9 of DHA bind in a compact, coiled orientation (Figure 9). The conformation of DHA in the COX-2 active site is similar to that of EPA in the active site of COX-1. In this orientation, C-15 of DHA, rather than C-13, is positioned below the phenolic oxygen of Tyr-385, resulting in the inefficient oxidation of DHA compared to AA (~10%) and the generation of monohydroperoxy fatty acid products (84).

Structural basis for COX-2 oxygenation of endocannabinoids. The endocannabinoids, AEA and 2-AG, are selectively oxygenated by COX-2 to form prostaglandin ethanolamides and glycerol esters, respectively. To date, a co-crystal structure of either AEA or 2-AG bound to COX-2 has not been published. However, the amino acid determinants of endocannabinoid oxygenation by COX-2 have been studied by mutagenesis. Substitution of the constriction site residue, Arg-120, for Gln resulted in a 9-fold reduction in 2-AG oxygenation, whereas the oxygenation of AEA was reduced more than 3-fold compared to WT enzyme (51,85). Further, mutation of Glu-524 to Leu

reduced the ability of COX-2 to oxygenate 2-AG, AEA, and also AA. Together, these results suggest that Arg-120 and Glu-524 at the constriction site play a critical role in the metabolism of endocannabinoids by COX-2. Interestingly, the third constriction site residue, Tyr-355, does not appear to be a determinant in endocannabinoid oxygenation.

Like AA, the endocannabinoids are not oxygenated by a Y385F mCOX-2 mutant enzyme, as an active tyrosyl radical at position 385 is required for catalysis. As described above, AA binds in an L-shaped conformation with its ω-tail inserted into a hydrophobic groove above Ser-530. The terminal carbon abuts Gly-533, and mutations that introduce steric bulk at position 533 dramatically reduce AA oxygenation. A Gly-533 to Val substitution also prevents the oxygenation of AEA and 2-AG. These results, combined with predicted interaction with constriction site residues, suggest that the endocannabinoids bind in a L-shaped conformation similar to that of AA.

The major difference in the active sites of COX-1 and COX-2 is the presence of a side pocket near the mouth of the active site in COX-2 that is not accessible in COX-1. The COX-2 side pocket is primarily comprised of Val-523, Arg-513, and Val-434. A COX-2 triple mutant, in which each of these residues has been mutated to its COX-1 counterpart (V523I/R513H/V434I), exhibits a dramatic reduction in 2-AG and AEA oxygenation (approximately 75%), while AA metabolism is unaffected. In subsequent studies, Arg-513 was identified as the side pocket residue primarily responsible for COX-2-selective oxygenation of endocannabinoids. Based on these findings, Kozak *et al*. developed molecular models for 2-AG and AEA binding to COX-2 (Figure 10) (51,85). In the models, the carbonyl is positioned at the constriction site between Arg-120 and Tyr-355 with the primary alcohol located near Glu-524 and participating in hydrogen

bonding interactions with Arg-513. The hypothetical binding mode shown in Figure 10 is supported by structure-activity studies which indicate that the primary hydroxyl moiety of 2-AG and AEA is an important determinant in the binding of these endocannabinoids to COX-2 (51,85).

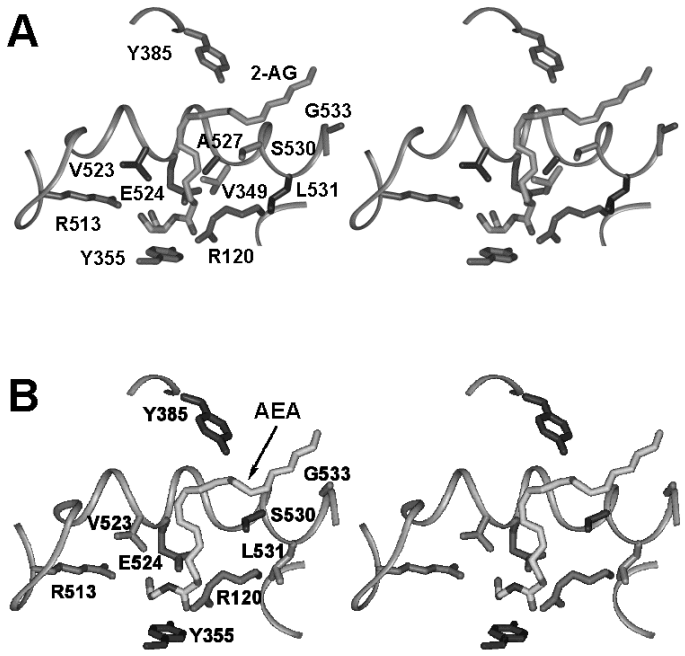

Figure 10. Computational models of 2-AG and AEA bound in the COX-2 active site. Reproduced from (85) and (51).

Mechanisms of NSAID action

Discovery of NSAIDs. Ancient civilizations documented the use of natural products in the treatment of pain, fever, and inflammation. The Ebers papyrus, arguably the world's oldest preserved medical text, indicates that ancient Egyptians used dried myrtle leaves to treat pain and fever as early as 1550 BC. The Greek physician Hippocrates recognized the analgesic and anti-pyretic properties of willow bark and leaf extracts in the 5th century BC. In addition to the Egyptians and the Greeks, it appears that Roman, Native American, African, and Chinese civilizations utilized these plant extracts for medicinal

purposes. Reverend Edward Stone published the first scientific record of the anti-pyretic effects of willow bark in his presentation to the Royal Society of London in 1763.

In 1829, the French pharmacist Henri Leroux identified salicin, the glucoside of salicylic alcohol, as the active ingredient in willow bark. Salicin can be modified to generate salicylic acid, but willow bark was difficult to obtain and purification from plant extracts was expensive so the supply of salicylic acid was limited (86). However, by the mid 19th century, Koble and Lautemann developed a method for the industrial production of salicylic acid from phenol, thereby facilitating its use by the general population in the treatment of pain and fever. To provide sufficient quantities of salicylic acid, the first drug factory, Salicylic Acid Works, was built in 1874. The widespread use of salicylic acid revealed its disadvantages; the low potency of the drug required patients to ingest several grams of the bitter compound per day, leading to gastric irritation and poor tolerance in many. To circumvent this problem, Felix Hoffman, a chemist at Friedrich Bayer and Co., developed acetylsalicylic acid. By acetylating the hydroxyl group of salicylic acid, Hoffman created a more palatable form of the drug with improved gastric tolerability. In 1899, acetylsalicylic acid was marketed by Bayer as aspirin, and soon became the world's best-selling drug.

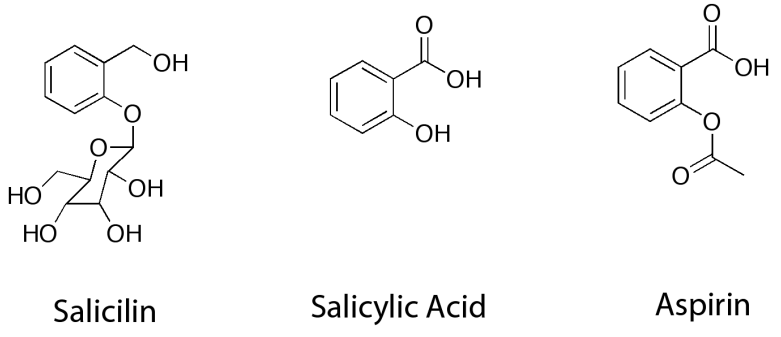

Figure 11. Chemical structures of salicilin, salicylic acid, and aspirin.

Animal models of pain and inflammation allowed the identification of several additional "aspirin-like" drugs, known today as non-steroidal anti-inflammatory drugs (NSAIDs), but the mechanism of action of these anti-inflammatory agents remained unclear until 1971. Upon the discovery that treatment of guinea pig lung homogenates with aspirin, sodium salicylate, or indomethacin causes a dose-dependent decrease in prostaglandin biosynthesis, sir John Vane concluded that NSAIDs exert their activity by inhibiting the enzyme responsible for prostaglandin production; the enzyme was later dubbed COX (87). Vane's findings were published alongside those of Smith and Willis, who observed that treatment of platelets with aspirin led to inhibition of prostaglandin biosynthesis (88).

Aspirin. Acetylsalicylic acid (aspirin) blocks prostaglandin production in both a time- and concentration-dependent manner (89). Notably, aspirin covalently modifies the COX enzymes as evident by the incorporation of radioactivity into the protein when incubated with [*acetyl*-^{3}H]aspirin (90,91). The active site residue Ser-530 was determined to be the single site of acetylation by aspirin, and the rate of acetylation closely corresponds to the rate of irreversible COX inactivation (91,92). Mutation of Ser-530 to alanine has no significant effect on COX activity, indicating that this residue is not essential for substrate binding or catalysis (93). However, S530A COX is not susceptible to covalent inhibition by aspirin, confirming that the hydroxyl moiety at position 530 is required for acetylation and subsequent irreversible inactivation of the enzyme by aspirin.

The crystal structure of COX-1 inactivated by the aspirin analog, 2-bromoacetoxy-benzoic acid, shows that acetylation of Ser-530 leads to significant steric

hindrance within the active site, effectively blocking substrate from interacting with the catalytic residue, Tyr-385, and thereby preventing catalysis (94). The bromoaspirin analog was shown to interact with COX-1 in a manner analogous to aspirin, and was employed in these studies so that the electron-dense halogen atom could be unambiguously located in a low-resolution electron density map (94). Upon acetylation of Ser-530, the bromoacetyl group occupies two rotameric states: in the primary conformer, the bromoacetyl group is positioned directly below Tyr-385 fully blocking the active site channel (Figure 12), while in the minor conformer, the bromoacetyl group extends into the hydrophobic groove above Ser-530, resulting in less hindrance of the main active site channel (not shown).

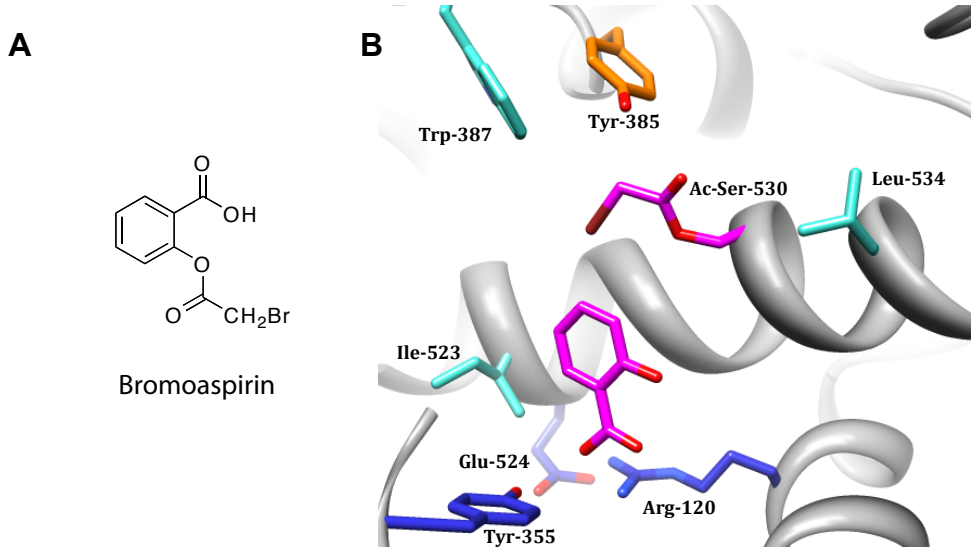

Figure 12. Crystal structure of bromoacetylated oCOX-1. *A.* Chemical structures of bromoaspirin analog 2-bromoacetoxy-benzoic acid. *B.* The primary conformer of the bromoacetyl serine and the by-product of the acetylation reaction, salicylic acid, are shown in magenta sticks within the COX-1 active site. The carboxylic acid moiety of salicylic acid participates in key interactions with Arg-120, while the carbonyl oxygen of the bromoacetyl group hydrogen-bonds to the phenolic oxygen of Tyr-385 (orange sticks) at the apex of the COX active site. (PDB ID: 1PTH)

Salicylic acid acts as the leaving group during the acetylation of COX-1 by aspirin. As shown in the oCOX-1:bromoaspirin crystal structure, salicylic acid is present within the COX active site approximately 5 Å away from the site of acetylation. The carboxylic acid moiety participates in ion-pairing interactions with Arg-120 at the base of the active site channel, and mutation of Arg-120 to glutamine or alanine results in a dramatic reduction in acetylation of COX upon treatment with aspirin (95). Mutagenesis studies performed within the COX-2 background indicate that Tyr-385 is also a critical determinant for acetylation by aspirin, as the extent of acetylation observed in Y385F COX-2 is reduced to levels similar to those observed in S530A mutant enzymes. In agreement with these studies, the oCOX-1:bromoaspirin crystal structure shows that the carbonyl oxygen of the bromoacetyl group participates in hydrogen-bonding interactions with the phenolic oxygen of Tyr-385. It has been proposed that this interaction acts to localize the acetyl group of aspirin near Ser-530 as well as to stabilize the negative charge of the tetrahedral intermediate of acetylation leading to increased reactivity (95).

A methionine substitution at Ser-530 most closely mimics the acetylation by aspirin, as three non-hydrogen atoms are added in both cases. Similar to the results obtained with S530M COX-1 and COX-2, aspirin acetylation inactivates oCOX-1 and causes the major product of the COX-2 reaction to become 15*R*-HpETE as opposed to 15*S*-PGG_2 (96). The ability of COX-2 to retain some enzymatic activity following acetylation by aspirin may also be related to the larger active site of COX-2 compared to COX-1. In support of this hypothesis, mutation of the residues that make up the COX-2 side pocket (Val-523, Arg-513, and Val-434) to the corresponding residues in COX-1 (Ile-523, His-513, and Ile-434) eliminates product formation by COX-2 upon treatment

with aspirin (97). It has been suggested that the larger COX-2 active site may lead to a change in the preferred rotameric state of the acetyl-serine side chain of COX-2 from that observed in the COX-1 crystallographic studies described above (94).

The irreversible inactivation of COX-1 by aspirin in the platelet is exploited therapeutically in cardiovascular prophylaxis. The cardioprotective effect of aspirin is attributed to sustained inhibition of COX-1 in the platelet, effectively preventing the biosynthesis of the vasoconstrictor, TXA_2. Because platelets are enucleated cells and cannot generate new COX-1 following acetylation, TXA_2 synthesis is blocked for the entire lifetime of the platelet. At low doses, aspirin does not dramatically affect the formation of the vasodilator, PGI_2, by COX-2 in the vascular endothelium, which can synthesize new enzyme molecules to replace those inactivated by acetylation (98).

Phenylpropionic acids. Aspirin is the only clinically used COX inhibitor to covalently modify the enzyme; all other NSAIDs are classified as either competitive and rapidly reversible or time-dependent, tight-binding and poorly reversible (89). The phenylpropionic acids, mefenamic acid and ibuprofen, interact with COX in a single-step kinetic mechanism characterized by the dissociation constant, K_I. Meclofenamic acid and flurbiprofen are structurally analogous to mefanamic acid and ibuprofen, respectively, but associate with the COX enzymes via a two-step mechanism in which the initial bimolecular association of the inhibitor with the enzyme is followed by a slower intramolecular step that results in a more tightly bound complex (eq 1) (89).

$$E + I \underset{k_{-1}}{\overset{k_1}{\rightleftharpoons}} EI \underset{k_{-2}}{\overset{k_2}{\rightleftharpoons}} EI^* \qquad \text{(eq 1)}$$

While ibuprofen and flurbiprofen exhibit different kinetic modes of inhibition, co-crystal structures indicate that the two inhibitors bind in a similar fashion within the COX active site (Figure 13) (64,65,99). As seen for AA, the carboxylic acid moiety of the inhibitor is positioned near the constriction site, where it participates in key interactions with Arg-120 and Tyr-355. Mutagenesis studies further demonstrate that an ion-pair with Arg-120 and a hydrogen bond with Tyr-355 are critical for potent inhibition of COX-1 and COX-2 by both ibuprofen and flurbiprofen (78,79). In addition, Tyr-355 is proposed to play a role in the stereospecificity of binding of 2-phenylpropionic acids. Although the majority of NSAIDs in this family are marketed as racemic mixtures, the *(S)*-enantiomer is significantly more potent than the (*R*)-enantiomer *in vivo*. The strict stereoselectivity is thought to arise from unfavorable steric interactions with the bulky phenolic side chain of Tyr-355 when the methyl group of the inhibitor is in the (*R*)-conformation. Bhattacharyya and colleagues provided support for this hypothesis in finding that decreasing the size of the side chain at position 355 (Tyr to Phe) results in significantly less specificity toward (*R*)- and (*S*)-ibuprofen compared to WT enzyme (78).

While phenylpropionic acids appear to be anchored within the COX active site by interactions between the carboxylic acid moiety and constriction site residues, the inhibitors make several contacts with additional protein residues in the active site cavity. The (*S*)-α-methyl group of 2-arylpropionic acids inserts into a small hydrophobic cleft near the base of the active site allowing it to participate in van der Waals interactions with Val-349 and Leu-359 (64,65). The distal portion of each inhibitor (i.e. the substituent on the phenyl ring) contacts amino acid residues located near the apex of the COX active site. Ibuprofen, the smallest NSAID of its class, is the exception, as the

isobutyl group is greater than 3.7 Å from neighboring protein residues (99). The fluorinated ring of flurbiprofen participates in van der Waals interactions with Val-349 and Ala-527. The fluorine atom itself contacts Ile-523 in COX-1, but makes no such interaction with the corresponding valine residue in COX-2 (65). In addition to several hydrophobic interactions, the unsubstituted phenyl ring of flurbiprofen contacts Ser-530 and stacks against Tyr-385 in both COX-1 and COX-2 (65,99).

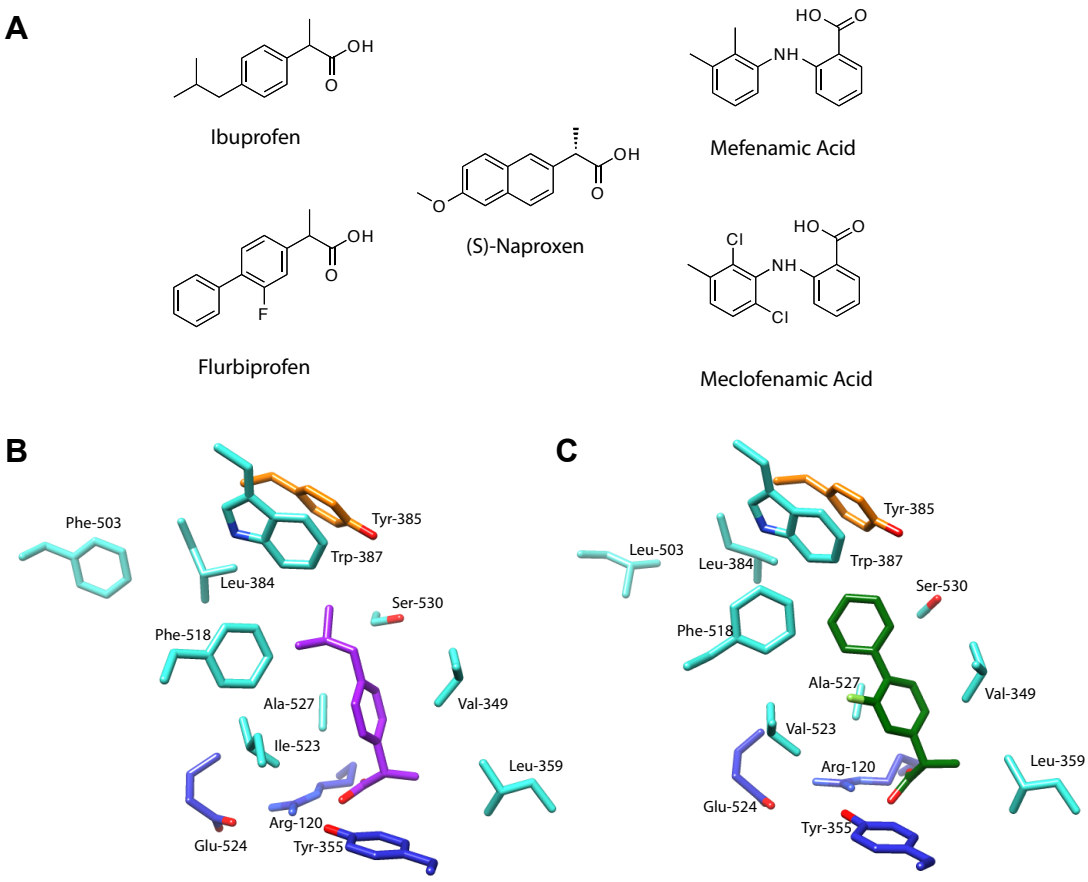

Figure 13. Phenylpropionic Acids. *A*. Chemical structures of phenylpropionic acids. *B*. Crystal structure of ibuprofen in the active site of oCOX-1 (1EQG). Ibuprofen (purple) interacts with constriction site residues Arg-120 and Tyr-355 (blue). *C*. Crystal structure of flurbiprofen (green) in the mCOX-2 active site (3PGH). Key active site residues are shown in turquoise and the catalytic tyrosine is shown in orange.

The unsubstituted ring of flurbiprofen approaches Leu-384 at the apex of the COX channel; Leu-384 is oriented differently in the active sites of COX-1 and COX-2 because of an amino acid change in the neighboring residue at position 503 (Phe in COX-1, Leu in COX-2). This substitution results in the presence of a small alcove in the COX-2 active site located above the phenyl ring of flurbiprofen. Based on the hypothesis that introduction of a lipophilic substituent at the 3'-position of the phenyl ring could be accommodated in the active site of COX-2, but not COX-1, Bayly and co-workers generated a series of potent and COX-2-selective flurbiprofen analogs (100). These studies provide a clear example of the importance of structural information in the rational design of COX inhibitors.

While crystallographic studies reveal critical information regarding the molecular determinants of inhibitor binding within the COX active site, they do not provide a complete explanation for the kinetic differences between competitive, reversible and slow, tight-binding inhibitors. As previously mentioned, flurbiprofen interacts with both COX-1 and COX-2 in a time-dependent, poorly reversible manner. In contrast, the flurbiprofen methyl ester binds to COX via a single-step mechanism like ibuprofen and mefenamic acid. Comparison of the co-crystal structures of flurbiprofen and methyl flurbiprofen bound to COX-1 reveals minor differences in the orientation of the inhibitors within the COX active site, but all major enzyme-inhibitor interactions are maintained (99). These studies illustrate that the structural basis for time-dependent inhibition is not related to a global conformational rearrangement of the enzyme structure and may be unique to each NSAID.

The 2-arylpropionic acid, naproxen, is one of the oldest and most widely used NSAIDs. Interestingly, naproxen is the only member of its class to be used exclusively as the (*S*)-enantiomer in the clinic. Previous kinetic studies suggest that naproxen binds to COX-1 in a time-independent manner but displays "mixed" inhibition for COX-2; "mixed" inhibition is defined as an initial time-dependent loss of enzyme activity followed by a non-zero plateau (101). A detailed investigation of the molecular basis for COX inhibition by naproxen will be presented in Chapters II and III of this dissertation.

Arylacetic acids. The indole based arylacetic acid, indomethacin, was first described as a time-dependent inhibitor of prostaglandin biosynthesis by Rome and Lands in 1975 (89). Similar to that of flurbiprofen, inhibition of COX by indomethacin is characterized as slowly reversible, rather than covalent, as intact inhibitor can be recovered following prolonged incubation with either COX enzyme (102). Following these early reports, in-depth studies have been performed in an effort to elucidate the molecular determinants of time-dependent COX inhibition by indomethacin. Examination of the COX-2:indomethacin co-crystal structure shows that the inhibitor is bound completely within the COX active site (Figure 14). As for the majority of carboxylate-containing NSAIDs, the carboxylic acid moiety is involved in critical interactions with Arg-120 and Tyr-355 at the constriction site. Salt-bridge formation between indomethacin and Arg-120 is essential for time-dependent inhibition of COX-1, but not COX-2, and as a result, conversion of the carboxylate moiety to various esters or amides generates potent COX-2-selective indomethacin derivatives (103) (104,105).

An important determinant of time-dependent inhibition by indomethacin appears to be the insertion of the 2′-methyl group into a small hydrophobic pocket formed by Val-349, Ala-527, Ser-530, and Leu-531 (106). Mutation of Val-349 to alanine increases the size of this pocket and renders the enzyme more sensitive to inhibition by indomethacin; decreasing the size of the pocket by mutation of Val-349 to leucine correspondingly decreases the potency of indomethacin. Interestingly, indomethacin exhibits significant reversibility in its inhibition of V349L COX-2 compared to WT. These mutagenesis studies have been corroborated by structure-activity studies showing that removal of the 2′-methyl group of indomethacin leads to poor and readily reversible inhibition of both COX-1 and COX-2.

Although binding of the 2′-methyl group in the hydrophobic pocket appears to be critical for the formation of the tightly bound enzyme-inhibitor complex, additional interactions help to anchor indomethacin within the COX active site. Inspection of the co-crystal structure of indomethacin in complex with COX-2 reveals that the *o*-methoxy group projects into a relatively large cleft comprised of Ser-353, Tyr-355, and Val-523 (65). The *para*-chlorobenzoyl group binds at the apex of the COX active site so that the chlorine atom interacts with Leu-384, and the benzoyl oxygen interacts with the side chains of Ser-530 and Val-349; hydrophobic interactions with Leu-384, Phe-381, Tyr-385, and Trp-387 act to stabilize the benzoyl group.

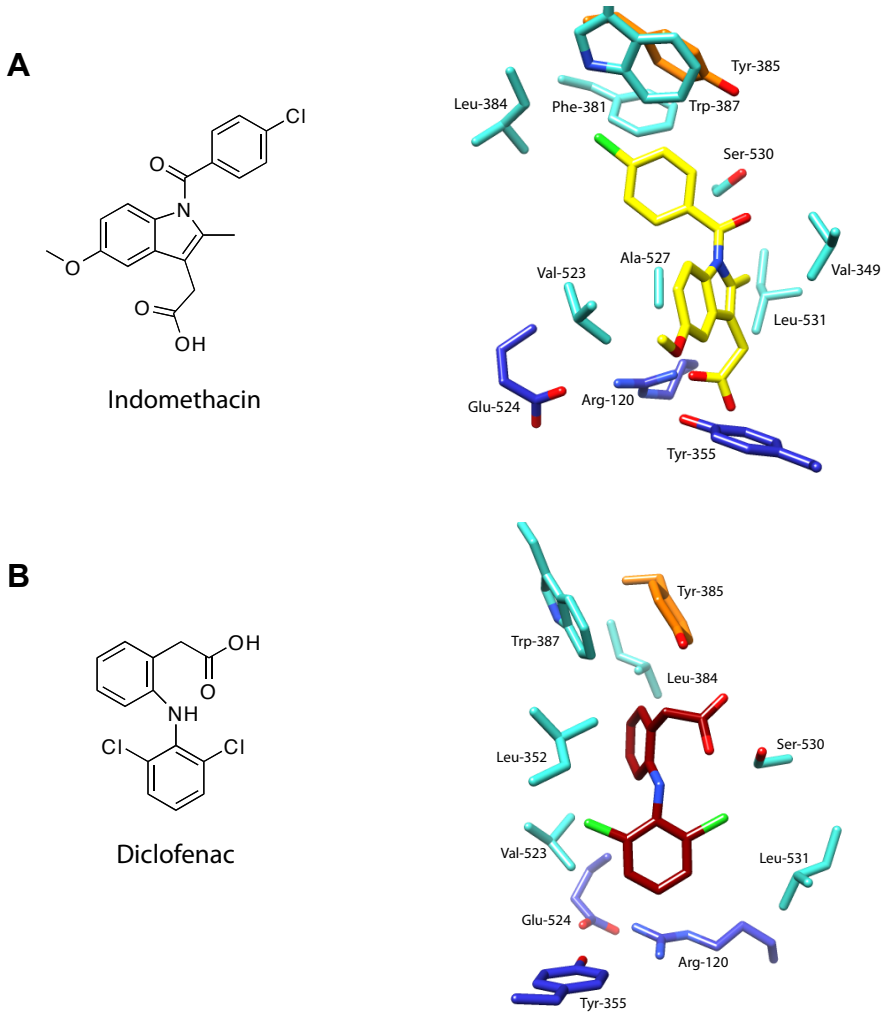

Figure 14. Binding of indomethacin and diclofenac in the mCOX-2 active site. A. Indomethacin (yellow) coordinates to constriction site residues Arg-120 and Tyr-355 (blue). The 2′-methyl group inserts into a small hydrophobic pocket comprised of Ser-530, Val-349, Leu-531, and Ala-527 (turquoise) (PDB ID: 4COX). B. Diclofenac (maroon) binds in an inverted conformation in the mCOX-2 active site with the carboxylate hydrogen-bonded to Ser-530 and Tyr-385 (PDB ID: 1PXX).

Diclofenac, like indomethacin, exhibits potent time-dependent inhibition of COX-1 and COX-2, but the binding mode of diclofenac is distinct among arylcarboxylic acid inhibitors. In this case, the inhibitor is positioned in an inverted conformation with its carboxylic acid hydrogen-bonded to Ser-530 and Tyr-385 at the top of the active site channel (Figure 14) (107). Mutation of constriction site residues at the base of the active

site does not affect diclofenac's inhibition of COX-2, whereas mutation of Ser-530 to alanine or methionine essentially abolishes its inhibitory activity (107,108). Although the strong hydrogen bonds to Tyr-385 and Ser-530 represent the only polar interactions between diclofenac and COX-2, the inhibitor makes hydrophobic contacts with several residues throughout the active site. The phenylacetic acid ring is encompassed by Tyr-385, Trp-387, Leu-384, and Leu-352, while the dichlorophenyl group participates in van der Waals interactions with Val-349, Ala-527, Leu-531, and Val-523 (107). Despite being similar in size and chemical composition, indomethacin and diclofenac display dramatically different binding modes within the COX-2 active site clearly demonstrating that each individual NSAID takes advantage of a unique set of active site residues in the formation of a tightly-bound enzyme-inhibitor complex. However, both NSAIDs appear to be anchored within the COX active at two primary locations. As described, the carboxylate of indomethacin is coordinated to constriction site residues while the 2′-methyl group binds in a hydrophobic depression bordered by Val-349. Diclofenac also has two major points of interaction in the COX active site as one of the chlorine atoms inserts into the hydrophobic pocket occupied by the of 2′-methyl group indomethacin and the carboxylate participates in H-bonding interactions with Ser-530 and Tyr-385.

Development of COX-2-selective inhibitors. Traditional NSAIDs, like those described above, are non-selective inhibitors of COX-1 and COX-2. The difference in the expression profiles of the COX enzymes suggests that the benefits of NSAID use, namely anti-inflammatory, analgesic, and antipyretic effects, arise from inhibition of COX-2, while deleterious side effects are associated with COX-1 inhibition. Side effects vary

greatly among individuals, and include gastrointestinal, liver, kidney, and nervous system toxicity. It was predicted that a COX-2-selective inhibitor would prevent inflammation without these undesired effects, specifically gastrointestinal toxicity. This hypothesis has since been validated in both animal models and human clinical trials, demonstrating that COX-2-selective inhibitors are anti-inflammatory and non-ulcerogenic (109-111).

Diarylheterocycles. The majority of COX-2-selective inhibitors used in the clinic belong to the diarylheterocycle structural class (Figure 15). In its search for novel anti-inflammatory agents with improved gastrointestinal safety, Dupont-Merck developed an aryl methyl sulfonyl inhibitor, DuP 697, prior to the discovery of COX-2. The finding that DuP 697 blocked prostaglandin biosynthesis in macrophages but not platelets suggested fundamental differences in its interactions with the COX enzymes in those cell types (112). This was substantiated by the discovery of COX-2 and the demonstration of its presence in macrophages (113). As such, DuP 697 acted as the principal lead compound in the development of COX-2-selective inhibitors culminating in the introduction of several diarylheterocycles to the market.

Diarylheterocycles, including DuP 697, appear to be rapid, reversible inhibitors of COX-1, but time-dependent, tight-binding inhibitors of COX-2 (114). Fluorescence quenching analysis has been used to directly monitor the kinetics of association of selective inhibitors to the COX enzymes, and indicates that diarylheterocycles follow a three-step mechanism of inhibition in which a fast bimolecular reaction is followed by two unimolecular steps (115,116). Traditional kinetic analysis of steady-state and time-dependent COX inhibition by the diarylheterocycles valdecoxib and celecoxib provided

further evidence for the three-step kinetic model (117). The third step of the inhibitor interaction with COX-2 results in the formation of a pseudo-irreversible complex and is thought to confer selectivity (116,117).

Structure-activity studies show that the presence of two aromatic rings at adjacent positions on a central heterocycle or carbocycle, with a 4-sulfunoamide or 4-methylsulfone substitution on one phenyl ring is critical for potent and selective inhibition of COX-2 (118). In support of this observation, mutagenesis and X-ray crystallography studies indicate that the final step of COX-2-diarylheterocycle association is the binding of the sulfonamide or sulfone moiety within a small pocket near the mouth of the COX-2 active site. The co-crystal structure of the celecoxib analog SC-558 bound to mCOX-2 clearly shows the insertion of the phenylsulfonamide moiety into this side pocket while the second phenyl ring binds in a hydrophobic cavity at the apex of the COX-2 active site bordered by Phe-381, Leu-384, Tyr-385, Trp-387, Phe-518, and Ser-530 similar to the binding of the phenyl ring of flurbiprofen and the benzoyl group of indomethacin (65).

Hydrophobic residues, including Leu-352, Tyr-355, Phe-518, and Val-523, surround the phenyl ring of the phenylsulfonamide moiety, while the sulfonamide interacts with His-90, Gln-192, and Arg-513. This region of the enzyme is less accessible in COX-1 largely due to the substitution of isoleucine for valine at position 523. Mutation of Val-523 to Ile in COX-2 eliminates time-dependent inhibition of COX-2 by diarylheterocycles but has only modest effects on the potency of traditional NSAIDs, suggesting that Val-523 is a critical determinant of selectivity in inhibitor binding (119,120). Secondary shell substitutions (Arg-513 for His and Val-434 for Ile) appear to

contribute to the accessibility of the COX-2 side pocket and therefore play a role in the selectivity of the diarylheterocycle class (65,121).

Recent reports indicate that the COX-2-selective inhibitor celecoxib can actually bind tightly within the active site of COX-1 (122). Overall, crystallographic studies indicate celecoxib adopts a similar conformation in COX-1 to that of SC-558 in the COX-2 active site. To accommodate the phenylsulfonamide moiety of celecoxib, Ile-523 adopts an extended rotamer conformation resulting in a shift in the positions of side chain residues 513-515 within the side pocket. While the sulfonamide group of SC-558 participates in hydrogen-bonding interactions with Arg-513 in COX-2, no such interactions occur between celecoxib and His-513 in COX-1. However, short hydrogen bonds are predicted to occur between the amide nitrogen of the sulfonamide moiety of celecoxib and Gln-192 and the backbone of Leu-352. The crystal structures of the COX-2 selective inhibitors nimesulide and indomethacin serinol amide bound within the active site of COX-1 also illustrate the ability of Ile-523 to adopt an alternate conformation to allow binding within the side-pocket region (123,124).

Lumiracoxib. Lumiracoxib, a close structural analog to diclofenac, represents the only example of a COX-2-selective inhibitor of the arylacetic acid class to be approved for use in the clinic. Crystallographic studies indicate that lumiracoxib binds in an inverted conformation similar to that of diclofenac in which the carboxylic acid is coordinated to Ser-530 and Tyr-385 at the apex of the COX active site. Selective inhibition of COX-2 by lumiracoxib is thought to arise form the insertion of the methyl group located on the phenylacetic acid ring into a small groove near Leu-384 at the top of the COX-2 active

site; in COX-1, bulky secondary shell residues surround Leu-384, restricting access to this region of the enzyme. Structure-activity studies illustrate that the presence of the methyl group is critical for COX-2 selectivity, as a *des*-methyl derivative of lumiracoxib is equally effective against COX-1 as it is COX-2 (125). A primary determinant of potency appears to be the binding of the chlorine atom of lumiracoxib within the small hydrophobic pocket comprised of Val-349, Ala-527, Ser-530, and Leu-531 in a manner analogous to that of the 2′-methyl group of indomethacin and the chlorine atom of diclofenac.

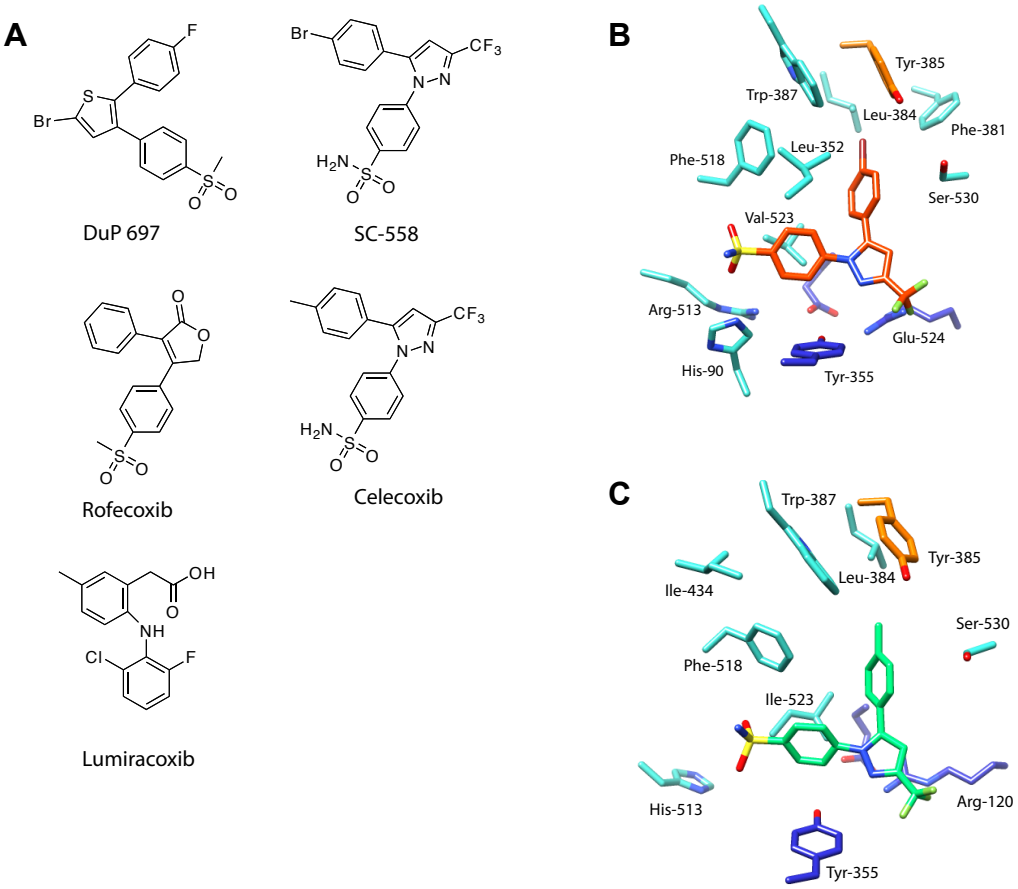

Figure 15. COX-2-selective inhibitors. *A*. Chemical structures of COX-2-selective inhibitors. *B*. Crystal structure of the celecoxib analog, SC-558 (red-orange), bound within the COX-2 active site. The sulfonamide moiety is inserted into the COX-2 side pocket lined by Val-523 and Arg-513 (PDB ID: 6COX). *C*. Crystal structure of celecoxib (green) bound in the active site of COX-1. Ile-523 adopts an extended conformation to allow for the binding of the sulfonamide moiety (PDB ID: 3KK6).

Partnering between COX monomers. The first evidence of cooperativity between COX monomers was the discovery that one molecule of a slow, tight-binding inhibitor (e.g. flurbiprofen, indomethacin) is sufficient to block substrate metabolism by the entire COX homodimer, suggesting that this class of inhibitors can achieve maximal inhibitory activity by binding to a single monomer (102). Preparation of COX heterodimers in which a WT hCOX-2 monomer was coupled to a monomer containing a mutation within the COX active site allowed for further investigation of possible cross-talk between COX subunits (126). Gly-533 is critical for the proper positioning of AA during catalysis and as such, G533A COX homodimers exhibit minimal catalytic activity compared to WT COX (75). However, the WT/G533A COX heterodimer is able to metabolize AA in a manner comparable to WT (126). The slow, tight-binding inhibitor, flurbiprofen is not an effective inhibitor of the R120Q/R120Q COX homodimer but exhibits potent, time-dependent inhibition of the WT/R120Q heterodimer (126). Together, these studies imply that COX enzymes exhibit half-of-sites reactivity, with only a single functioning monomer during catalysis. These findings are consistent with recent reports by the Malkowski group (described above) in which substrates occupy alternate conformations in the each COX active site of the biological dimer; further suggesting that only one monomer is functional at any given time.

Recently, structural studies have been performed in an attempt to elucidate the mechanism of communication between partnered COX monomers. Cross-linking studies indicate that the loop containing Ser-126 and Pro-127 as well as the loop containing Ser-541 and Ala-543, both located at the dimer interface of COX-2, are altered during

inhibitor binding (127). The crystal structure of celcoxib bound to COX-1 provides further evidence for a conformational change at the dimer interface. In the oCOX-1:celecoxib structure, one monomer is 100% occupied by celecoxib while the partner monomer is approximately 50% occupied. In the partially unoccupied monomer, positive difference density (F_o-F_c) revealed an alternate conformation of the loop containing residues 121-129 (Figure 16)(122). In agreement with the cross-linking studies, when the loop is present in the alternate conformation, Ser-126 closely neighbors Glu-543 as shown in Figure 16.

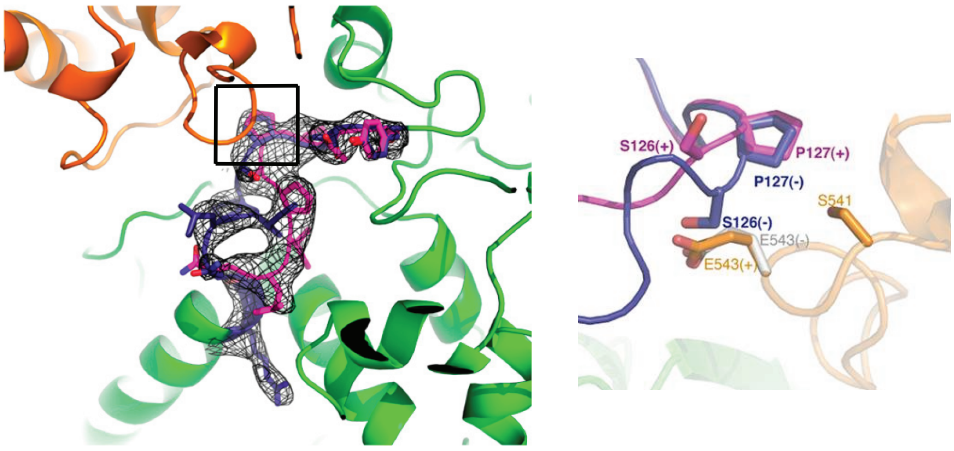

Figure 16. Alternate conformations of residues 121-129 at the dimer interface in the oCOX-1:celecoxib crystal structure. Reproduced from (122).

Movement of the 123-129 loop is also visible in the crystal structure of flurbiprofen bound to the WT/R120Q COX-1 heterodimer further indicating that this mobile loop may play a key role in the cross-talk between COX monomers (123).

COX-2 inhibitors and cardiovascular toxicity. The Vioxx Gastrointestinal Outcome Research (VIGOR) study provided the first evidence for an increased risk of cardiovascular events associated with the use of COX-2-selective inhibitors (110). In the VIGOR trial, the efficacy and safety of the potent and highly selective inhibitor, rofecoxib (Vioxx), was evaluated in comparison to the non-selective NSAID, naproxen, in patients with rheumatoid arthritis. Rofecoxib proved to be equally efficacious to naproxen with a reduced number of GI adverse events. However, patients treated with rofecoxib exhibited a 4-fold increase in acute myocardial infarction compared to those treated with naproxen. The long half-life of naproxen in humans leads to sustained inhibition of COX-1-driven production of the prothrombotic and atherogenic, TXA_2 (128). When administered at doses of > 500 mg twice daily, the biosynthesis of platelet-derived TXA_2 is inhibited throughout the dosage interval, and the inhibition of platelet COX-1 at the end of the dosage interval approaches but does not equal that of aspirin. As such, authors of the VIGOR study claimed that rofecoxib was neutral with regard to cardiovascular toxicity, and that the apparent increased risk was reflective of a cardioprotective effect of naproxen. It should be noted that this aspirin-like sustained inhibition of platelet COX-1 is not observed when lower doses of naproxen (e.g. 220 mg twice daily) are administered. The Celecoxib Long-term Arthritis Safety Study (CLASS) trial was a similar study in which celecoxib (400 mg twice daily) was compared to diclofenac and ibuprofen in patients with osteoarthritis or rheumatoid arthritis (111). Initial reports indicated that celecoxib was associated with fewer upper gastrointestinal events compared to the traditional NSAIDS, but no statistically significant differences were observed after twelve months of follow up (129). This is consistent with reports that

celecoxib and diclofenac show a similar degree of COX-2 selectivity in human whole blood assays (130). Furthermore, no significant differences in the incidence of cardiovascular events between celecoxib and the comparator non-selective NSAIDs were observed.

Colon polyp recurrence trials allowed for further evaluation of a potential cardiovascular hazard associated with COX-2 inhibitors. COX-2 is overexpressed in human colon cancers and is thought to play a role in tumorigenesis. Therefore, COX-2-selective inhibitors are attractive candidates for novel chemopreventive agents. The Adenomatous Polyp Prevention on Vioxx (APPROVE) trial evaluated the recurrence of polyps in individuals treated with rofecoxib (25 mg) versus placebo. The study showed a clear reduction in polyp recurrence (24%) in patients treated with rofecoxib after three years. However, treatment with rofecoxib also resulted in a roughly 2-fold increase in cardiovascular events, including myocardial infarction and stroke, compared to placebo (131,132). The cardiovascular side effects reported in the APPROVE trial led to the immediate withdrawal of rofecoxib from the market. Similarly, the Adenoma Prevention with Celecoxib (APC) trial measured polyp recurrence in patients receiving either 200 or 400 mg celecoxib twice daily compared to placebo and reported a dose-dependent reduction in the recurrence of polyps following treatment with celecoxib. Cardiovascular events also increased in a dose-dependent manner with a 2.6-fold increase in patients allocated to low-dose celecoxib and a 3.4-fold increase in the high-dose group. Together, these trials illustrate the potential for COX-2-selective inhibitors as an effective therapy in the prevention of colon polyp recurrence but also establish that prolonged use of COX-2 inhibitors is associated with an increased risk of adverse cardiovascular events.

It has been hypothesized that the cardiovascular toxicity of COX-2-selective inhibitors is thought to arise from the inhibition of the COX-2-driven production of the anti-thrombotic and anti- atherogenic PGI_2 or PGI_2-G by vascular endothelial cells (63,133). As such, there is some debate as to whether or not the cardiovascular risk associated with selective COX-2 inhibitors extends to non-selective NSAIDs, which also block PGI_2 biosynthesis. Long-term, placebo-controlled studies of significant power must be conducted in order to make definitive conclusions regarding the cardiovascular outcomes associated with the use of non-selective NSAIDs. However, evolving data from meta-analyses of clinical trials as well as retrospective cohort studies suggest that high-doses of traditional NSAIDS, including ibuprofen, indomethacin, and diclofenac, carry an increased risk similar to that of the COX-2 selective inhibitor celecoxib (134-136). Naproxen, a non-selective inhibitor of COX-1 and COX-2, is the outlier in these studies and appears to be of neutral risk and may convey a mild protective effect at high doses. As mentioned above, inhibition of TXA_2 biosynthesis throughout the dosing interval, which is not observed with other commonly used NSAIDs, such as ibuprofen, may offset reductions in PGI_2 or PGI_2-G biosynthesis and contribute to the reduced cardiovascular adverse effects of the higher doses of naproxen (137).

Dissertation Aims

The major goal of the research described herein was to provide further insight into the structural and functional determinants of COX inhibition by NSAIDs. A significant effort was made to identify the molecular basis for the activity of the non-selective NSAID, naproxen, because of its unique pharmacological properties and long history of human use. An investigation of the kinetics of COX inhibition by naproxen and an analysis of the structure-activity relationship of naproxen are presented in Chapter II. As an extension of these studies, an in-depth mutagenesis study was performed, in which naproxen was tested against a library of COX-2 active site mutants to identify amino acid residues that are critical for naproxen binding. These results are discussed in Chapter III. Crystallographic analysis of the binding mode of naproxen within the active site of COX-2 is also described in Chapter III. Together, these studies provide a comprehensive understanding of naproxen activity. Chapter IV will summarize my examination of the ability of NSAIDs to inhibit the oxygenation of the endocannabinoid, 2-AG, as compared to AA. The finding that weak inhibitors of AA metabolism are in some cases potent inhibitors of 2-AG oxygenation prompted the investigation of the activity of (*R)*-enantiomers of 2-arylpropionic acids against endocannabinoids. These studies are presented in Chapter V. Chapters IV and V together provide novel information regarding the molecular determinants for substrate-selective inhibition. In sum, the findings presented in Chapters II-V provide a greater understanding of COX structure and function as well as the actions of NSAIDS *in vivo*. Chapter VI will contain a brief discussion of the implications of this research.

References

1. Smith, W. (1997) *Adv Exp Med Biol* **400B**, 989-1011

2. Funk, C. D. (2001) *Science* **294**, 1871-1875

3. Fitzgerald, G. A., Catella, F., and Oates, J. A. (1987) *Hum. Pathol.* **18**, 248-252

4. Murata, T., Ushikubi, F., Matsuoka, T., Hirata, M., Yamasaki, A., Sugimoto, Y., Ichikawa, A., Aze, Y., Tanaka, T., Yoshida, N., Ueno, A., Oh-ishi, S., and Narumiya, S. (1997) *Nature* **388**, 678-682

5. Cheng, Y., Austin, S. C., Rocca, B., Koller, B. H., Coffman, T. M., Grosser, T., Lawson, J. A., and FitzGerald, G. A. (2002) *Science* **296**, 539-541

6. Thomas, D. W., Mannon, R. B., Mannon, P. J., Latour, A., Oliver, J. A., Hoffman, M., Smithies, O., Koller, B. H., and Coffman, T. M. (1998) *J. Clin. Invest.* **102**, 1994-2001

7. Patrono, C., and Dunn, M. J. (1987) *Kidney. Int.* **32**, 1-12

8. Robert, A. (1979) *Gastroenterology* **77**, 761-767

9. Sheng, H., Shao, J., Kirkland, S. C., Isakson, P., Coffey, R. J., Morrow, J., Beauchamp, R. D., and DuBois, R. N. (1997) *J. Clin. Invest.* **99**, 2254-2259

10. Hwang, D., Scollard, D., Byrne, J., and Levine, E. (1998) *J. Natl. Cancer Inst.* **90**, 455-460

11. Samad, T. A., Sapirstein, A., and Woolf, C. J. (2002) *Trends. Mol. Med.* **8**, 390-396

12. Levy, G. N. (1997) *FASEB j* **11**, 234-247

13. Hamberg, M., and Samuelsson, B. (1967) *J. Biol. Chem.* **242**, 5344-5354

14. Morita, I., Schindler, M., Regier, M. K., Otto, J. C., Hori, T., DeWitt, D. L., and Smith, W. L. (1995) *J. Biol. Chem.* **270**, 10902-10908

15. Miyamoto, T., Ogino, N., Yamamoto, S., and Hayaishi, O. (1976) *J. Biol. Chem.* **251**, 2629-2636

16. Ogino, N., Ohki, S., Yamamoto, S., and Hayaishi, O. (1978) *J. Biol. Chem.* **253**, 5061-5068

17. Hamberg, M., and Samuelsson, B. (1973) *Proc. Natl. Acad. Sci. U.S.A.* **70**, 899-903

18. Ohki, S., Ogino, N., Yamamoto, S., and Hayaishi, O. (1979) *J. Biol. Chem.* **254**, 829-836

19. Dietz, R., Nastainczyk, W., and Ruf, H. H. (1988) *Eur. J. Biochem.* **171**, 321-328

20. Landino, L. M., Crews, B. C., Gierse, J. K., Hauser, S. D., and Marnett, L. J. (1997) *J. Biol. Chem.* **272**, 21565-21574

21. Smith, W. L., and Lands, W. E. (1972) *Biochemistry* **11**, 3276-3285

22. Mizuno, K., Yamamoto, S., and Lands, W. E. (1982) *Prostaglandins* **23**, 743-757

23. Koshkin, V., and Dunford, H. B. (1999) *Biochim. Biophys. Acta.* **1431**, 47-52

24. Hamberg, M., and Samuelsson, B. (1967) *J. Biol. Chem.* **242**, 5336-5343

25. Samuelsson, B. (1965) *J. Am. Chem. Soc.* **87**, 3011-3013

26. Schreiber, J., Mason, R. P., and Eling, T. E. (1986) *Arch. Biochem. Biophys.* **251**, 17-24

27. Wu, G., Wei, C., Kulmacz, R. J., Osawa, Y., and Tsai, A. L. (1999) *J. Biol. Chem.* **274**, 9231-9237

28. Wu, G., Rogge, C. E., Wang, J. S., Kulmacz, R. J., Palmer, G., and Tsai, A. L. (2007) *Biochemistry* **46**, 534-542

29. Markey, C. M., Alward, A., Weller, P. E., and Marnett, L. J. (1987) *J. Biol. Chem.* **262**, 6266-6279

30. Siegel, M. I., McConnell, R. T., Abrahams, S. L., Porter, N. A., and Cuatrecasas, P. (1979) *Biochem. Biophys. Res. Commun.* **89**, 1273-1280

31. Hashimoto, Y., Naito, C., Kume, S., Kato, H., Watanabe, T., Kawamura, M., Teramoto, T., and Oka, H. (1985) *Biochim. Biophys. Acta.* **841**, 283-291

32. Kent, R. S., Diedrich, S. L., and Whorton, A. R. (1983) *J. Clin. Invest.* **72**, 455-465

33. Xie, W. L., Chipman, J. G., Robertson, D. L., Erikson, R. L., and Simmons, D. L. (1991) *Proc. Natl. Acad. Sci. U.S.A.* **88**, 2692-2696

34. Yu, Y., Fan, J., Hui, Y., Rouzer, C. A., Marnett, L. J., Klein-Szanto, A. J., FitzGerald, G. A., and Funk, C. D. (2007) *J. Biol. Chem.* **282**, 1498-1506

35. Kulmacz, R. J. (2005) *Biochem. Biophys. Res. Commun.* **338**, 25-33

36. Bambai, B., Rogge, C. E., Stec, B., and Kulmacz, R. J. (2004) *J. Biol. Chem.* **279**, 4084-4092

37. Ueno, N., Takegoshi, Y., Kamei, D., Kudo, I., and Murakami, M. (2005) *Biochem. Biophys. Res. Commun.* **338**, 70-76

38. Mbonye, U. R., Wada, M., Rieke, C. J., Tang, H. Y., Dewitt, D. L., and Smith, W. L. (2006) *J. Biol. Chem.* **281**, 35770-35778

39. Matsuda, L. A., Lolait, S. J., Brownstein, M. J., Young, A. C., and Bonner, T. I. (1990) *Nature* **346**, 561-564

40. Munro, S., Thomas, K. L., and Abu-Shaar, M. (1993) *Nature* **365**, 61-65

41. Herkenham, M., Lynn, A. B., Little, M. D., Johnson, M. R., Melvin, L. S., de Costa, B. R., and Rice, K. C. (1990) *Proc. Natl. Acad. Sci. U.S.A.* **87**, 1932-1936

42. Devane, W. A., Hanus, L., Breuer, A., Pertwee, R. G., Stevenson, L. A., Griffin, G., Gibson, D., Mandelbaum, A., Etinger, A., and Mechoulam, R. (1992) *Science* **258**, 1946-1949

43. Liu, J., Wang, L., Harvey-White, J., Huang, B. X., Kim, H. Y., Luquet, S., Palmiter, R. D., Krystal, G., Rai, R., Mahadevan, A., Razdan, R. K., and Kunos, G. (2008) *Neuropharmacology* **54**, 1-7

44. Wang, J., and Ueda, N. (2009) *Prostaglandins Other Lipid. Mediat.* **89**, 112-119

45. Sugiura, T., Kondo, S., Sukagawa, A., Nakane, S., Shinoda, A., Itoh, K., Yamashita, A., and Waku, K. (1995) *Biochem. Biophys. Res. Commun.* **215**, 89-97

46. Mechoulam, R., Ben-Shabat, S., Hanus, L., Ligumsky, M., Kaminski, N. E., Schatz, A. R., Gopher, A., Almog, S., Martin, B. R., Compton, D. R., and et al. (1995) *Biochem. Pharmacol*. **50**, 83-90

47. Stella, N., Schweitzer, P., and Piomelli, D. (1997) *Nature* **388**, 773-778

48. Long, J. Z., Li, W., Booker, L., Burston, J. J., Kinsey, S. G., Schlosburg, J. E., Pavon, F. J., Serrano, A. M., Selley, D. E., Parsons, L. H., Lichtman, A. H., and Cravatt, B. F. (2009) *Nat. Chem. Biol.* **5**, 37-44

49. Yu, M., Ives, D., and Ramesha, C. S. (1997) *J. Biol. Chem.* **272**, 21181-21186

50. So, O. Y., Scarafia, L. E., Mak, A. Y., Callan, O. H., and Swinney, D. C. (1998) *J. Biol. Chem.* **273**, 5801-5807

51. Kozak, K. R., Prusakiewicz, J. J., Rowlinson, S. W., Prudhomme, D. R., and Marnett, L. J. (2003) *Biochemistry* **42**, 9041-9049

52. Kozak, K. R., Rowlinson, S. W., and Marnett, L. J. (2000) *J. Biol. Chem.* **275**, 33744-33749

53. Kozak, K. R., Crews, B. C., Morrow, J. D., Wang, L. H., Ma, Y. H., Weinander, R., Jakobsson, P. J., and Marnett, L. J. (2002) *J. Biol. Chem.* **277**, 44877-44885

54. Kondo, S., Kondo, H., Nakane, S., Kodaka, T., Tokumura, A., Waku, K., and Sugiura, T. (1998) *FEBS Lett.* **429**, 152-156

55. Rouzer, C. A., and Marnett, L. J. (2005) *J. Biol. Chem.* **280**, 26690-26700

56. Hu, S. S., Bradshaw, H. B., Chen, J. S., Tan, B., and Walker, J. M. (2008) *Br. J. Pharmacol.* **153**, 1538-1549

57. Correa, F., Docagne, F., Clemente, D., Mestre, L., Becker, C., and Guaza, C. (2008) *Biochem. J.* **409**, 761-770

58. Krauss, A. H., and Woodward, D. F. (2004) *Surv. Ophthalmol.* **49 Suppl 1**, S5-11

59. Liang, Y., Woodward, D. F., Guzman, V. M., Li, C., Scott, D. F., Wang, J. W., Wheeler, L. A., Garst, M. E., Landsverk, K., Sachs, G., Krauss, A. H., Cornell, C., Martos, J., Pettit, S., and Fliri, H. (2008) *Br. J. Pharmacol.* **154**, 1079-1093

60. Nirodi, C. S., Crews, B. C., Kozak, K. R., Morrow, J. D., and Marnett, L. J. (2004) *Proc. Natl. Acad. Sci. U.S.A.* **101**, 1840-1845

61. Sang, N., Zhang, J., and Chen, C. (2006) *J. Physiol.* **572**, 735-745

62. Sang, N., Zhang, J., and Chen, C. (2007) *J. Neurochem.* **102**, 1966-1977

63. Ghosh, M., Wang, H., Ai, Y., Romeo, E., Luyendyk, J. P., Peters, J. M., Mackman, N., Dey, S. K., and Hla, T. (2007) *J. Exp. Med.* **204**, 2053-2061

64. Picot, D., Loll, P. J., and Garavito, R. M. (1994) *Nature* **367**, 243-249

65. Kurumbail, R. G., Stevens, A. M., Gierse, J. K., McDonald, J. J., Stegeman, R. A., Pak, J. Y., Gildehaus, D., Miyashiro, J. M., Penning, T. D., Seibert, K., Isakson, P. C., and Stallings, W. C. (1996) *Nature* **384**, 644-648

66. Rouzer, C. A., and Marnett, L. J. (2009) *J. Lipid. Res.* **50**, S29 - S34

67. Van der Ouderaa, F. J., Buytenhek, M., Nugteren, D. H., and Van Dorp, D. A. (1977) *Biochim. Biophys. Acta.* **487**, 315-331

68. Picot, D., and Garavito, R. M. (1994) *FEBS Lett.* **346**, 21-25

69. Shimokawa, T., and Smith, W. L. (1991) *J. Biol. Chem.* **266**, 6168-6173

70. Liu, J., Seibold, S. A., Rieke, C. J., Song, I., Cukier, R. I., and Smith, W. L. (2007) *J. Biol. Chem.* **282**, 18233-18244

71. Gupta, K., Selinsky, B. S., and Loll, P. J. (2006) *Acta. Crystallogr. D. Biol. Crystallogr.* **62**, 151-156

72. Chubb, A. J., Fitzgerald, D. J., Nolan, K. B., and Moman, E. (2006) *Biochemistry* **45**, 811-820

73. Luong, C., Miller, A., Barnett, J., Chow, J., Ramesha, C., and Browner, M. F. (1996) *Nat. Struct. Biol.* **3**, 927-933

74. Malkowski, M. G., Ginell, S. L., Smith, W. L., and Garavito, R. M. (2000) *Science* **289**, 1933-1937

75. Rowlinson, S. W., Crews, B. C., Lanzo, C. A., and Marnett, L. J. (1999) *J. Biol. Chem.* **274**, 23305-23310

76. Kiefer, J. R., Pawlitz, J. L., Moreland, K. T., Stegeman, R. A., Hood, W. F., Gierse, J. K., Stevens, A. M., Goodwin, D. C., Rowlinson, S. W., Marnett, L. J., Stallings, W. C., and Kurumbail, R. G. (2000) *Nature* **405**, 97-101

77. Vecchio, A. J., Simmons, D. M., and Malkowski, M. G. (2010) *J. Biol. Chem.* **285**, 22152-22163

78. Bhattacharyya, D. K., Lecomte, M., Rieke, C. J., Garavito, M., and Smith, W. L. (1996) *J. Biol. Chem.* **271**, 2179-2184

79. Rieke, C. J., Mulichak, A. M., Garavito, R. M., and Smith, W. L. (1999) *J. Biol. Chem.* **274**, 17109-17114

80. Thuresson, E. D., Lakkides, K. M., Rieke, C. J., Sun, Y., Wingerd, B. A., Micielli, R., Mulichak, A. M., Malkowski, M. G., Garavito, R. M., and Smith, W. L. (2001) *J. Biol. Chem.* **276**, 10347-10357

81. Harman, C. A., Rieke, C. J., Garavito, R. M., and Smith, W. L. (2004) *J. Biol. Chem.* **279**, 42929-42935

82. Schneider, C., Boeglin, W. E., Prusakiewicz, J. J., Rowlinson, S. W., Marnett, L. J., Samel, N., and Brash, A. R. (2002) *J. Biol. Chem.* **277**, 478-485

83. Malkowski, M. G., Thuresson, E. D., Lakkides, K. M., Rieke, C. J., Micielli, R., Smith, W. L., and Garavito, R. M. (2001) *J. Biol. Chem.* **276**, 37547-37555

84. Laneuville, O., Breuer, D. K., Xu, N., Huang, Z. H., Gage, D. A., Watson, J. T., Lagarde, M., DeWitt, D. L., and Smith, W. L. (1995) *J. Biol. Chem.* **270**, 19330-19336

85. Kozak, K. R., Prusakiewicz, J. J., Rowlinson, S. W., Schneider, C., and Marnett, L. J. (2001) *J. Biol. Chem.* **276**, 30072-30077

86. Jack, D. B. (1997) *Lancet* **350**, 437-439

87. Vane, J. R. (1971) *Nat. New. Biol.* **231**, 232-235

88. Smith, J. B., and Willis, A. L. (1971) *Nat. New. Biol.* **231**, 235-237

89. Rome, L. H., and Lands, W. E. (1975) *Proc. Natl. Acad. Sci. U.S.A.* **72**, 4863-4865

90. Van Der Ouderaa, F. J., Buytenhek, M., Nugteren, D. H., and Van Dorp, D. A. (1980) *Eur. J. Biochem.* **109**, 1-8

91. Roth, G. J., Machuga, E. T., and Ozols, J. (1983) *Biochemistry* **22**, 4672-4675

92. Rome, L. H., Lands, W. E., Roth, G. J., and Majerus, P. W. (1976) *Prostaglandins* **11**, 23-30

93. DeWitt, D. L., el-Harith, E. A., Kraemer, S. A., Andrews, M. J., Yao, E. F., Armstrong, R. L., and Smith, W. L. (1990) *J. Biol. Chem.* **265**, 5192-5198

94. Loll, P. J., Picot, D., and Garavito, R. M. (1995) *Nat. Struct. Biol.* **2**, 637-643

95. Hochgesang, G. P., Jr., Rowlinson, S. W., and Marnett, L. J. (2001) *J. Am. Chem. Soc.* **122**, 6514-6515

96. Meade, E. A., Smith, W. L., and DeWitt, D. L. (1993) *J. Biol. Chem.* **268**, 6610-6614

97. Rowlinson, S. W., Crews, B. C., Goodwin, D. C., Schneider, C., Gierse, J. K., and Marnett, L. J. (2000) *J. Biol. Chem.* **275**, 6586-6591

98. FitzGerald, G. A., Oates, J. A., Hawiger, J., Maas, R. L., Roberts, L. J., 2nd, Lawson, J. A., and Brash, A. R. (1983) *J. Clin. Invest.* **71**, 676-688

99. Selinsky, B. S., Gupta, K., Sharkey, C. T., and Loll, P. J. (2001) *Biochemistry* **40**, 5172-5180

100. Bayly, C. I., Black, W. C., Leger, S., Ouimet, N., Ouellet, M., and Percival, M. D. (1999) *Bioorg. Med. Chem. Lett.* **9**, 307-312

101. Gierse, J. K., Koboldt, C. M., Walker, M. C., Seibert, K., and Isakson, P. C. (1999) *Biochem. J.* **339 (Pt 3)**, 607-614

102. Kulmacz, R. J., and Lands, W. E. (1985) *J. Biol. Chem.* **260**, 12572-12578

103. Mancini, J. A., Riendeau, D., Falgueyret, J. P., Vickers, P. J., and O'Neill, G. P. (1995) *J. Biol. Chem.* **270**, 29372-29377

104. Kalgutkar, A. S., Crews, B. C., Rowlinson, S. W., Marnett, A. B., Kozak, K. R., Remmel, R. P., and Marnett, L. J. (2000) *Proc. Natl. Acad. Sci. U.S.A.* **97**, 925-930

105. Kalgutkar, A. S., Marnett, A. B., Crews, B. C., Remmel, R. P., and Marnett, L. J. (2000) *J. Med. Chem.* **43**, 2860-2870

106. Prusakiewicz, J. J., Felts, A. S., Mackenzie, B. S., and Marnett, L. J. (2004) *Biochemistry* **43**, 15439-15445

107. Rowlinson, S. W., Kiefer, J. R., Prusakiewicz, J. J., Pawlitz, J. L., Kozak, K. R., Kalgutkar, A. S., Stallings, W. C., Kurumbail, R. G., and Marnett, L. J. (2003) *J. Biol. Chem.* **278**, 45763-45769

108. Mancini, J. A., Vickers, P. J., O'Neill, G. P., Boily, C., Falgueyret, J. P., and Riendeau, D. (1997) *Mol. Pharmacol.* **51**, 52-60

109. Masferrer, J. L., Zweifel, B. S., Manning, P. T., Hauser, S. D., Leahy, K. M., Smith, W. G., Isakson, P. C., and Seibert, K. (1994) *Proc. Natl. Acad. Sci. U.S.A.* **91**, 3228-3232

110. Bombardier, C., Laine, L., Reicin, A., Shapiro, D., Burgos-Vargas, R., Davis, B., Day, R., Ferraz, M. B., Hawkey, C. J., Hochberg, M. C., Kvien, T. K., and Schnitzer, T. J. (2000) *New. Engl. J. Med.* **343**, 1520-1528, 1522 p following 1528

111. Silverstein, F. E., Faich, G., Goldstein, J. L., Simon, L. S., Pincus, T., Whelton, A., Makuch, R., Eisen, G., Agrawal, N. M., Stenson, W. F., Burr, A. M., Zhao,

W. W., Kent, J. D., Lefkowith, J. B., Verburg, K. M., and Geis, G. S. (2000) *J. Amer. Med. Assoc.* **284**, 1247-1255

112. Gans, K. R., Galbraith, W., Roman, R. J., Haber, S. B., Kerr, J. S., Schmidt, W. K., Smith, C., Hewes, W. E., and Ackerman, N. R. (1990) *J. Pharmacol. Exp. Ther.* **254**, 180-187

113. Lee, S. H., Soyoola, E., Chanmugam, P., Hart, S., Sun, W., Zhong, H., Liou, S., Simmons, D., and Hwang, D. (1992) *J. Biol. Chem.* **267**, 25934-25938

114. Copeland, R. A., Williams, J. M., Giannaras, J., Nurnberg, S., Covington, M., Pinto, D., Pick, S., and Trzaskos, J. M. (1994) *Proc. Natl. Acad. Sci. U.S.A.* **91**, 11202-11206

115. Lanzo, C. A., Beechem, J. M., Talley, J., and Marnett, L. J. (1998) *Biochemistry* **37**, 217-226

116. Lanzo, C. A., Sutin, J., Rowlinson, S., Talley, J., and Marnett, L. J. (2000) *Biochemistry* **39**, 6228-6234

117. Walker, M. C., Kurumbail, R. G., Kiefer, J. R., Moreland, K. T., Koboldt, C. M., Isakson, P. C., Seibert, K., and Gierse, J. K. (2001) *Biochem. J.* **357**, 709-718

118. Leblanc, Y., Gauthier, J. Y., Ethier, D., Guay, D., Mancini, J., Riendeau, D., Tagari, P., Vickers, P., Wong, E., and Prasit, P. (1995) *Biorg. Med. Chem. Lett.* **5**, 2123-2128

119. Guo, Q., Wang, L. H., Ruan, K. H., and Kulmacz, R. J. (1996) *J. Biol. Chem.* **271**, 19134-19139

120. Gierse, J. K., McDonald, J. J., Hauser, S. D., Rangwala, S. H., Koboldt, C. M., and Seibert, K. (1996) *J. Biol. Chem.* **271**, 15810-15814

121. Wong, E., Bayly, C., Waterman, H. L., Riendeau, D., and Mancini, J. A. (1997) *J. Biol. Chem.* **272**, 9280-9286

122. Rimon, G., Sidhu, R. S., Lauver, D. A., Lee, J. Y., Sharma, N. P., Yuan, C., Frieler, R. A., Trievel, R. C., Lucchesi, B. R., and Smith, W. L. (2010) *Proc. Natl. Acad. Sci. U.S.A.* **107**, 28-33

123. Sidhu, R. S., Lee, J. Y., Yuan, C., and Smith, W. L. (2010) *Biochemistry* **49**, 7069-7079

124. Harman, C. A., Turman, M. V., Kozak, K. R., Marnett, L. J., Smith, W. L., and Garavito, R. M. (2007) *J. Biol. Chem.* **282**, 28096-28105

125. Blobaum, A. L., and Marnett, L. J. (2007) *J. Biol. Chem.* **282**, 16379-16390

126. Yuan, C., Rieke, C. J., Rimon, G., Wingerd, B. A., and Smith, W. L. (2006) *Proc. Natl. Acad. Sci. U.S.A.* **103**, 6142-6147

127. Yuan, C., Sidhu, R. S., Kuklev, D. V., Kado, Y., Wada, M., Song, I., and Smith, W. L. (2009) *J. Biol. Chem.* **284**, 10046-10055

128. Capone, M. L., Tacconelli, S., Sciulli, M. G., Anzellotti, P., Di Francesco, L., Merciaro, G., Di Gregorio, P., and Patrignani, P. (2007) *J. Pharmacol. Exp. Ther.* **322**, 453-460

129. Juni, P., Rutjes, A. W., and Dieppe, P. A. (2002) *Brit. Med. J.* **324**, 1287-1288

130. Warner, T. D., Giuliano, F., Vojnovic, I., Bukasa, A., Mitchell, J. A., and Vane, J. R. (1999) *Proc. Natl. Acad. Sci. U.S.A.* **96**, 7563-7568

131. Bresalier, R. S., Sandler, R. S., Quan, H., Bolognese, J. A., Oxenius, B., Horgan, K., Lines, C., Riddell, R., Morton, D., Lanas, A., Konstam, M. A., and Baron, J. A. (2005) *New Engl. J. Med.* **352**, 1092-1102

132. Solomon, S. D., McMurray, J. J., Pfeffer, M. A., Wittes, J., Fowler, R., Finn, P., Anderson, W. F., Zauber, A., Hawk, E., and Bertagnolli, M. (2005) *New Engl. J. Med.* **352**, 1071-1080

133. McAdam, B. F., Catella-Lawson, F., Mardini, I. A., Kapoor, S., Lawson, J. A., and FitzGerald, G. A. (1999) *Proc. Natl. Acad. Sci. U.S.A.* **96**, 272-277

134. Graham, D. J., Campen, D., Hui, R., Spence, M., Cheetham, C., Levy, G., Shoor, S., and Ray, W. A. (2005) *Lancet* **365**, 475-481

135. Kearney, P. M., Baigent, C., Godwin, J., Halls, H., Emberson, J. R., and Patrono, C. (2006) *Brit. Med. J.* **332**, 1302-1308

136. McGettigan, P., and Henry, D. (2006) *J. Amer. Med. Assoc.* **296**, 1633-1644

137. Grosser, T., Fries, S., and FitzGerald, G. A. (2006) *J. Clin. Invest.* **116**, 4-15

CHAPTER II

FUNCTIONAL ANALYSIS OF NAPROXEN ACTIVITY AGAINST CYCLOOXYGENASE-1 AND CYCLOOXYGENASE-2

Introduction

Cyclooxygenases (COX-1 and COX-2) are bifunctional enzymes that catalyze the *bis*-dioxygenation of arachidonic acid (AA) to form the hydroxy endoperoxide, PGH_2. PGH_2 serves as the precursor to several biologically active prostanoids that are formed by the enzymatic activity of tissue specific synthases (1). The two COX isoforms have high sequence identity and similar three-dimensional structures, but differ in their expression profiles. COX-1 is constitutively expressed in most tissues and contributes predominantly to homeostatic prostaglandin biosynthesis. In contrast, COX-2 is inducibly expressed in most tissues in response to a broad range of physiological and pathophysiological stimuli. Recently, however, it has become evident that COX-2 is also constitutively expressed in the brain, kidney, and vascular systems, and that COX-1 plays a role in some inflammatory responses (2,3).

The primary mechanism of the anti-inflammatory and antipyretic action of NSAIDs is inhibition of COX. Naproxen is one of the oldest and largest selling NSAIDs (Figure 1). It was introduced in prescription form as Naprosyn in 1976 and as the over-the-counter drug, Aleve, in 1994 (4). It exhibits analgesic, anti-pyretic, and anti-inflammatory activity and was recently reported to be effective in the prevention of bladder cancer progression even when administered several weeks after the tumor-initiating agent (5). Naproxen is a non-selective NSAID that inhibits both COX-1 and

COX-2 with IC_{50} values in the low micromolar range for human recombinant enzymes (6). Inhibition of prostaglandin biosynthesis by naproxen has been confirmed in several human clinical studies (7,8). It exhibits significant gastrointestinal side effects, but recent mounting evidence suggests it does not exert cardiovascular side effects when administered in the higher doses that provide sustained inhibition of platelet COX-1 throughout the dosing interval (e.g.$\geq$ 500 mg twice daily) (7,9,10). This latter property has taken on increasing importance as evolving data suggest that the cardiovascular toxicity first exhibited by the COX-2-selective inhibitors rofecoxib and celecoxib extends to other selective or non-selective COX inhibitors including diclofenac, indomethacin, and ibuprofen (10-12).

The precise mechanism by which naproxen interacts with COX is still unknown. Therefore, we performed a functional analysis of naproxen activity against the COX enzymes by examining the kinetics of COX inhibition and the structure-activity relationship of naproxen. Our results suggest that, although there is a time-dependent component for inhibition of both COX-1 and COX-2 by naproxen, COX-1 is more sensitive to time-independent inhibition at low substrate concentrations. Further, the structure-activity analyses indicate that each of the pendant groups of the naphthyl scaffold is essential for COX inhibition, and only minimal substitutions are tolerated.

Experimental Procedures

Materials - (*S*)-Naproxen, 6-methoxy naphthalene acetic acid, and PGE_2-d_4 were purchased from Cayman Chemical Company (Ann Arbor, MI). 6-*O*-desmethyl naproxen and (*R*)–naproxen were purchased from Sigma-Aldrich (Milwaukee, WI). Arachidonic

acid (AA) for mass-spectrometry experiments was purchased from Nu-Check Prep, Inc. (Elysian, MN). [1-^{14}C]-AA was purchased from PerkinElmer Life Sciences (Boston, MA) and diluted using 0.1 N NaOH. Chemicals used for the synthesis of naproxen analogs were purchased from Sigma-Aldrich (Milwaukee, WI). The expression and purification of recombinant murine COX-2 (mCOX-2) and human COX-2 (hCOX-2) from SF-9 cells and the purification of ovine COX-1 (oCOX-1) from ram seminal vesicles were performed as previously described (13).

Synthesis and characterization of naproxen analogs – Matthew Walters performed the synthesis of all naproxen analogs, and a detailed report of this chemistry has been published previously (14); a brief description is reported herein. A Methyl 2-(6-methoxynaphthalen-2-yl)propanoic acid and 2-(6-methoxynapthalen-2-yl)-2-methylpropanoic acid were synthesized as previously described by Stock *et al.* (15). To synthesize 2-(6-methoxynaphthalen-2-yl)butanoic acid, a Grignard reagent was formed with 2-bromo-6-methoxynapthalene, and this newly formed Grignard was then reacted with methyl 2-bromobutyrate. The resultant ester was subjected to hydrolysis under basic conditions to afford the desired acid.

(2-(6-Ethylnapthalen-2-yl)propanoic acid and 2-(6-(methylthio)napthalen-2-yl)propanoic acid were synthesized starting from the common intermediate (*S*)-methyl 2-(6-(trifluoromethylsulfonyloxy)napthalen-2-yl)propanoate. This intermediate was synthesized starting from (*S)*-naproxen, which was converted to *des*-methyl naproxen under acidic conditions (16), followed by methyl ester protection of the acid group (17) and trifiate protection of the phenolic oxygen. For 2-(6-ethylnapthalen-2-yl)propanoic

acid, the triflic intermediate was coupled with potassium vinyltrifluoroborate using a Suzuki reaction, and the resulting alkene was reduced to the corresponding alkane followed by hydrolysis under basic conditions to afford the desired acid. 2-(6-(Methylthio)napthalen-2-yl)propanoic acid was synthesized starting from the triflic intermediate, which was coupled to sodium triisopropylsilanethiolate (18), the resulting product was then deprotected using tetrabutylammonium fluoride followed by alkylation with iodomethane. The racemic acid was then obtained by basic hydrolysis. The enantiomers were separated by chiral HPLC using either a Chiralpak AD or Chiralpak IC column, respectively.

2-(6-(Methylthio)napthalen-2-yl)propanoic acid was oxidized to form 2-(6-(methylsulfinyl)naphthalen-2-yl)propanoic acid using chloroperoxybenzoic acid. 2-(6-(Methylsulfonyl)naphthalen-2-yl)propanoic acid was formed by oxidation of 2-(6-(methylthio)napthalen-2-yl)propanoic acid with oxone. The structures and their purity were confirmed by ^{1}H-NMR and mass spectrometry.

Time dependence of COX inhibition – To measure time independent inhibition, naproxen (1, 10, or 50 μM) and AA (1, 10, or 50 μM) were added simultaneously to hematin-reconstituted enzyme (mCOX-2 = 50 nM, oCOX-1 = 25 nM) in 100 mM Tris-HCl buffer containing 500 μM phenol at 37 °C. For time-dependent inhibition, naproxen was allowed to incubate with the enzyme for 3 min at 37 °C before the addition of AA. The reactions were quenched after 8 s by the addition of an extraction solution of ethyl acetate containing 0.5% acetic acid and 1 μM PGE_2-d_4. To examine the effect of the length of pre-incubation time, naproxen and COX were incubated for periods varying from 0 to 3

minutes prior to reaction with AA. Following extraction, the organic layer was evaporated to near-dryness under nitrogen and reconstituted in 1:1 MeOH: H_2O (v:v). Samples were chromatographed by liquid chromatography-mass spectrometry (LC-MS) using a Luna C18(2) column (50 × 2 mm, 3 μm) with an isocratic elution method (66:34 (v:v), 5 mM ammonium acetate, pH 3.3: acetonitrile containing 10% A) at a flow rate of 0.375 mL/min. Tandem mass-spectrometry (MS/MS) was conducted on a Quantum triple quadrupole mass spectrometer operated in positive ion mode. A mass transition of *m/z* = 370→ 317 was monitored to measure the production of PGE_2/D_2 and *m/z* = 374→ 321 for PGE_2-d_4. Peak areas for PGE_2/D_2 were normalized to PGE_2-d_4. Prostaglandin production for incubations containing inhibitor was normalized to the appropriate dimethyl sulfoxide (DMSO) control.

Standard COX inhibition screening assay – Concentration-dependent inhibition reactions were performed by pre-incubating inhibitor and hematin-reconstituted enzyme in 100 mM Tris-HCl buffer with 500 μM phenol for 17 min at room temperature followed by a 3 min incubation at 37 °C. Following the addition of 50 μM [1-^{14}C]-AA, samples were incubated for 30 s at 37 °C, and the reactions were then terminated by extraction with diethyl ether/methanol/citrate (30:4:1). The extracts were analyzed for substrate consumption by thin-layer chromatography (TLC) as previously described (19). All inhibitor concentrations for 50% enzyme activity (IC_{50}) were determined by nonlinear regression analysis using Graphpad Prism software and were the average of at least two independent experiments. Inhibitors were prepared as stock solutions in DMSO, and diluted into reaction buffer so that the final DMSO concentration was 2.5%. Reactions

were run with hematin-reconstituted proteins at final enzyme concentrations adjusted to give approximately 30-35% substrate consumption (mCOX-2 = 154 nM, hCOX-2 = 94 nM, oCOX-1 = 31.6 nM). AA was prepared as a stock solution in 0.1 N NaOH. For IC_{50} determinations using 5 μM AA, the conditions were as described for the standard assay with a lowered enzyme concentration to allow for the appropriate amount of metabolism (oCOX-1 = 7.6 nM, mCOX-2 = 40 nM).

COX inhibition assay for a substrate concentration of 500 nM – The COX inhibition assay described above was modified to perform IC_{50} determinations in the presence of sub-micromolar concentrations of AA (20). Hematin-reconstituted enzyme and inhibitor were incubated for 0 or 5 min at 37 °C before the addition of 0.5 μM [1-^{14}C]-AA. The reaction was terminated after 8 sec, and substrate consumption was analyzed as described above. Enzyme concentrations were adjusted to allow approximately 30-50% substrate consumption under the modified conditions (mCOX-2 = ~20 nM, oCOX-1 = ~15 nM).

Time course for product formation by COX- To examine the time course of product formation in the presence of inhibitor, 5 or 50 μM naproxen was incubated with enzyme (oCOX-1 = 31.6 nM, mCOX-2 = 154 nM) for 3 min at 37 °C. [1-^{14}C]-AA was added at 5 μM or 50 μM to naproxen-bound enzyme and allowed to react for 30 s, 1 min, 2 min, 3 min, or 5 min to establish a time course for AA oxygenation. To measure reversibility at a low substrate concentration, hematin-reconstituted enzyme (oCOX-1 = 15 nM, mCOX-2 = 20 nM) was incubated with 10 μM naproxen for 3 minutes prior to the addition of 1 μM [1-^{14}C]-AA. The reaction was allowed to proceed for 8, 15, 30, 45, 60, 90, 120, or

180 s. Naproxen was prepared as a stock solution in DMSO as described above. Enzymes were reconstituted with approximately 2 molar equivalents of heme. The study was performed in 100 mM Tris-HCl buffer containing 500 μM phenol, pH 8. Assays were terminated and analyzed for substrate consumption by TLC as described above. The amount of enzyme activity as compared to a DMSO control was plotted against the incubation times and fit to a single-exponential association with a plateau to determine $k_{obs.}$ The values reported were the average of two or more independent experiments.

Results

NSAIDs appear to follow a multistep kinetic mechanism for inhibition of COX enzymes (eq 1). Initial bimolecular association of the inhibitor with the enzyme is followed by a slower intramolecular step that results in a more tightly bound complex. In the case of aspirin, the intramolecular step results from acetylation of the active site residue, Ser-530, but in all other cases the inhibitor-enzyme association is non-covalent (21,22). The magnitude of the individual rate constants determines the apparent type of inhibition (eq 1).

$$E + I \underset{k_{-1}}{\overset{k_1}{\rightleftharpoons}} EI \underset{k_{-2}}{\overset{k_2}{\rightleftharpoons}} EI^* \qquad \text{(eq 1)}$$

Inhibitors with a very low k_2/k_{-2} ratio appear to be rapid, reversible inhibitors, exhibiting kinetics consistent with simple competitive inhibition as k_2/k_{-2} approaches zero. In contrast, inhibitors with a significant k_2/k_{-2} ratio exhibit time-dependent inhibition, often consistent with the behavior of slow, tight-binding inhibitors. If the k_2/k_{-2} ratio is high, these inhibitors are functionally irreversible; however some NSAIDs that show time-

dependent inhibition are reversible as revealed by the existence of a non-zero plateau for maximal inhibition.

Gierse et al. reported that naproxen displays no time-dependence for inhibition of COX-1 and "mixed" inhibition for COX-2. "Mixed" inhibition in this context was characterized by an initial time-dependent loss of enzyme activity followed by a non-zero plateau (23). This type of inhibition is characteristic of a weakly binding, readily reversible inhibitor. We explored the time-dependence of COX inhibition by naproxen using a very low concentration of AA (500 nM; ~ 0.1 K_m). In the absence of a preincubation, the IC_{50} value for naproxen inhibition of oCOX-1 was approximately 5.6 μM, and nearly 100% inhibition was achieved at 25 μM inhibitor (Figure 1A). For mCOX-2, the extent of inhibition was very low so that an IC_{50} value could not be determined at concentrations of up to 25 μM naproxen (Figure 1B). Following a three-min incubation of COX and naproxen prior to the addition of AA, we observed substantial concentration-dependent inhibition of AA turnover for both COX isoforms. Naproxen inhibited oCOX-1 with an IC_{50} value of 340 nM and mCOX-2 with an IC_{50} value of 180 nM and demonstrated greater than 80% inhibition of both isoforms in the presence of 500 nM AA (Figure 1). These data suggest the existence of a significant time-dependent component of naproxen inhibition for both COX-1 and COX-2. This time-dependence was observed with higher concentrations of AA as well (1, 10, and 50 μM – Figure 2).

In an attempt to determine the kinetic constants for time-dependent inhibition, naproxen was preincubated with COX-2 for varying lengths of time before the addition of 50 μM AA. As shown in Figure 3, maximal inhibition was reached within eight

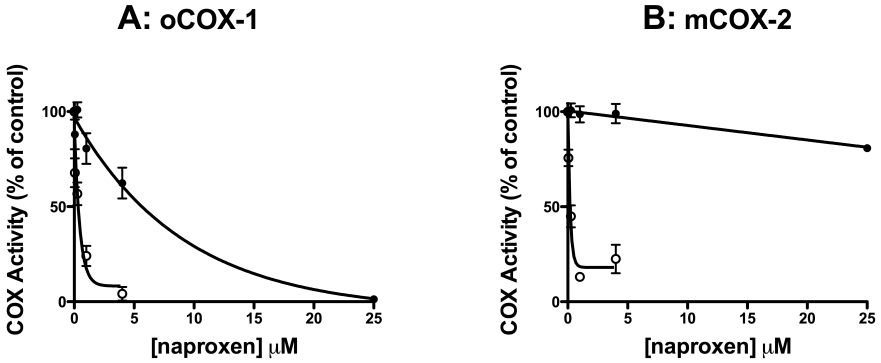

Figure 1. Effect of pre-incubation of enzyme and inhibitor on COX inhibition by naproxen. Closed circles (●) represent incubations in which naproxen (0.05 – 25 μM) and AA (500 nM) were added simultaneously to COX. For the incubations represented by open circles (○), COX was pre-incubated with naproxen (0.05-4 μM) for 5 minutes before the addition of 500 nM AA. *Panel A* is representative of incubations with oCOX-1 and *Panel B* represents reactions with mCOX-2. The reaction with substrate was allowed to proceed for 8 seconds before quenching. Substrate consumption was analyzed by TLC as described in Experimental Procedures to determine approximate IC_{50} values. Each data point is the mean of at least two experiments in duplicate.

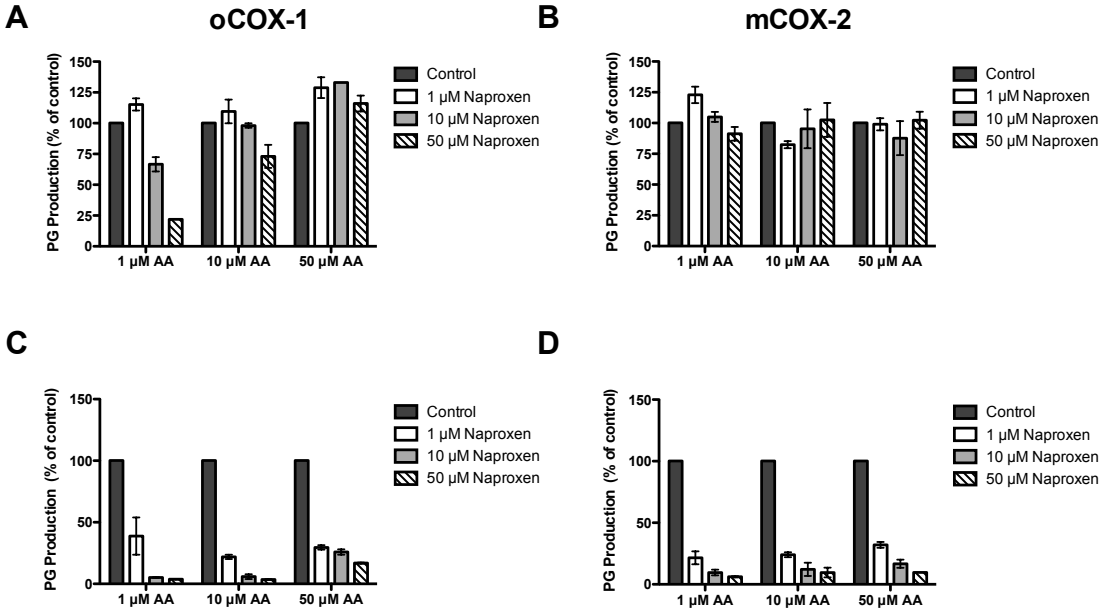

Figure 2. Kinetic basis of COX by naproxen. *Upper panels*: DMSO or 1, 10, or 50 μM naproxen and 1, 10, or 50 μM AA were added simultaneously to hematin-reconstitued oCOX-1 (*A*) or mCOX-2 (*B*) and allowed to react for 8 sec. *Lower Panels*: DMSO or naproxen was incubated with enzyme (*C* - oCOX-1, *D* - mCOX-2) for 3 min at 37 °C prior to the addition of 500 nM AA for 8 sec. PG production was measured by LC/MS/MS as described under "Experimental Procedures".

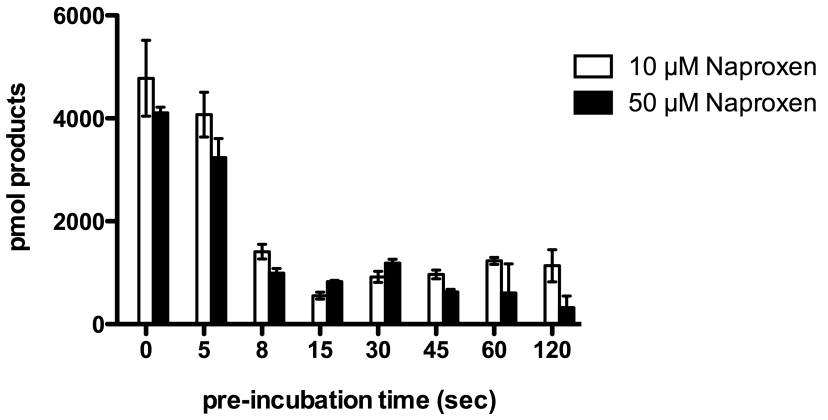

Figure 3. Effect of pre-incubation time on the inhibition of COX-2 by naproxen. Naproxen (10 or 50 μM) was pre-incubated with COX-2 for 0, 5, 8, 15, 30, 45, 60, or 120 seconds prior to the addition of AA for 30 seconds. Reactions were terminated with organic solvent containing PGE_2-d_4, and prostaglandin production was measured by tandem-mass spectrometry as described in Experimental Procedures.

seconds so that kinetic parameters could not be determined. Similar results were obtained with COX-1.

In subsequent studies, we utilized an IC_{50} assay designed for time-dependent inhibitors to elucidate tight-binding interactions critical for the formation of the naproxen-mCOX-2 complex. Under our standard assay conditions, enzyme and inhibitor were preincubated for 20 min prior to the addition of a saturating concentration of substrate (50 μM) for 30 sec. In this assay, the inhibition of oCOX-1 activity reached a plateau at approximately 50% inhibition and an IC_{50} value could not be determined at concentrations up to 25 μM. Naproxen appeared to be a slightly more potent inhibitor of mCOX-2 in that an IC_{50} value of 0.90 μM (~70% inhibition) could be measured (Figure 4). An inhibition assay was performed using hCOX-2 (data not shown), and the IC_{50} was determined to be 0.75 μM with an inhibition curve that plateaued at approximately 55%.

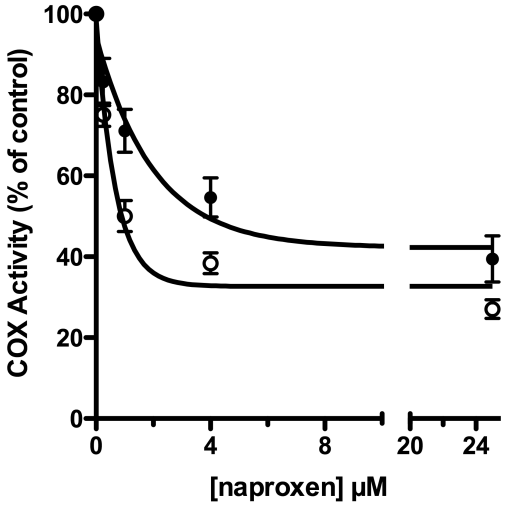

Figure 4. COX inhibition by naproxen. Naproxen was screened in a standard time-dependent IC_{50} screen against wt mCOX-2 (○) and oCOX-1 (●). Naproxen (0.25 – 25 μM) was pre-incubated with the enzyme for 20 min prior to the addition of substrate (50 μM) for 30s at 37 °C as described under "Experimental Procedures." Each point represents the average of two or more independent determinations.

The inhibition curves shown in Figure 4 reach a non-zero plateau value, which is consistent with a time-dependent, reversible inhibitor (23). To investigate this apparent residual activity in greater detail, the time course of product formation in the presence of maximally inhibiting naproxen concentrations and saturating AA was obtained. Naproxen (5 or 50 μM) was prebound to purified enzymes for 3 min at 37 °C, followed by the addition of AA at a concentration of 50 μM. The reaction was allowed to progress for various times up to five minutes, and the extent of conversion of AA to prostaglandins was determined. The amount of product formation was plotted against the incubation time and fit to the equation $Y = V_o/k_{obs}(1-\exp(k_{obs}*t))$ (R^2 = .95 - .99), where V_o is the initial reaction velocity and k_{obs} is the first order rate constant for the change in reaction rate. COX enzymes undergo a first order self-inactivation, which is the primary

contributor to k_{obs}. However, in the presence of a prebound reversible inhibitor, increasing reaction times should lead to a decrease in the extent of inhibition and an increasing reaction rate, which counteracts the self-inactivation. Enzyme inhibition can also directly slow the rate of self-inactivation by slowing the generation of inactivating species. Consequently, the k_{obs} values obtained are likely the result of a combination of multiple factors.

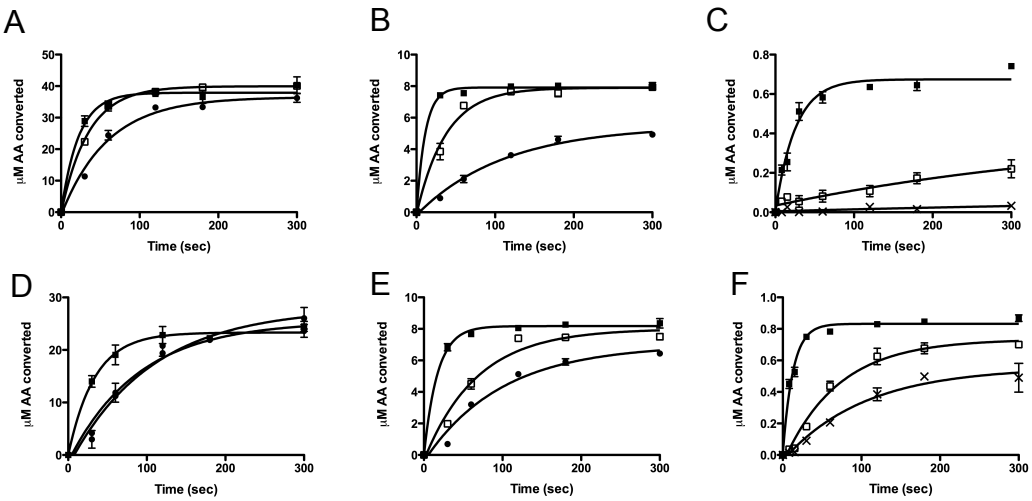

Figure 5. Time course for product formation in the presence of naproxen. In panels A & D, DMSO (■), 5 (□) or 50 (●) µM naproxen was preincubated with oCOX-1 (**A**) or mCOX-2 (**D**) for 3 minutes before the addition of 50 µM AA. The reaction was allowed to proceed for 30, 45, 60, 120, 180, or 300 sec. Panels **B** (oCOX-1) & **E** (mCOX-2) are representative of experiments identical to panels A & D with addition of 10 µM AA. In panels C & F, 1 µM AA was added to 5 (□) or 10 (×) µM naproxen (or DMSO (■)) prebound to oCOX-1 (**C**) or mCOX-2 (**F**) for 8,15,30,60,90,120,180 or 300 s. Substrate consumption was analyzed as described.

Table I summarizes values for initial velocity and maximal product (V_o/k_{obs}) formed in the presence and absence of inhibitor. Although the inhibitor consistently reduced the initial velocity of the reaction in a concentration-dependent manner, the time course of the reaction was prolonged in the presence of naproxen, as shown in Figure 5. In the case of COX-2, this effect actually led to greater levels of total product in the presence of the inhibitor than in its absence, while the total levels of product formed by

Table I. Initial velocity and maximal product formation by COX in the presence and absence of naproxen.

COX-1				
	DMSO	5 μM naproxen	10 μM naproxen	50 μM naproxen
1 μM AA				
V_o	0.026	n.a.	n.a.	n.d.
plateau	0.670	no plateau	no plateau	n.d.
10 μM AA				
V_o	0.710	0.210	n.d.	0.049
plateau	7.900	7.900	n.d.	5.500
50 μM AA				
V_o	1.700	1.200	n.d.	0.620
plateau	38.00	40.00	n.d.	37.00
COX-2				
	DMSO	5 μM naproxen	10 μM naproxen	50 μM naproxen
1 μM AA				
V_o	0.032	0.011	0.0054	n.d.
plateau	0.830	0.730	0.560	n.d.
10 μM AA				
V_o	0.470	0.120	n.d.	0.071
plateau	8.200	8.000	n.d.	7.000
50 μM AA				
V_o	0.690	0.290	n.d.	0.270
plateau	23.00	25.00	n.d.	28.00

Methods described in Figure 5. V_o is expressed in μM/sec and the quantity of maximum products, or plateau, in μM. n.d. indicates a value was not determined.

COX-1 in the presence of naproxen approached, but did not exceed, those of control samples. The results of experiments in which 10 μM AA was used were similar to those conducted using 50 μM AA, in that the initial velocity was significantly lower and the reaction proceeded for a longer period time in the presence of both 5 and 50 μM naproxen compared to uninhibited enzyme. At this substrate concentration, the total amount of products only reached those of control samples at 5 μM naproxen for both COX-1 and COX-2 in the allotted time. We also attempted these experiments at a substrate concentration of 1 μM, which is near that of the K_m for COX. Here, no plateau was reached for reactions involving COX-1, and total product formation in the presence

of 5 μM naproxen was less than 30% of uninhibited enzyme after a five-minute incubation with substrate; at 10 μM naproxen, product formation was essentially undetectable. In contrast, we were able to observe significant product formation under thesame conditions for COX-2. Together, these results highlight the importance of assay conditions in measuring inhibitory activity of NSAIDs, as the amount of observable inhibition is highly dependent upon the allowed reaction time, particularly at high substrate concentrations, and as such comparing IC_{50} values determined using different assays is difficult. The results also suggest that slowing of enzyme self-inactivation in the presence of inhibitor can lead to greater total product formation than would be expected from measurements of initial velocity alone.

Structure-activity analysis. In addition to examining the kinetics of COX inhibition, we sought to elucidate structure-activity relationships for naproxen. Early structure-activity studies were conducted before the identification of the COX enzymes as the molecular targets for non-steroidal anti-inflammatory drugs. These studies indicated that the carboxylate group of naproxen was required for activity. We confirmed the importance of this moiety by synthesizing a naproxen methyl ester analog and found that it was unable to inhibit either COX isoform at concentrations up to 25 μM.

The early studies conducted by Harrison *et al*. also indicated that the presence of an a-methyl group improved potency in animal models of pain and inflammation (24). To determine whether the α-methyl group was an important determinant of the interaction between naproxen and COX, 2-*des*-methylnaproxen was assayed against WT COX-1 and COX-2. Elimination of the methyl group resulted in a significant decrease in

inhibition of WT COX-1 and COX-2 (maximum inhibition 10-20% at concentrations up to 25 μM) (Table II). The addition of extra steric bulk at the α-position also resulted in a loss of potency, as the α-ethyl analog of naproxen displayed no inhibition of either wild-type COX-1 or COX-2 enzymes in our standard IC_{50} assay (Table II). Similarly, bulkier substitutions at the α-position of another 2-arylpropionic acid, flurbiprofen, result in a complete loss of inhibition of COX-1 (25). Thus, the (*S*)-α-methyl group is a critical determinant of naproxen efficacy, and it cannot be replaced with smaller (hydrogen) or larger (ethyl) substituents.

The majority of NSAIDs of the 2-arylpropionic acid family are marketed as racemic mixtures, but naproxen is sold exclusively as the *(S)*-enantiomer. The *(S)*-enantiomer is significantly more potent than the (*R*)-enantiomer in inflammatory models *in vivo*, which is typical of members of the 2-arylpropionic acid class of inhibitors (24). In the presence of saturating substrate concentrations, the (*R)*-enantiomer did not inhibit oCOX-1 or mCOX-2 to any appreciable extent at concentrations up to 25 μM (Table II). Previous studies suggest that the strict stereoselectivity of the 2-arylpropionic acid class of inhibitors is due to unfavorable steric interactions with Tyr-355 when the methyl group of the inhibitor is in the *(R)*-stereochemistry (26) (27,28). However, the lack of inhibition observed with the *des*-methyl naproxen analog raised the possibility that the inability of the (*R*)-enantiomer to inhibit is due to the absence of the *(S)*-methyl group. To address this possibility, the α,α-dimethyl analog was synthesized and tested for its ability to inhibit mCOX-2 (29). Assuming that this compound occupies the active site in a manner analogous to naproxen, the *(S)*-methyl group should be in position to interact with the

TABLE II. Determination of IC_{50} values of naproxen analogs with WT COX

Analog	COX-1	COX-2
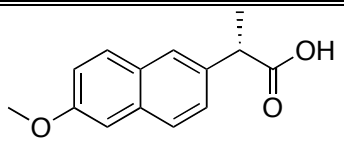	>25 μM (50%)	0.9 μM (70%)
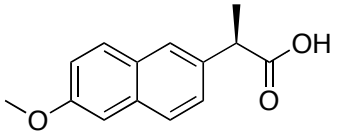	>25 μM (20%)	>25 μM (10%)
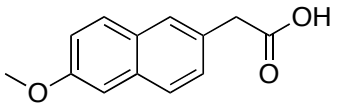	>25 μM (10%)	>25 μM (20%)
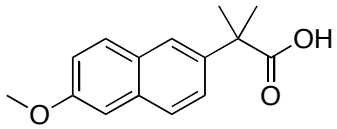	no inhib.	>25 μM (10%)
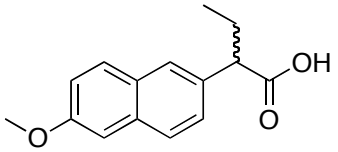	no inhib.	no inhib.
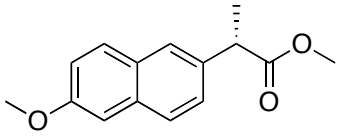	>25 μM (20%)	>25 μM (10%)
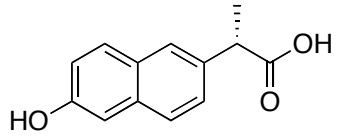	>25 μM (30%)	>25 μM (30%)
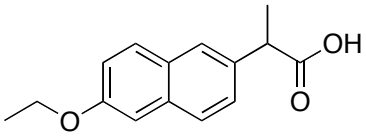	>25 μM (10%)	>25 μM (25%)
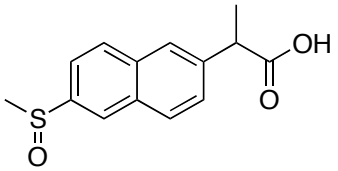	14 μM (50%)	12.5 μM (50%)
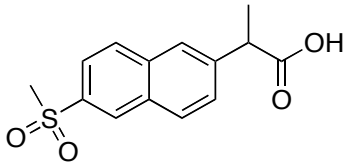	>25 μM (30%)	20 μM (60%)

Each naproxen analog was assayed against purified oCOX-1 and mCOX-2 as described under Experimental Procedures for standard COX inhibition assays (50 μM AA). "No inhib" indicates less than 10% inhibition up to inhibitor concentrations of 25 μM. The number in parentheses represents the extent of inhibition indicating where the plateau for inhibition is reached for each inhibitor.

pocket below Val-349 in the COX active site. However, the α,α-dimethyl analog was completely inactive against oCOX-1 or mCOX-2 (Table I). This is consistent with previous reports demonstrating that a dimethyl substitution for the α-methyl group of flurbiprofen eliminates COX-1 inhibition (25). While the presence of an (*R*)-methyl substituent clearly eliminates inhibition, the *(S)*-methyl group makes key interactions within the COX active site that are essential for binding and inhibition.

To probe the importance of the *p*-methoxy group, we synthesized a series of analogs with different substituents in the *para* position. The *p*-hydroxy analog (*O*-desmethyl naproxen), which is the major *in vivo* metabolite of naproxen, was a very weak inhibitor, exhibiting roughly 30% inhibition up to 25 μM (Table II) (30). Further, the *o*-ethoxy analog was completely inactive against both COX-1 and COX-2, indicating that changes in size at this position are not tolerated (Table II). To further investigate potential interactions between the *p*-methoxy moiety of naproxen and surrounding COX residues, we synthesized two naproxen analogs, in which an ethyl or methylthio group was substituted for *p*-methoxy to introduce variations in size and polarity as well as eliminate the possibility of hydrogen-bonding interactions. The methylthio analog has been reported to exhibit anti-inflammatory activity *in vivo* but has not been tested *in vitro*. The ethyl analog has not been reported. Both the *p*-ethyl and *p*-methylthio analogs were able to inhibit wild-type mCOX-2 to the same extent as naproxen (IC_{50} = 0.67 μM and 0.77 μM in the presence of 50 μM AA) (Table II). Interestingly, both analogs exhibited a loss of potency compared to naproxen when tested against oCOX-1 so that no IC_{50} value could be determined at inhibitor concentrations up to 25 μM (Table II). We also observed an increase in COX-2 selectivity at reduced substrate concentrations (500 nM and 5 μM

Table III: **IC_{50} values for the inhibition of WT COX by naproxen and naproxen analogs in the presence of varying substrate concentrations.**

	Analog	COX-1	COX-2
50 μM AA	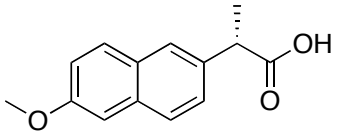	>25 μM (50%)	0.9 μM (70%)
	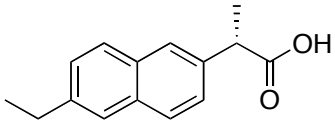	>25 μM (45%)	0.67 μM (65%)
	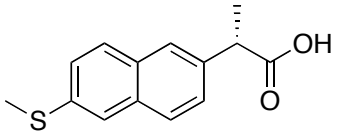	>25 μM (40%)	0.77 μM (70%)
5 μM AA	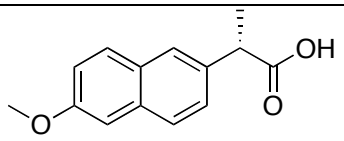	200 nM (70%)	610 nM (80%)
	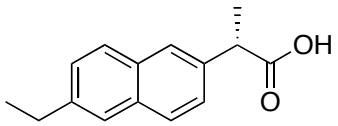	2.6 μM (50%)	270 nM (80%)
	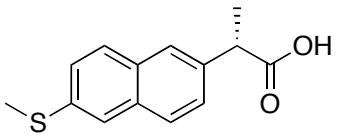	1.0 μM (70%)	450 nM (70%)
500 nM AA	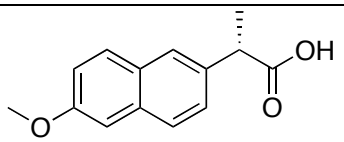	230 nM (75%)	53 nM (90%)
	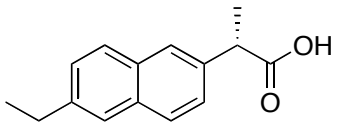	880 nM (75%)	72 nM (90%)
	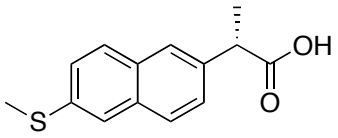	570 nM (75%)	63 nM (95%)

Naproxen and the naproxen analogs were screened against purified oCOX-1 and mCOX-2 as described under Experimental Procedures for 50 μM, 5 μM, and 0.5 μM substrate concentrations. Reactions were quenched with an extraction solution of ethyl acetate containing 0.5% acetic acid (v/v) and 1 μM PGE_2-d_4. PGE_2/D_2 production was analyzed by LC-MS/MS as described under Experimental Procedures. Numbers in parenthesis represent the extent of inhibition.

AA) (Table III). As an extension of these studies, we tested the ability of naproxen derivates with *p*-methylsulfinyl and *p*-methylsulfonyl substitutents to inhibit the COX enzymes and found that both analogs appeared to be weak, nonselective inhibitors of both isoforms (Table II). The IC_{50} values for the *p*-methylsulfinyl naproxen derivative against COX-1 and COX-2 were approximately 14 μM and 12 μM (approximately 50% inhibition), respectively. No IC_{50} value could be determined for the *p*-methylsulfonyl analog when tested against COX-1, and the IC_{50} value for COX-2 was approximately 20 μM. Taken together, the results with these analogs suggest important and specific interactions between the *p*-methoxy group and COX active site residues.

Discussion

Naproxen has been an FDA-approved drug since the mid-1970s, but there are few literature reports regarding its precise mechanism of action. Previous kinetic studies indicated that naproxen exhibits time-dependent "mixed" inhibition for COX-2 and no time dependence for COX-1 as measured by loss of arachidonate-driven peroxidase activity (23). Consistent with these studies, our analyses indicate that, while COX-1 is more sensitive to time-independent inhibition, there is a time-dependent component for inhibition of both COX isoforms by naproxen (Figures 1 and 2). We observed a rapid dissociation of preformed COX-naproxen complexes as determined by the time course of oxygenation of AA when added at saturating concentrations (Figure 4). The k_{obs} value for AA oxygenation by mCOX-2 in the presence of naproxen remains relatively constant regardless of substrate concentration. In the presence of saturating concentrations of substrate, the dissociation rate of naproxen from oCOX-1 is slightly higher than mCOX-

2. However, the rate of reversibility for naproxen appears to be significantly slower for COX-1 compared to COX-2 at 1 μM AA. The results at low substrate concentrations may partially explain why a more complete inhibition of thromboxane synthesis (COX-1-mediated) as compared to prostacyclin synthesis (COX-2-mediated) is observed in humans (7,31).

Naproxen is a relatively simple molecule with only three functional groups distributed on opposite ends of the naphthyl scaffold. Our data indicate that each of these substituents is required for potent inhibition of both COX isoforms and that very little structural variation is tolerated. Early SAR studies concluded that three structural components were crucial for the activity of naproxen: an acidic group at position 1, an aromatic system, and a small lipophilic group at position 6 (6). Additionally, introduction of a methyl group in the alpha position further increased anti-inflammatory activity. These studies were conducted using animal models, as the target of naproxen had not yet been identified. Since the discovery of COX enzymes, no further work has been conducted to examine the molecular interaction between naproxen and COX, and as such, it was unclear what naproxen moieties are key for inhibition of the individual COX enzymes. Therefore, we performed a structure-activity analysis to investigate the importance of each functional group in the inhibition of COX-1 compared to COX-2.

As previous studies suggested, the carboxylic acid appears to be critical for the binding as evidenced by the minimal inhibitory activity of a methyl ester naproxen analog. The α-methyl group of naproxen also appears to be involved in critical interactions with the COX enzymes. Introduction of a range of substituents of varying size and stereochemistry at the α-position suggests the steric requirements for this

interaction are stringent while removal of the α-methyl group also results in a dramatic loss of potency (Table II). The region of the enzyme that interacts with the *p*-methoxy moiety of naproxen appears to be strict in its ability to bind functional groups; the *p*-hydroxy and *p*-ethoxy analogs were very weak inhibitors whereas a methylene or sulfur substitution for the oxygen atom of the *p*-methoxy group of naproxen generated potent inhibitors of WT mCOX-2. Further, the *p*-methylsulfinyl and *p*-methylsulfonyl naproxen derivatives were significantly less potent than the *p*-methylthio analog and naproxen itself.

It is clear that there is great diversity and subtlety in the types of molecular interactions that result in COX inhibition and selectivity for isoforms. Even viewed from this perspective, our discoveries of the effect of methylene and sulfur substitution for the oxygen atom of the *p*-methoxy group of naproxen seem extraordinary, in that a single atom substitution increases their COX-2-selectivity. Together with the evidence that naproxen exhibits unique kinetics of inhibition for each of the COX enzymes, these data suggest that naproxen adopts a unique binding conformation within each of the COX active sites. This hypothesis is supported by the finding that naproxen is unable to inhibit a mutant hCOX-2 enzyme in which Val-523 has been replaced by the corresponding COX-1 residue, Ile, despite being an effective inhibitor of both COX-1 and COX-2 (32). The distinct binding modes may arise from the difference in size between the COX-1 and COX-2 active sites, as the COX-2 site is approximately 20-30% larger, combined with the inflexibility of naproxen due to the rigid naphthyl backbone. The elucidation of the critical interactions between naproxen and mCOX-2 can be used in the specific design of more potent or selective naproxen analogs. In the future, a truly COX-2-selective

naproxen analog may be used as a tool to determine whether or not increased cardiovascular risk is linked to isoform selectivity.

References

1. Hamberg, M., and Samuelsson, B. (1973) *Proc. Natl. Acad. Sci. U.S.A.* **70**, 899-903

2. Smith, W. L., DeWitt, D. L., and Garavito, R. M. (2000) *Ann. Review Biochem.* **69**, 145-182

3. Rouzer, C. A., and Marnett, L. J. (2009) *J. Lipid Res.* **50**, S29 - S34

4. FDA Statement on Naproxen. (2004) Press Announcements, U.S. Department of Health & Human Services

5. Lubet, R. A., Steele, V. E., Juliana, M. M., and Grubbs, C. J. (2010) *J. Urol.* **183**, 1598-1603

6. Laneuville, O., Breuer, D. K., Dewitt, D. L., Hla, T., Funk, C. D., and Smith, W. L. (1994) *J. Pharmacol. Exp. Ther.* **271**, 927-934

7. Capone, M. L., Tacconelli, S., Sciulli, M. G., Anzellotti, P., Di Francesco, L., Merciaro, G., Di Gregorio, P., and Patrignani, P. (2007) *J. Pharmacol. Exp. Ther.* **322**, 453-460

8. Van Hecken, A., Schwartz, J. I., Depre, M., De Lepeleire, I., Dallob, A., Tanaka, W., Wynants, K., Buntinx, A., Arnout, J., Wong, P. H., Ebel, D. L., Gertz, B. J., and De Schepper, P. J. (2000) *J. Clin. Pharm.* **40**, 1109-1120

9. Ray, W. A., Varas-Lorenzo, C., Chung, C. P., Castellsague, J., Murray, K. T., Stein, C. M., Daugherty, J. R., Arbogast, P. G., and Garcia-Rodriguez, L. A. (2009) *Circ. Cardiovasc. Qual. Outcomes* **2**, 155-163

10. Kearney, P. M., Baigent, C., Godwin, J., Halls, H., Emberson, J. R., and Patrono, C. (2006) *Brit. Med. J. (Clinical research ed)* **332**, 1302-1308

11. Graham, D. J., Campen, D., Hui, R., Spence, M., Cheetham, C., Levy, G., Shoor, S., and Ray, W. A. (2005) *Lancet* **365**, 475-481

12. McGettigan, P., and Henry, D. (2006) *J. Amer. Med. Assoc.* **296**, 1633-1644

13. Rowlinson, S. W., Crews, B. C., Lanzo, C. A., and Marnett, L. J. (1999) *J. Biol. Chem* **274**, 23305-23310

14. Duggan, K. C., Walters, M. J., Musee, J., Harp, J. M., Kiefer, J. R., Oates, J. A., and Marnett, L. J. (2010) *J. Biol. Chem.* **285**, 34950-34959

15. Stock, N., Munoz, B., Wriley, J. D. J., Shearman, M. S., Beher, D., Peachey, J., Williamson, T. L., Bain, G., Chen, W., Jiang, X., St-Jacques, R., and Prasit, P. (2006) *Bioorg. Med. Chem. Lett.* **16**, 2219-2223

16. Gant, T. G., Sarshar, S., and Woo, S. H. (2007) Preparation and utility of substituted carboxylic acid compounds. Auspex Pharmaceuticals, I. ed., USA
17. Arewang, C. J., Lahmann, M., Oscarson, S., and Tiden, A. (2007) *Carbohydr. Res.* **342**, 970 - 974

18. Kovacs, I., Belanger-Gariepy, F., and Shaver, A. (2003) *Inorg. Chem.* **42**, 2988-2991

19. Kalgutkar, A. S., Crews, B. C., Rowlinson, S. W., Garner, C., Seibert, K., and Marnett, L. J. (1998) *Science* **280**, 1268-1270

20. Boutaud, O., Aronoff, D. M., Richardson, J. H., Marnett, L. J., and Oates, J. A. (2002) *Proc. Natl. Acad. Sci. U.S.A.* **99**, 7130-7135
21. Rome, L. H., and Lands, W. E. (1975) *Proc. Natl. Acad. Sci. U.S.A.* **72**, 4863-4865

22. Blobaum, A. L., and Marnett, L. J. (2007) *J. Biol. Chem.* **282**, 16379-16390

23. Gierse, J. K., Koboldt, C. M., Walker, M. C., Seibert, K., and Isakson, P. C. (1999) *Biochem. J.* **339 (Pt 3)**, 607-614

24. Harrison, I. T., Lewis, B., Nelson, P., Rooks, W., Roszkowski, A., Tomolonis, A., and Fried, J. H. (1970) *J. Med. Chem.* **13**, 203-205

25. Peretto, I., Radaelli, S., Parini, C., Zandi, M., Raveglia, L. F., Dondio, G., Fontanella, L., Misiano, P., Bigogno, C., Rizzi, A., Riccardi, B., Biscaioli, M., Marchetti, S., Puccini, P., Catinella, S., Rondelli, I., Cenacchi, V., Bolzoni, P. T., Caruso, P., Villetti, G., Facchinetti, F., Del Giudice, E., Moretto, N., and Imbimbo, B. P. (2005) *J. Med. Chem.* **48**, 5705-5720

26. Loll, P. J., Picot, D., Ekabo, O., and Garavito, R. M. (1996) *Biochemistry* **35**, 7330-7340

27. Bhattacharyya, D. K., Lecomte, M., Rieke, C. J., Garavito, M., and Smith, W. L. (1996) *J. Biol. Chem.* **271**, 2179-2184

28. Picot, D., Loll, P. J., and Garavito, R. M. (1994) *Nature* **367**, 243-249

29. Stock, N., Munoz, B., Wrigley, J. D., Shearman, M. S., Beher, D., Peachey, J., Williamson, T. L., Bain, G., Chen, W., Jiang, X., St-Jacques, R., and Prasit, P. (2006) *Bioorg. Med. Chem. Lett.* **16**, 2219-2223

30. Miners, J. O., Coulter, S., Tukey, R. H., Veronese, M. E., and Birkett, D. J. (1996) *Biochem. Pharmacol.* **51**, 1003-1008

31. Graff, J., Skarke, C., Klinkhardt, U., Watzer, B., Harder, S., Seyberth, H., Geisslinger, G., and Nusing, R. M. (2007) *J. Thromb. Haemost.* **5**, 2376-2385

32. Gierse, J. K., McDonald, J. J., Hauser, S. D., Rangwala, S. H., Koboldt, C. M., and Seibert, K. (1996) *J. Biol. Chem.* **271**, 15810-15814

CHAPTER III

AMINO ACID DETERMINANTS OF CYCLOOXGYENASE INHIBITION BY THE NON-SELECTIVE NON-STEROIDAL ANTI-INFLAMMATORY DRUG, NAPROXEN

Introduction

Cyclooxygenase (COX) enzymes are the targets for inhibition by a diverse array of non-steroidal anti-inflammatory drugs (NSAIDs) that contain functional groups such as arylacetic acids, arylpropionic acids, β-ketoenols, and diarylheterocycles. Investigation of the molecular determinants of inhibition by different classes of compounds reveals that the protein residues in the active site maintain similar orientations and that each chemical class forms distinct sets of interactions within the active site (1). Compounds with nanomolar binding affinity – and in many cases, COX-2 selectivity – have been successfully designed for multiple chemical series, in spite of their diverse binding modes.

COX-1 and COX-2 are functional homodimers, and each monomer consists of three major structural domains: the epidermal growth factor domain located at the N-terminus, a membrane binding domain, and a large globular catalytic domain containing the cyclooxygenase and peroxidase active sites (2,3). The cyclooxygenase and peroxidase sites are structurally distinct but mechanistically coupled. Substrate and inhibitors travel through the membrane-binding domain at a site termed the "lobby" to enter the cyclooxgenase active site. The COX active site is separated from the lobby by a constriction composed of three residues: Arg-120, Tyr-355, and Glu-524. While the

COX-1 and COX-2 active sites are very similar, the COX-2 active site is approximately 20-30% larger than that of COX-1; the size difference is partially attributed to a single amino acid change (Ile-523 in COX-1, Val in COX-2) which limits stable binding in a pocket of the main cyclooxygenase active site (4).

Naproxen is a widely used over-the-counter NSAID with analgesic and antipyretic properties. Despite the fact that it has been marketed for many years, relatively little is known of the structural determinants of naproxen's interaction with the COX enzymes. No crystal structures have been reported for naproxen bound to COX-1 or COX-2 and relatively little information has been reported on the amino acid determinants of naproxen interaction with the COX active sites (5). Considering its continuing importance in the treatment of a range of inflammatory disorders and its intriguing side effect profile, we conducted an investigation of naproxen-COX interactions using site-directed mutagenesis and X-ray crystallography. The results reveal a novel molecular determinant of COX binding not seen with other NSAIDs.

Experimental Procedures

Materials - (*S*)-Naproxen was purchased from Cayman Chemical Company (Ann Arbor, MI). Reagents used in the synthesis of naproxen analogs were purchased from Sigma-Aldrich (Milwaukee, WI). Synthetic procedures are described in Chapter II. [1-^{14}C]-Arachidonic acid (AA) was purchased from PerkinElmer Life Sciences (Boston, MA) and diluted using 0.1 N NaOH. Crystallography reagents were purchased from Hampton Research (Aliso Viejo, CA).

Enzymes –The expression and purification of recombinant murine COX-2 (mCOX-2), and site-directed mutagenesis to generate various active site mutants (V349A, V349I, V349L, R120A, R120Q, Y355F, W387F) was performed according to published methods (6-8). The specific activities of W387F mCOX-2 and R120Q mCOX-2 were 2.1 and 23.9 μM AA per μM enzyme per min, respectively (compared to 13.7 for WT mCOX-2); the specific activities of all other mutant enzymes have been reported previously (7,8).

Standard COX inhibition screening assay – Hematin-reconstituted enzyme and inhibitor were pre-incubated for 17 min at room temperature then 3 min at 37 °C prior to addition of 50 μM [1-^{14}C]-AA for 30 sec at 37 °C. The reactions were terminated by extraction with diethyl ether/methanol/1 M sodium citrate (30:4:1, v:v:v) and analyzed for substrate consumption by thin-layer chromatography as previously reported (9). Reactions were run with hematin-reconstituted proteins at final enzyme concentrations adjusted to give approximately 30-35% substrate consumption (mCOX-2 = 154 nM, hCOX-2 = 94 nM, oCOX-1 = 31.6 nM, V349A = 250 nM, V349I = 268 nM, V349L = 113 nM, R120A = 100 nM, R120Q = 159 nM, Y355F = 174 nM, W387F = ~750 nM, V523I = 83 nM). AA was prepared as a stock solution in 0.1 N NaOH, and inhibitors were prepared as stock solutions in dimethyl sulfoxide (DMSO). IC_{50} values (inhibitor concentrations for 50% enzyme activity) were determined by nonlinear regression analysis and are the average of multiple determinations of duplicate analyses.

COX-2 crystallization – Murine recombinant COX-2 was purified from Sf21 insect cells as previously described (10). Following the initial anion-exchange and gel filtration

columns, anion-exchange chromatography was repeated on an 8 mL Mono-Q column followed by size-exclusion chromatography using the same conditions as the first two columns. mCOX-2 was stored at -80 °C at 1-2 mg/mL for further use. For crystallization, protein was concentrated to approximately 10 mg/mL and reconstituted with 1 eq. of heme from a 15 mM stock in DMSO. Hematin-reconstituted mCOX-2 was dialyzed overnight at 4 °C in exchange buffer containing 100 mM NaCl, 20 mM Na_3PO_4, pH 6.7, 0.6% beta-octyl glucoside (β-OG), and 0.01% NaN_3. Inhibitor complexes were formed by the addition of 1 mM inhibitor from a 50 mM stock in ethanol for 15-20 min on ice immediately before setting up hanging-drop crystallization trays. mCOX-2 crystals were grown as previously described with the following alterations to the procedure (11). The crystallizations were conducted in darkness, and crystals were transferred into a cryosolution of a diffusion-equilibrated sitting drop containing a 1:1 ratio of COX-2 inhibitor complex and well solution (28% polyethylene glycol monomethyl ether 550, 100 mM $MgCl_2$, 50 mM N-[Hydroxyethyl]piperazine-N'-[3-propane-sulfonic acid] (EPPS), pH 8.0) that was set up at the time of the initial crystallization.

Crystals were flash frozen and data were collected at the Southeastern Regional Collaborative Access Team (SER-CAT) beam line 22-ID or the Life Sciences Collaborative Access Team (LS-CAT) beam line 21-ID-F at the Advanced Photon Source at Argonne National Laboratory. The mCOX-2:naproxen co-crystal belongs to space group I222 with unit cell dimensions a=122.3 Å, b=133.2 Å, c=181.3 Å, and $\alpha = \beta = \gamma = 90°$. The crystal diffracted X-rays to a 1.7 Å resolution. There was a single mCOX-2 dimer in the asymmetric unit. The mCOX-2:*p*-methylthio naproxen crystal belongs to space group $P2_12_12$ with unit cell parameters a=181.2 Å, b=134.2 Å, c=122.0 Å, and $\alpha =$

$\beta = \gamma = 90°$. The asymmetric unit consisted of two mCOX-2 dimers; inhibitor was bound in each monomer. The structures were determined by molecular replacement using a Pfizer high resolution structure as the search model and the program MOLREP (12). Data collection and refinement statistics can be found in Table I. The models were refined using REFMAC5 (13) with iterated manual fitting using COOT (14). The coordinates and structure factors have been deposited in the Protein Data Bank under accession codes: 3NT1 for naproxen and 3NTB for the naproxen analog.

Results

Arylcarboxylic acid inhibitors bind in one of two orientations in the COX active site (Figure 1). Flurbiprofen binds in the canonical fashion with its carboxylate moiety ion-paired and hydrogen-bonded to the constriction site residues Arg-120 and Tyr-355 (Figure 1B) (2,11)**.** In contrast, diclofenac binds in an inverted orientation in which its carboxylate is hydrogen bonded to the sidechains of Tyr-385 and Ser-530 (Figure 1C) (7). These two orientations can be discriminated by mutations of constriction site residues, which abolish inhibition by flurbiprofen but have no effect on inhibition by diclofenac. Mutation of Tyr-355 to Phe in mCOX-2 abolished inhibition by naproxen (Figure 2A); whereas, mutation of Arg-120 to Gln slightly increased the potency of inhibition as compared to WT as exhibited by an improved IC_{50} and a greater extent of inhibition (~90%). Mutation of Arg-120 to Ala resulted in a complete loss of enzyme inhibition by naproxen (Figure 2A). Together, these results imply that the carboxylate group of naproxen binds at the constriction site in the canonical orientation, coordinated to Tyr-355 and Arg-120.

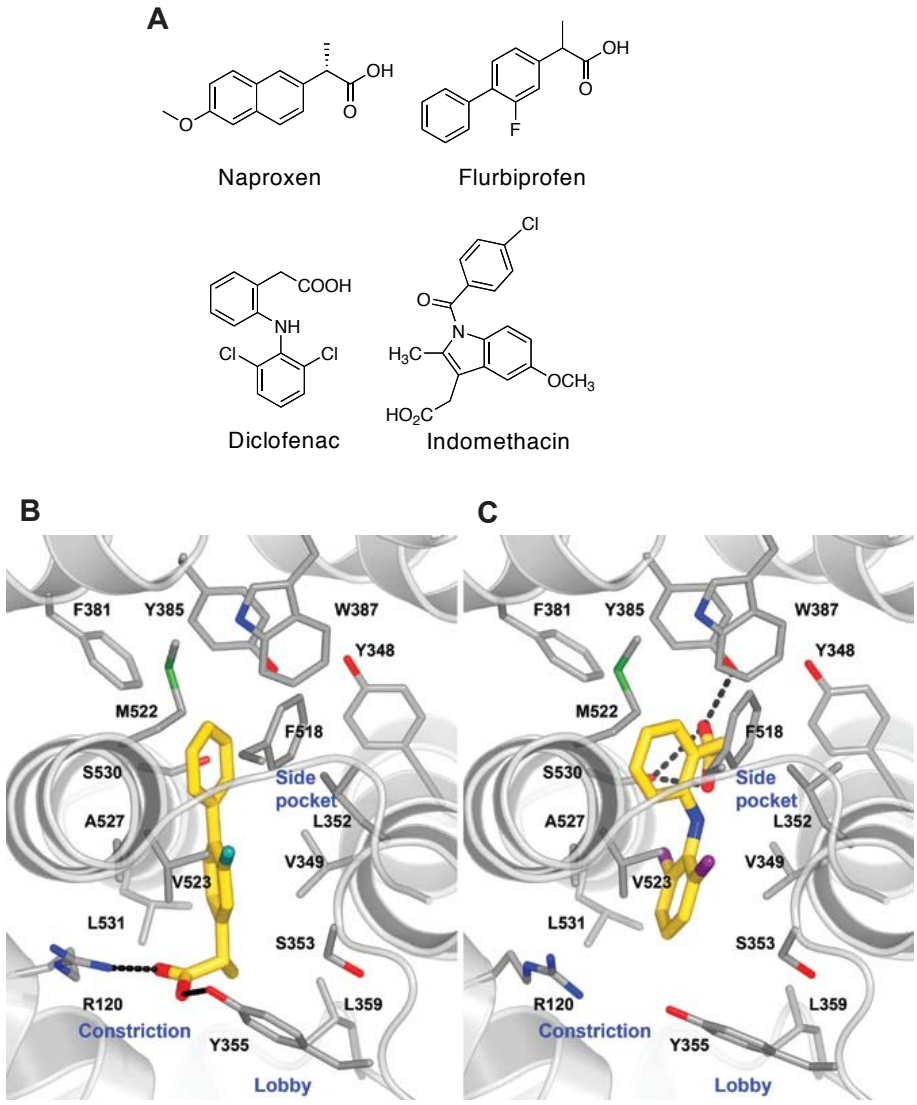

Figure 1. Chemical structures of NSAIDs and crystal structures of flurbiprofen and diclofenac bound in mCOX-2 active site. *A.* Chemical structures of naproxen, flurbiprofen, diclofenac, and indomethacin. *B*. The structure of flurbiprofen (3PGH, inhibitor carbon atoms colored gold) and *C.* diclofenac (1PXX) bound at the COX-2 active site show the opposing binding modes that position their acidic groups either coordinated to the constriction residues Arg-120 and Tyr-355 at the base of the active site or to the catalytic Tyr-385 as well as Ser-530 at the top of the pocket.

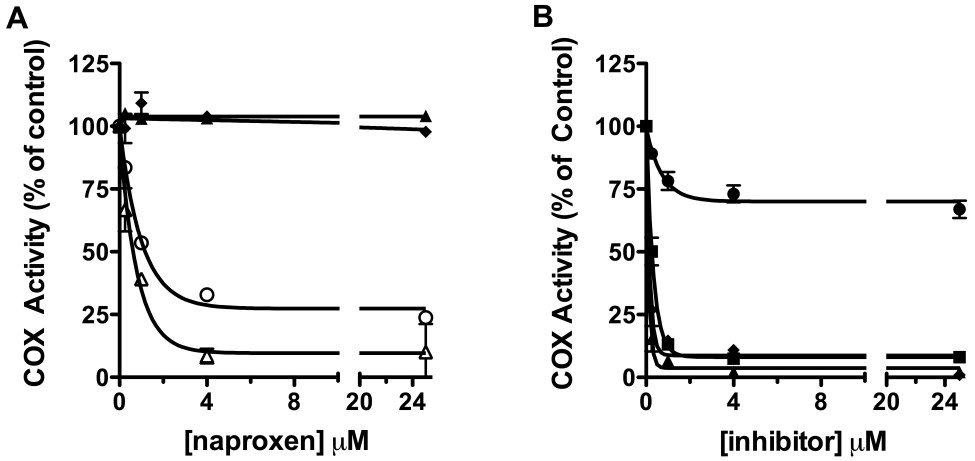

Figure 2. Inhibition of mCOX-2 active site mutants by naproxen and nonselective NSAIDs. *A*. Naproxen (0.25 – 25 μM) was pre-incubated with WT mCOX-2 (○) or R120A (▲), R120Q (△) and Y355F (◆) mCOX-2 mutant enzymes for 20 min prior to the addition of substrate (50 μM) for 30s at 37 °C. *B*. Naproxen (●), indomethacin (■), diclofenac (▲) or flurbiprofen (◆) was preincubated with mCOX-2 W387F for 20 min prior to the addition of substrate (50 μM). Inhibitor concentrations ranged from 0.25 – 25 μM. Data were fit to a one-phase decay model to determine approximate IC_{50} values. Data points represent the mean of duplicate determinations. Data points for naproxen against W387F represent the mean of five independent experiments in duplicate.

In order to rigorously examine the binding mode predicted from these studies, we determined the co-crystal structure of naproxen bound to mCOX-2 at 1.7 Å resolution, the highest resolution COX structure to date and among the highest resolution membrane protein structures described. The topology of the COX dimer and active site resemble those of previous studies, though we have resolved additional solvent, ion, and detergent molecules not observed in lower resolution structures. Somewhat surprisingly, the residues lining the active site were observed in single conformations, despite the fact that many of them were bordered only by solvent. The resolution of this structure enabled the identification of a β-OG molecule lying on the external side of the constriction, at the base of the funnel-shaped entrance to the active site (lobby region). Similar observations were reported for high resolution structures of COX-1 (e.g., 2AYL) (15). A solvent

molecule is often observed hydrogen bonded to Tyr385 and Ser 530 in the active site; however, when this density was fitted with a water molecule in the current structure, a 5σ residual electron density peak remained at that position. When fitted with a chlorine atom, the residual peak disappeared, and the atom refined to a temperature factor similar to neighboring protein and inhibitor atoms. A peak in the anomalous difference map at the same location provided further evidence that the peak was a chlorine atom. While the physiological significance of chloride binding at this position is unknown, chloride ions have been used previously to identify the binding site of molecular oxygen in various proteins including dioxygenases (16,17). This raises the possibility that the chloride ion may be indicative of the position of molecular oxygen prior to incorporation into COX substrates.

Strong electron density was observed for a single orientation of naproxen binding within the COX-2 active site, making no contacts in the COX-2 side pocket or lobby region (Figure 3). As predicted by the mutagenesis data, the binding mode of naproxen is similar to that of other members of the 2-arylpropionic acid family of NSAIDs with the carboxylate group of naproxen participating in hydrogen-bonding interactions with Arg-120 (2.8 Å and 2.9 Å) and Tyr-355 (2.5 Å) at the base of the active site. The remainder of the interactions between the compound and protein were van der Waals contacts. The (*S*)-α-methyl group of naproxen inserts into the hydrophobic cleft adjacent to Val-349 while the naphthyl backbone of naproxen makes hydrophobic contacts with Ala-527,

Table 1. X-ray data collection and refinement statistics

Data set	**naproxen**	***p*-methylthio naproxen**
Beamline	LS-CAT APS 21 ID-F	SER-CAT APS 22 ID
Wavelength	0.97856	1.0000
Space group	I222	$P2_12_12$
Unit cell dimensions	a=122.3Å, b=133.2Å, c=181.3Å, a=b=g=90°	a=181.2Å, b=134.2Å, c=122.0Å, a=b=g=90°
# molecules / ASU	2	4
Resolution (all, highest bin)	35.0-1.73Å, 1.79-1.73Å	20.0-2.27Å, -2.35-2.27Å
R-factor (all, highest bin)	6.7%, 40.9%	12.4%, 50.9%
I/sI (all, highest bin)	23.3, 2.0	12.2, 2.0
Completeness (all, highest bin)	98.6%, 97.8%	97.8%, 91.9%
Redundancy	4.6	4.9
Refinement		
Resolution (all, highest bin)	30.0 – 1.73Å	19.9-2.27Å
# reflections	142,975	131,041
R-factor	16.7%	23.4%
R_{free}	18.6%	26.3%
Rmsd ideal values		
Bond lengths	0.006Å	0.006Å
Bond angles	1.063°	0.895°
B-factors		
Protein	26.5 $Å^2$	50.1 $Å^2$
Ligand	22.1 $Å^2$	42.3 $Å^2$

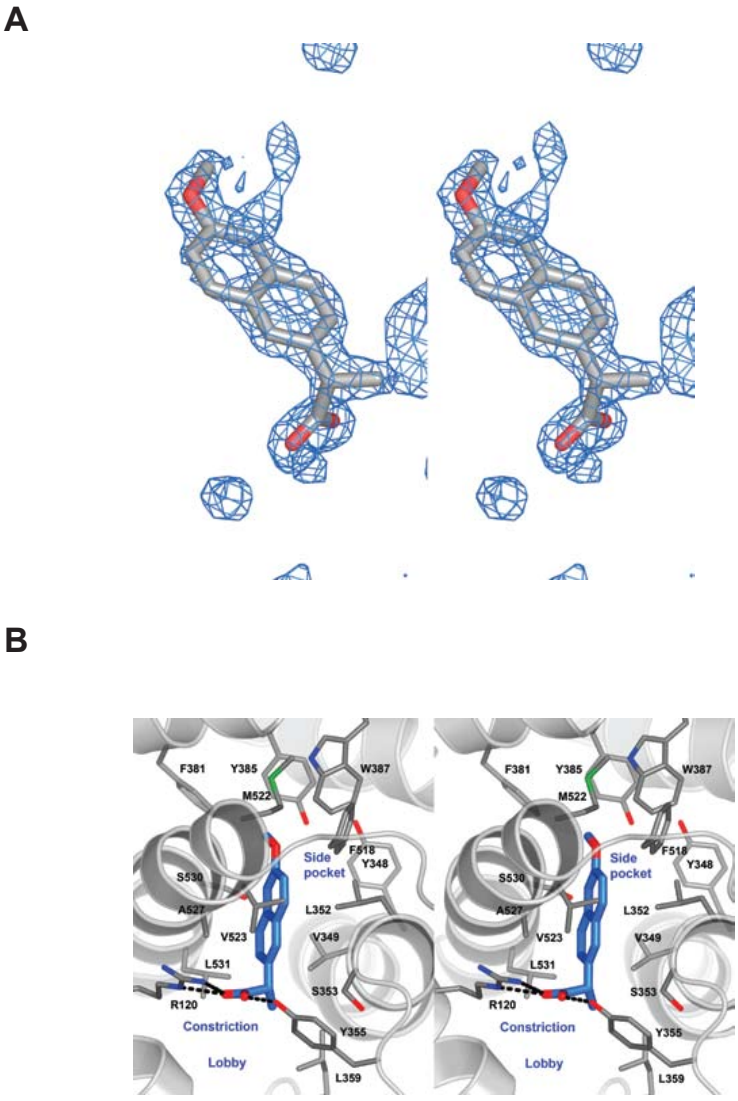

Figure 3. Crystal structure of naproxen bound to mCOX-2. *A*. Difference electron density map (F_O-F_C) contoured at 3.5σ of the COX-2 active site prior to the addition of naproxen to the model or modification of sidechain positions in the binding pocket. This and other molecular graphics images were composed with PyMol (Delano Scientific). *B.* Stereoview of the crystal structure of naproxen (blue carbon atoms) bound at the COX-2 active site reveals that it forms extensive van der Waals contacts within the binding pocket and hydrogen bonds, similar to flurbiprofen, to the sidechains of Tyr 355 and Arg 120. The inhibitor does not enter the side pocket into which the phenyl sulfonamide or phenyl sulfone moieties of diaryl heterocyclic compounds protrude.

Gly-526 and Leu-352. Interestingly, the side chain of Leu-352 adopts an alternate conformation from that observed in the co-crystal structures of flurbiprofen, indomethacin, and diclofenac bound to mCOX-2. The *p*-methoxy group of naproxen is oriented towards the apex of the COX active site and forms van der Waals interactions with Trp-387 and Tyr-385.

The mCOX-2:naproxen crystal structure indicates that the (*S*)-α-methyl group of naproxen is oriented in a conformation similar to that of the α-methyl group of flurbiprofen and makes hydrophobic contacts with Val-349 as well as Leu-359 (11). To further probe these interactions, we quantified the ability of naproxen to inhibit V349A, V349L, and V349I mutant enzymes. Naproxen inhibited V349A mCOX-2 with a similar potency and extent of inhibition as WT mCOX-2 (IC_{50} = 3.5 μM, 75% inhibition) but the V349I and V349L mutants were both more sensitive to inhibition (IC_{50} = 0.28 μM and 0.35 μM, greater than 95% inhibition) (Figure 4). The increase in inhibition observed when naproxen was tested against V349I or V349L could arise from increased hydrophobic interactions between the α-methyl group and residue 349. This is consistent with the finding that 2-*des*-methylnaproxen is significantly less potent than naproxen against WT mCOX-2 (described in Chapter II).

The naproxen-COX-2 crystal structure shows that the *p*-methoxy group interacts with Trp-387 by van der Waals contacts to two carbon atoms of the sidechain, Cζ2 (3.4 Å) and Cη2 (3.6 Å), the latter being the position of the sidechain unique spatially to tryptophans. Trp-387 is located at the top of the COX active site near the catalytic residue, Tyr-385, and has been shown to be a critical residue for the proper positioning of

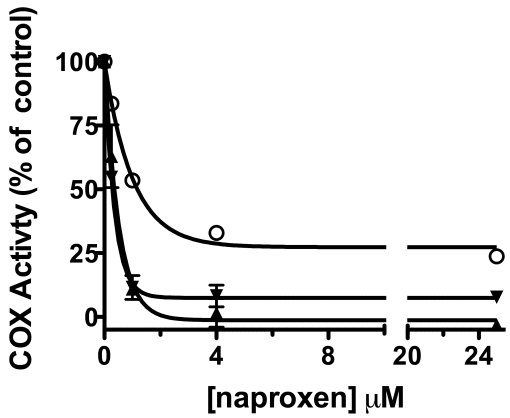

Figure 4. Inhibition of Val-349 mCOX-2 mutants by naproxen. Naproxen (0.25 – 25 μM) was preincubated with WT mCOX-2 (○), V349L (▲), and V349I (▼) for 20 min prior to the addition of substrate (50 μM). Each reaction was terminated and analyzed as described under "Experimental Procedures." IC_{50} values are reported under "Results". Each data point is the average of at least two independent determinations.

AA within the active site to yield the cyclooxygenase product, PGG_2. The W387F mCOX-2 mutant enzyme forms relatively low amounts of PGG_2 but increased amounts of the uncyclized product, 11-hydroxy-eicosatetraenoic acid (18). We tested the W387F mutant for sensitivity to naproxen inhibition. A higher protein concentration was used because of the mutant's reduced catalytic activity. Naproxen had a minimal inhibitory effect on W387F exhibiting only 25% inhibition at 25 μM (Figure 2B). The W387F mutation has not been studied with other inhibitors, so we tested it against several other carboxylate-containing NSAIDs. Surprisingly, the IC_{50} values for diclofenac, flurbiprofen, and indomethacin against the W387F mutant enzyme were similar to previously reported values against WT enzyme (~87 nM, ~120 nM, and ~250 nM, respectively) (Figure 2B). Diclofenac and indomethacin, only form a single contact point to the tryptophan sidechain, at the Cζ2 position, which is closely mimicked by phenylalanine (7,11). While flurbiprofen forms interactions with both carbon atoms of

the Trp residue, they originate from a phenyl ring of the inhibitor that is already buttressed by other interactions, making the one with the Trp perhaps less important for binding. In the case of naproxen, the oxygen of the *p*-methoxy group lies within van der Waals contact range only of the Trp sidechain. Therefore, the interaction between Trp-387 and naproxen appears to be unique among carboxylate-containing NSAIDs.

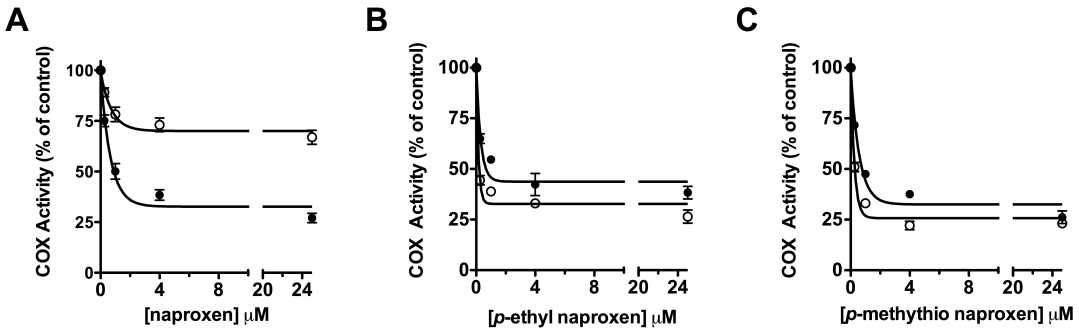

Figure 5. Inhibition of WT and W387F mCOX-2 by naproxen and naproxen analogs. Following a 20 minute preincubation of naproxen (*A*), *p*-ethyl naproxen (*B*), or a *p*-methylthio naproxen (*C*) with mCOX-2 (●) or W387F mCOX-2 (○), [1-^{14}C]-AA (50 μM) was added and allowed to react for 30 seconds prior to termination with organic solvent. Concentrations of inhibitors ranged from 0.25 – 25 μM. Product formation was measured by TLC as described. Each data point is the mean of at least two independent experiments.

As described in Chapter II, we synthesized a *p*-ethyl and *p*-methylthio naproxen analog and tested their ability to inhibit the COX enzymes. Both analogs were potent inhibitors of mCOX-2 but displayed a loss of potency against COX-1 as compared to naproxen. More remarkable however, both analogs inhibited W387F as well as they inhibited wild-type enzyme (Figure 5). The difference in sensitivity of W387F mCOX-2 to naproxen and the *p*-ethyl and *p*-methylthio analogs prompted us to crystallize the complex of mCOX-2 with the *p*-methylthio naproxen derivative. A structure of this complex was refined at 2.3 Å resolution (Figure 6). Like naproxen, the inhibitor is bound

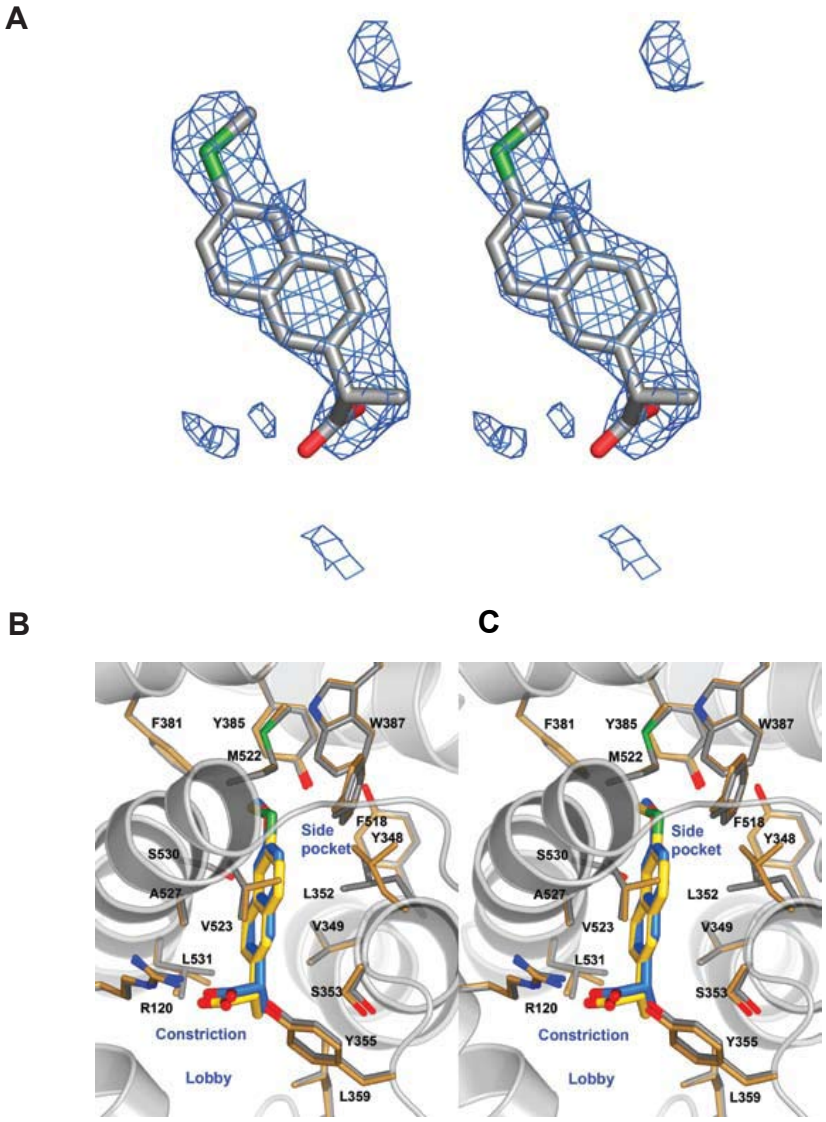

Figure 6. Crystal structure of *p*-methylthio naproxen bound to mCOX-2. *A.* Stereoview of the $(F_O\text{-}F_C)$ difference electron density map contoured at 3.0σ prior to the addition of the inhibitor to the model. *B.* Stereoview of the *p*-methylthio naproxen analog bound within the mCOX-2 active site. The carboxylate participates in hydrogen-bonding interactions with Arg-120 and Tyr-355 at the base of the active site; this interaction is represented by the dashed, yellow lines.

entirely within the main channel of the COX active site. The closest equivalent atoms (distance = 0.2 Å) between the two compounds are the sulfur and oxygen atoms of the *p*-methylthio and *p*-methoxy groups, respectively. The carboxylate tails of the compounds differ greatest in position, with the *p*-methylthio-substituted compound extending approximately 0.5 Å less deeply into the binding site. The *p*-methylthio naproxen analog adopts a binding conformation similar to that of naproxen, maintaining many of the same interactions with surrounding residues. For example, the carboxylate makes hydrogen-bonding interactions with Arg-120 (2.9 and 3.0 Å) and Tyr-355 (2.5 Å) and the (*S*)- α-methyl group makes hydrophobic contacts with Val-349 and Leu-359. The naphthyl backbone participates in van der Waals interactions with Ala-527 and Gly-526 while the methylthio substitutent at the 6-position contacts Tyr-385 and Trp-387. In contrast to naproxen, the *p*-methylthio naproxen analog is not within van der Waals distances of Leu-352. This difference arises from the fact that the Leu sidechain exhibits different conformations in the two structures, with that observed in the methylthio analog being consistent with that seen in the previously published NSAID:mCOX-2 co-crystal structures (3 of 4 monomers). No explanation for the rotation of the residue in the naproxen structure, or its failure to rotate in the methylthio derivative structure, is readily apparent. Comparison of the two crystal structures also indicates that Val-523 makes hydrophobic contacts with the naphthyl backbone of the *p*-methylthio naproxen analog but does not contact naproxen. This observation results from the relative shift of the compounds within the active site.

Discussion

The pharmacological effects of NSAIDs, including naproxen, arise from the suppression of prostaglandin biosynthesis by inhibiting the cyclooxygenase enzymes, COX-1 and COX-2. Despite long-term use in the clinic, the molecular basis for COX inhibition by naproxen is not well-defined. We utilized an extensive mutagenesis study and X-ray crystallography, in combination with the previously described exploration of structure-activity relationships, to identify the molecular determinants of COX inhibition by naproxen. By using a combined approach to probe the importance of naproxen-COX-2 interactions, we were able to elucidate key interactions that would not have been identified by one technique alone. We found critical interactions between the inhibitor and constriction site residues as well as a novel interaction with Trp-387 (Figure 2). Substitution of an ethyl or methylthio group for the *p*-methoxy substituent generated COX-2-preferring naproxen analogs that were unaffected by mutation of Trp-387 to Phe (Figure 5). We determined the X-ray crystal structures of both naproxen and the *p*-methylthio analog bound to mCOX-2. The combination of mutagenesis, chemical elaboration of naproxen analogs, and structural studies, clearly defined the contribution of protein and inhibitor atoms to affinity (Figures 3 and 6).

Naproxen appears to bind in the canonical conformation, with the carboxylic acid oriented towards the mouth of the mCOX-2 active site. Mutagenesis data suggests that one possibility regarding the nature of the interaction between the carboxylate moiety of naproxen and mCOX-2 is that the carboxylate interacts with Arg-120 via hydrogen bonding rather than ion-pairing interactions (Figure 3A). In contrast, the crystal structure of flurbiprofen in complex with mCOX-2 indicates that the carboxylate forms a salt

bridge with the guanidinium group of Arg-120 (11) Furthermore, previous studies have shown a 1000-fold increase in the IC_{50} value for flurbiprofen against R120Q oCOX-1 compared to wild-type enzyme, suggesting that ion-pairing interactions are more important for inhibition by flurbiprofen than naproxen (19).

Our data indicate that the α-methyl group inserts into a small hydrophobic cleft below Val-349, which may serve to anchor naproxen within the mCOX-2 active site and thereby reinforce the canonical binding orientation. The X-ray crystal structures of other 2-arylpropionic acids and the diaryl heterocyclic compound, SC-558 bound to the COX enzymes indicate that the α-methyl group (or 4-trifluoromethyl, in the case of SC-558) is bound in a similar fashion to the naproxen structure (11,20). Carboxylate-containing COX inhibitors without a methyl group in the α-position utilize alternate interactions to reinforce binding within the COX active site. For example, the indolyl-2′-methyl group of indomethacin inserts into a hydrophobic pocket above Val-349 lined by Ala-527, Ser-530, and Leu-531 to form a tightly bound complex (8,11). Similarly, while diclofenac binds in an inverted orientation with the carboxylate coordinated to Ser-530 and Tyr-385, a chlorine atom on the lower aniline ring also inserts into the hydrophobic pocket above Val-349 (7).

A key interaction between naproxen and Trp-387 was uncovered during our mutagenesis screen by the finding that the W387F mutant was largely insensitive to naproxen inhibition. This interaction appears to be unique to naproxen as the same mutation had no appreciable effect on inhibition of mCOX-2 by diclofenac, flurbiprofen, or indomethacin (Figure 3B). The interaction with Trp-387 may result from a combination of hydrophobic packing of the methyl group and electrostatic interactions

with the polarized methoxy group. Unlike naproxen, the p-ethyl and *p*-methylthio analogs are effective inhibitors of W387F mCOX-2. This suggests that either the interaction with Trp-387 is not required for inhibition by the naproxen analogs or that they are able to interact more effectively with W387F COX-2 than is naproxen. Crystal structures of naproxen and the *p*-methylthio naproxen analog show the substituents at the 6-position oriented in a very similar fashion at the top of the COX active site providing no definitive basis for differential inhibition of W387F mCOX-2. Moreover, with the exception of Leu-352, there are no dramatically different interactions throughout the rest of the active site. The substitution of Phe for Trp at position 387 creates a larger active site for the mutant enzyme compared to WT mCOX-2. The ability of the *p*-ethyl and *p*-methylthio naproxen analogs to inhibit W387F mCOX-2 as well as WT suggests that the analogs may be able to adopt an alternate conformation in the larger active site of W387F mCOX-2 compensating for the loss of the interaction with Trp-387 in the wild-type enzyme.

Crystallographic studies may provide some insight into the nature of the COX-2 selectivity of the *p*-ethyl and *p*-methylthio analogs compared to naproxen. The crystal structure of the *p*-methylthio naproxen analog bound to mCOX-2 is suggestive of hydrophobic interactions between Val-523 and the proximal ring of the napthyl backbone. Thus, steric interactions at the top of the channel may put additional pressure on Val-523 near the base of the active site so that inhibition of COX-1, where a bulkier isoleucine is located at residue 523, is significantly more difficult. Mutation of Val-523 to Ile in COX-2 greatly reduces the selectivity of potent COX-2-selective inhibitors like celecoxib and rofecoxib. Consistent with this hypothesis, the naproxen analogs were

unable to significantly inhibit V523I mCOX-2. However, interpretation of these results is difficult, as it has previously been reported that a V523I mutation in the hCOX-2 background completely abrogates inhibition of hCOX-2 by naproxen as measured by a PGE_2 ELISA assay (21). Consistent with these results, naproxen was not an effective inhibitor of V523I mCOX-2 in our standard IC_{50} assay; the maximal extent of inhibition was approximately 20% (data not shown). This appears to be the first case of a non-COX-2-selective inhibitor making a key interaction with this area of the active site.

References

1. Blobaum, A. L., and Marnett, L. J. (2007) *J. Med. Chem.* **50**, 1425-1441

2. Picot, D., Loll, P. J., and Garavito, R. M. (1994) *Nature* **367**, 243-249

3. Xiao, G., Chen, W., and Kulmacz, R. J. (1998) *J. Biol. Chem.* **273**, 6801-6811

4. Luong, C., Miller, A., Barnett, J., Chow, J., Ramesha, C., and Browner, M. F. (1996) *Nat. Struct. Biol.* **3**, 927-933

5. Harrison, I. T., Lewis, B., Nelson, P., Rooks, W., Roszkowski, A., Tomolonis, A., and Fried, J. H. (1970) *J. Med. Chem.* **13**, 203-205

6. Rowlinson, S. W., Crews, B. C., Lanzo, C. A., and Marnett, L. J. (1999) *J. Biol. Chem.* **274**, 23305-23310

7. Rowlinson, S. W., Kiefer, J. R., Prusakiewicz, J. J., Pawlitz, J. L., Kozak, K. R., Kalgutkar, A. S., Stallings, W. C., Kurumbail, R. G., and Marnett, L. J. (2003) *J. Biol. Chem.* **278**, 45763-45769

8. Prusakiewicz, J. J., Felts, A. S., Mackenzie, B. S., and Marnett, L. J. (2004) *Biochemistry* **43**, 15439-15445

9. Kalgutkar, A. S., Crews, B. C., Rowlinson, S. W., Garner, C., Seibert, K., and Marnett, L. J. (1998) *Science* **280**, 1268-1270

10. Stevens, A. M., Pawlitz, J. L., Kurumbail, R. G., Gierse, J. K., Moreland, K. T., Stegeman, R. A., Loduca, J. Y., and Stallings, W. C. (1999) *J. Cryst. Growth* **196**, 350-355

11. Kurumbail, R. G., Stevens, A. M., Gierse, J. K., McDonald, J. J., Stegeman, R. A., Pak, J. Y., Gildehaus, D., Miyashiro, J. M., Penning, T. D., Seibert, K., Isakson, P. C., and Stallings, W. C. (1996) *Nature* **384**, 644-648

12. Vagin, A., and Teplyakov, A. (1997) *J. Appl. Cryst*. 1022-1025

13. Murshudov, G. N., Vagin, A. A., and Dodson, E. J. (1997) *Acta. Crystallogr. D. Biol. Crystallogr.* **53**, 240-255

14. Emsley, P., and Cowtan, K. (2004) *Acta. Crystallogr. D. Biol. Crystallogr.* **60**, 2126-2132

15. Gupta, K., Selinsky, B. S., and Loll, P. J. (2006) *Acta. Crystallogr. D. Biol. Crystallogr.* **62**, 151-156

16. Colloc'h, N., Gabison, L., Monard, G., Altarsha, M., Chiadmi, M., Marassio, G., Sopkova-de Oliveira Santos, J., El Hajji, M., Castro, B., Abraini, J. H., and Prange, T. (2008) *Biophys. J.* **95**, 2415-2422

17. Steiner, R. A., Janssen, H. J., Roversi, P., Oakley, A. J., and Fetzner, S. (2010) *Proc. Natl. Acad. Sci. U.S.A.* **107**, 657-662

18. Thuresson, E. D., Lakkides, K. M., and Smith, W. L. (2000) *J. Biol. Chem.* **275**, 8501-8507

19. Rieke, C. J., Mulichak, A. M., Garavito, R. M., and Smith, W. L. (1999) *J. Biol. Chem.* **274**, 17109-17114

20. Selinsky, B. S., Gupta, K., Sharkey, C. T., and Loll, P. J. (2001) *Biochemistry* **40**, 5172-5180

21. Gierse, J. K., McDonald, J. J., Hauser, S. D., Rangwala, S. H., Koboldt, C. M., and Seibert, K. (1996) *J. Biol. Chem.* **271**, 15810-15814

CHAPTER IV

DIFFERENTIAL SENSITIVITY AND MECHANISM OF INHIBITION OF CYCLOOXYGENASE-2 OXYGENATION OF ARACHIDONIC ACID AND 2-ARACHIDONOYLGLYCEROL BY RAPIDLY REVERSIBLE NON-STEROIDAL ANTI-INFLAMMATORY DRUGS

Introduction

Cyclooxygenase-2 (COX-2) oxygenates a range of fatty acyl substrates including fatty acids, esters, and amides. Arachidonic acid (AA) and the endocannabinoid 2-arachidonoylglycerol (2-AG) are the best acid and ester hCOX-2 substrates, respectively, and display comparable k_{cat}/K_m ratios for oxygenation (1). Despite this similarity, this laboratory recently reported that COX-2 oxygenation of 2-AG is dramatically more sensitive to inhibition by ibuprofen and mefenamic acid than is oxygenation of AA (2). In fact, these compounds, which have been considered relatively weak COX inhibitors, inhibit 2-AG oxygenation at concentrations that are orders of magnitude lower than the concentrations required for inhibition of AA oxygenation. Further, ibuprofen and mefenamic acid appear to be competitive inhibitors of AA oxygenation, but non-competitive inhibitors of 2-AG oxygenation by COX-2 (Figure 1).

These data suggest that ibuprofen and mefenamic acid inhibit COX-2 oxygenation of AA and 2-AG by different mechanisms and with different potencies. An interpretation of the experimental findings that is consistent with recent results establishes that the two subunits of the homodimeric COX-2 protein are not identical once substrate or inhibitor is bound (3). In the case of 2-AG oxygenation, binding of a single molecule of ibuprofen or mefenamate at one subunit prevents productive binding of 2-AG at the other subunit

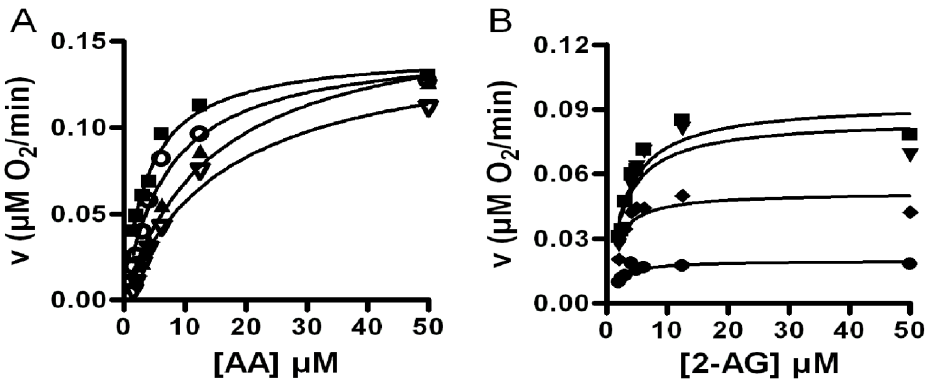

Figure 1. **Inhibition of mCOX-2 oxygenation of AA and 2-AG by ibuprofen**. Ibuprofen and substrate were mixed in an oxygraph cell, and the reaction was initiated by addition of COX-2. The initial velocity of O_2 uptake was determined from a tangent to the most rapidly descending portion of the curve. Data were fit using the Michaelis-Menten model. (A) Ibuprofen at 0 μM (■), 50 μM (○), 200 μM (▲), and 300 μM (●). (B) Instantaneous COX-2 inhibition of 2-AG oxidation by ibuprofen at 0 μM (■), 0.5 μM (▼), 1.25 μM (◆), and 2.5 μM (●). Reproduced from (2).

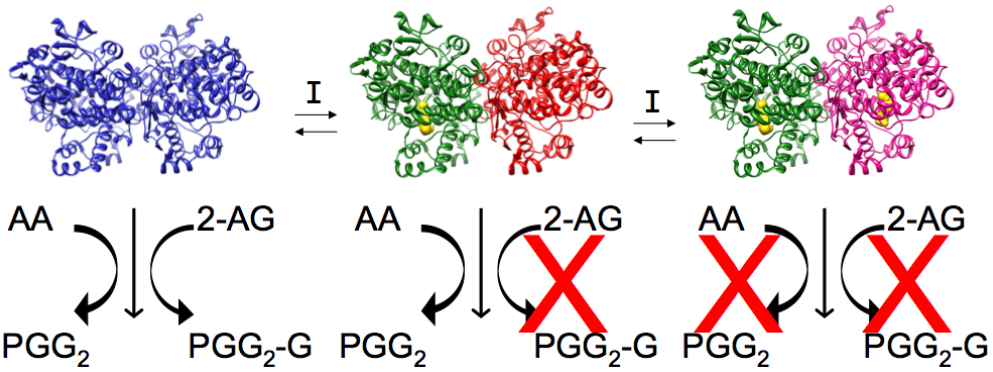

Figure 2. Model for differential inhibition 2-AG and AA oxygenation by COX-2. The uninhibited mCOX-2 homodimer (blue) is able to effectively metabolize both AA and 2-AG to form PGG_2 and PGG_2-G. Binding of an inhibitor (yellow) to a single monomer (green) precludes the productive binding of 2-AG in the partner monomer (red) but still allows for AA oxygenation. Metabolism of AA is inhibited only when an inhibitor occupies both active sites of the COX dimer as shown on the far right.

(Figure 2). This hypothesis is consistent with the apparent non-competitive inhibition of 2-AG oxygenation by ibuprofen and mefenamic acid. In contrast to the observations with 2-AG, inhibition of COX-2 oxygenation of AA by ibuprofen or mefenamate requires much higher concentrations of inhibitor and displays kinetic behavior typical of competitive inhibition. The most straightforward interpretation of these results is that inhibition of AA oxygenation requires inhibitor molecules to bind in both active sites. Binding in the first active site is necessary but not sufficient to inhibit AA oxygenation; inhibition is only observed when the second molecule of inhibitor competes with AA for binding at the remaining active site (Figure 2).

To explore the generality of this phenomenon, we surveyed the inhibition of COX-2-dependent 2-AG and AA oxygenation by different classes of NSAIDs. The results of these studies indicate that compounds classified as weak, reversible inhibitors of AA oxygenation are potent inhibitors of 2-AG oxygenation by COX-2 while compounds classified as slow, tight-binding inhibitors exhibit potent inhibition of both 2-AG and AA oxidation with comparable IC_{50} values for both substrates.

Experimental Procedures

Materials. mCOX-2 was expressed and purified as described (4). AA was purchased from Nu-Check Prep, Inc. (Elysian, MN) and prepared as a stock solution in DMSO. 2-AG and prostaglandin E_2-d_4 (PGE_2-d_4) was purchased from Cayman Chemical Company (Ann Arbor, MI). The internal standard prostaglandin E_2-glycerol-d_5 (PGE_2-G-d_5) was synthesized by transesterification from PGE_2 and glycerol-d_5 purchased from Sigma

(Milwaukee, WI). Naproxen, diclofenac, flurbiprofen, indomethacin and celecoxib were also purchased from Sigma-Aldrich (Milwaukee, WI). Lumiracoxib, 2′-*des*-methylindomethacin (DM-INDO), and rofecoxib were synthesized according to published methods (5-7). Reagents used in the crystallization of mCOX-2 were purchased from Hampton Research (Aliso Viejo, CA).

Inhibition of AA and 2-AG oxygenation as measured by oxygen uptake. For AA experiments, 440 nM mCOX-2 was preincubated with inhibitor for 2 min at 37 °C prior to the addition of 50 μM AA. For experiments in which 2-AG was used as the substrate, the concentration of mCOX-2 was increased to 890 nM to allow for a similar extent of oxygenation of 2-AG compared to AA. Because of the relatively low sensitivity of the oxygen monitor, high protein concentrations were required to obtain measurable oxygenation. Initial reaction velocity was determined from the linear portion of oxygen uptake curves as measured by an Instech 210 Fiber Optic oxygen monitor (Plymouth Meeting, PA) and normalized to a DMSO control.

Analysis of NSAID inhibition of AA and 2-AG oxygenation by mCOX-2 by mass spectrometry - A fixed concentration of mCOX-2 (approximately 50 nM for 5 μM substrate or 200 nM for 50 μM substrate) was incubated with inhibitor (or DMSO control) for five or twenty minutes at 37 °C before the addition of substrate; pre-incubation time was determined based on previous reports of the time necessary to achieve maximal inhibition. The concentration of inhibitor ranged from 16 nM – 25 μM. The enzyme-inhibitor complex was allowed to react with 5 or 50 μM AA or 2-AG for 30

seconds before quenching with an extraction solution of ethyl acetate with 0.5% acetic acid and deuterated internal standards. The organic layer was separated and evaporated to near-dryness under nitrogen and stored at -20 °C until analysis. Samples were reconstituted with 1:1 MeOH:water (v/v) and analyzed using liquid chromatography-tandem mass spectrometry (LC-MS/MS) analysis. The solvent system consisted of 5 mM ammonium acetate, pH 3.5 (Buffer A) and acetonitrile with 6% Buffer A (v/v) (Buffer B). Samples were chromatographed using a 50 Å C18 Luna column (5 x 0.2 cm, 3 μm) using an isocratic method at 34% B with a flow rate of 375 mL/min. Prostaglandin (PG) and glycerol prostaglandin (PG-G) products were measured by SRM using the following transitions: for PGE_2/D_2 *m/z* 370 → 317, for PGE_2/D_2-d_4 *m/z* 374 → 321, for PGE_2/D_2 - G *m/z* 444 → 391 and for PGE_2/D_2 - G-d_5 *m/z* 449→ 396. In order to quantitate PG and PG-G production, the ratio of the area of the peak to its corresponding internal standard was determined and normalized to a DMSO control.

Co-crystallization of mCOX-2 and DM-INDO. Purification and crystallization were performed according to the methodology described for the co-crystallization of naproxen and mCOX-2 (8). Data collection and refinement statistics are shown in Table 1.

Results

Indomethacin and DM-INDO. Several arylcarboxylic acids or diarylheterocycles are slow, tight-binding inhibitors of COX-2 (9). These compounds exhibit low K_d values for binding and potent inhibition but only after a lengthy preincubation period. The indoleacetic acid derivative indomethacin is a classic slow, tight-binding inhibitor of both

COX-2 and COX-1 (10). Inhibition of AA oxygenation by COX-2 requires a preincubation period of up to 15 min, and its inhibition potency increases dramatically during this time. Following preincubation of enzyme and inhibitor, indomethacin displayed an IC_{50} of 2 μM for inhibition of AA oxygenation and 5.5 μM for inhibition of 2-AG oxygenation as measured by an oxygen uptake assay (Figure 3). It has been reported previously that binding of a single molecule of indomethacin to a COX homodimer is sufficient to maximally inhibit AA oxygenation (11). The similar IC_{50} values for inhibition of AA and 2-AG suggests that a single indomethacin molecule bound in one subunit is sufficient to inhibit the oxygenation of either a fatty acid or fatty acid ester substrate in the other subunit.

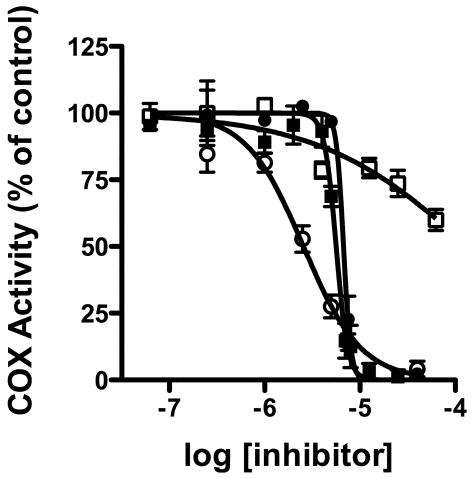

Figure 3. Determination of IC_{50} values for the inhibition of mCOX-2 oxygenation of AA and 2-AG by indomethacin and DM-INDO. mCOX-2 was preincubated with indomethacin (●) or DM-INDO(■) for 2 min before the addition of 2-AG. For AA, maximal inhibition was achieved following a 15 min preincubation with indomethacin (○) and a 2 min preincubation with DM-INDO(□). Inhibitor concentrations ranged from 250 nM to 500 μM. Following the addition of 50 μM substrate, initial rates of oxygen uptake were determined and normalized to a DMSO control.

The steep dose-response curve observed for the inhibition of 2-AG oxygenation

by indomethacin may indicate that the K_d's of these inhibitors are lower than the concentration of enzyme used in the oxygen uptake assay (12). In this case, the measured IC_{50} values are a reflection of the enzyme concentration and not the true K_d. Therefore, an alternative assay was employed that measured PGD_2/E_2-G or PGD_2/E_2 formation by LC-MS/MS following a 15 min preincubation of inhibitor with enzyme to assure maximal inhibition of the oxygenation of both substrates. Saturating concentrations of both 2-AG and AA (50 μM for both) were used as in the oxygen uptake assay. The increased sensitivity of the mass-spectrometry assay allowed the use of enzyme concentrations significantly lower than the concentration required for the oxygen uptake assay (200 nM versus approximately 900 nM for 2-AG). The IC_{50} values for inhibition of AA and 2-AG by indomethacin were 180 nM and 10 nM, respectively; complete inhibition was observed for both substrates. These findings are in agreement with the trends observed in the oxygen uptake experiments in that indomethacin potently inhibits the oxygenation of both AA and 2-AG with similar IC_{50} values.

A major determinant of the slow, tight binding of indomethacin to COX-2 is insertion of the 2′-methyl group on the indole ring into a hydrophobic depression in the side of the COX-2 active site (6). Removal of the 2′-methyl group generates a molecule, DM-INDO, which exhibits rapid reversible inhibition of AA oxygenation with a much higher IC_{50}. Figure 3 demonstrates that removal of the 2′-methyl group from indomethacin increases the IC_{50} for inhibition of AA oxygenation from 2 μM for indomethacin to ~500 μM for DM-INDO. In contrast to the results with AA, removal of the 2′-methyl group from indomethacin has no effect on the inhibition of 2-AG oxygenation; the IC_{50} for inhibition of 2-AG oxygenation by DM-INDO is 6.8 μM,

essentially the same as the IC_{50} of indomethacin (Figure 3). Like indomethacin, DM-INDO has a steep dose-response curve for the inhibition of 2-AG. Therefore, we evaluated the inhibition of both AA and 2-AG oxygenation by DM-INDO in the LC-MS/MS assay. The IC_{50} value for 2-AG was 110 nM (100% inhibition), while no value could be determined for inhibition of AA oxygenation at concentrations of DM-INDO up to 25 μM (30% inhibition)(Table II). Therefore, like the reversible inhibitors ibuprofen and mefenamic acid, DM-INDO appears to be a weak inhibitor of COX-2 mediated oxygenation of AA, but a potent inhibitor of 2-AG oxygenation.

A conformational change at the dimer interface upon inhibitor binding is thought to be associated with the negative cooperativity between COX monomers. The results above suggest that indomethacin and DM-INDO utilize different mechanism of inhibition to prevent 2-AG oxygenation. To examine potential differences at the dimer interface following the binding of indomethacin compared to DM-INDO, and to verify that indomethacin and DM-INDO occupy similar conformations within the mCOX-2 active site, we determined the 2.4 Å crystal structure of DM-INDO bound within the COX-2 active site; the 2.9 Å crystal structure of indomethacin bound to COX-2 was reported by Kurumbail *et al*. in 1996 (13). As shown in Figure 4, clear electron density for DM-INDO was observed in both monomers of the COX-2 homodimer. Like indomethacin, DM-INDO appears to bind completely within the COX active site, with the carboxylic acid coordinated to active site residues Try-355 and Arg-120. The p-chlorobenzoyl moiety of DM-INDO also occupies a similar conformation to that of indomethacin at the apex of the COX active site channel. While it is difficult to make definitive conclusions regarding differences in the binding mode of indomethacin and DM-INDO due to the low

to moderate resolution of the structures, it appears that the indole ring and benzoyl oxygen of DM-INDO occupy slightly altered conformations compared to indomethacin (Figure 4). This can likely be attributed to the absence of the 2′-methyl group, which anchors indomethacin in a small hydrophobic pocket comprised of Val-349, Leu-531, Ser-530 and Ala-527. Insertion of the 2′-methyl group of indomethacin into this pocket is the major determinant of time-dependent inhibition of COX, and is thought to result in a conformational change of the enzyme-inhibitor complex leading to functionally irreversible inhibition.

We hypothesize that binding of a single molecule of inhibitor in one active site is sufficient to prevent the productive binding of 2-AG in the active site of the partner monomer. This hypothesis is based on recent work that indicates that the two monomers of each COX enzyme are functionally interdependent and that binding of a substrate or inhibitor at one active site alters the properties of the other active site (3). The communication between subunits occurs through the dimer interface (14). Further, it has recently been reported that a shift in the position of the loop containing residues 121-127 at the dimer interface is observed when celecoxib is bound in one monomer of the oCOX-1 homodimer, while the active site of the partner monomer remains empty (15). However, the concentration of inhibitor was seven times that of the enzyme in the crystallization conditions used to determine the mCOX-2:DM-INDO structure so that both monomers appeared to be fully occupied with DM-INDO, and no changes were observed along the dimer interface.

Table 1. Crystallographic data collection and refinement statistics.

Beamline	APS (NE-CAT)
Wavelength (Å)	0.979
Temperature (K)	100
Space group	I222
Unit cell (a, b, c; Å)	123.23, 132.59, 180.29
Resolution range (Å)	30-2.5
Highest resolution shell	2.59-2.5
No. of measurements	1280205
No. of unique reflections	49403 (4936)
Redundancy	3.7 (3.7)
Completeness (%)	97.1 (98.6)
R_{merge} (%)	10.6 (47.2)
Signal to noise ($I/\sigma I$)	15.1 (2.5)
Solvent content (%)	59.6
Model composition (asymmetric unit)	
No. amino acid residues	1102
No. water molecules	405
R_f (%)	19.0
R_{free} (%)	25.6
rms deviation	
Bond lengths (Å)	0.009
Bond angles (°)	1.3
B-factors	
Protein	39.445
Ligand	35.052

[a] Values in parentheses correspond to the highest resolution shells.
[b] $R_{merge} = \Sigma_{hkl} \Sigma_{j=1,N} \left| \langle I_{hkl} \rangle - I_{hklj} \right| / \Sigma_{hkl} \Sigma_{j=1,N} \left| I_{hklj} \right|$ where the outer sum (hkl) is taken over the unique reflections.
[c] $R_f = \Sigma_{hkl} ||F_{o,hkl}| - k|F_{c,hkl}|| / \Sigma_{hkl} |F_{o,hkl}|$, where $|F_{o,hkl}|$ and $|F_{c,hkl}|$ are the observed and calculated structure factor amplitudes, respectively.
[d] R_{free} is same as for R_f for the set of reflections (5-10% of the total) omitted from the refinement process.
APS, Advanced Photon Source; NE-CAT, North Eastern Collaborative Access Team; rms deviation, root mean square deviation.

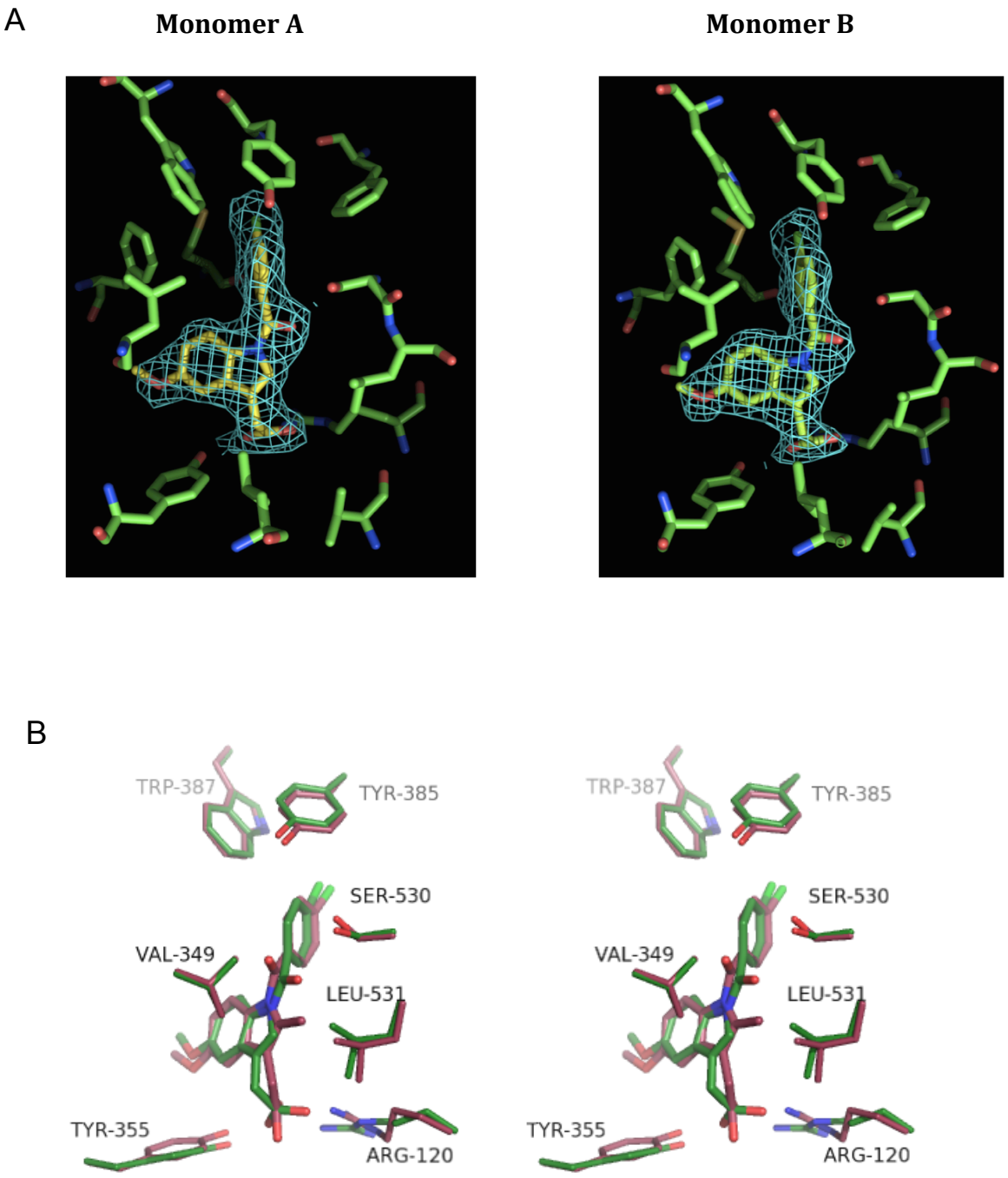

Figure 4. Crystal structure of DM-INDO bound in the active site of COX-2. *A*. $2F_O$-F_C difference electron density map contoured at 1.0σ for DM-INDO in the active site of mCOX-2. B. Stereoview of an overlay of DM-INDO (green) and indomethacin (purple) in the mCOX-2 active site. PDB ID for indomethacin structure: 4COX.

Naproxen. The non-selective NSAID naproxen displays a unique kinetic mechanism of COX inhibition. It is clear that naproxen does not associate with the COX enzymes by a single-step mechanism (like ibuprofen or mefenamic acid), as a short preincbuation time is required for maximal inhibition. However, in contrast to slow, tight-binding inhibitors like indomethacin, the enzyme-inhibitor complex remains readily reversible. Previous studies describe this mode of inhibition as "mixed", which was characterized by an initial time-dependent loss of enzyme activity followed by a non-zero plateau (16). As such, it was of interest to determine whether naproxen would be a more potent inhibitor of 2-AG compared to AA oxygenation similar to other rapidly reversible inhibitors, despite interacting with the enzyme in a time-dependent manner. Following a short preincubation, naproxen inhibited AA oxygenation by mCOX-2 with an IC_{50} value of 4.5 μM while the IC_{50} value was 430 nM for 2-AG. These results indicate that naproxen is, in fact, a more potent inhibitor of 2-AG oxygenation compared to AA (Figure 5). In subsequent experiments, the substrate concentration was reduced from a saturating concentration of 50 μM to 5 μM, which is closer to the reported K_m values for AA and 2-AG. Under these conditions, the IC_{50} values decreased (AA: 340 nM, 2-AG: 30 nM) but the fold-change in potency for 2-AG versus AA was similar (Figure 5). The shift in IC_{50} values may also be partially attributed to differing assay conditions as values for 50 μM substrate were determined by monitoring the change in the initial rate of oxygen uptake as measured by an oxygen electrode, while the IC_{50} values for reduced substrate concentrations were determined by monitoring decrease in product formation using mass spectrometry.

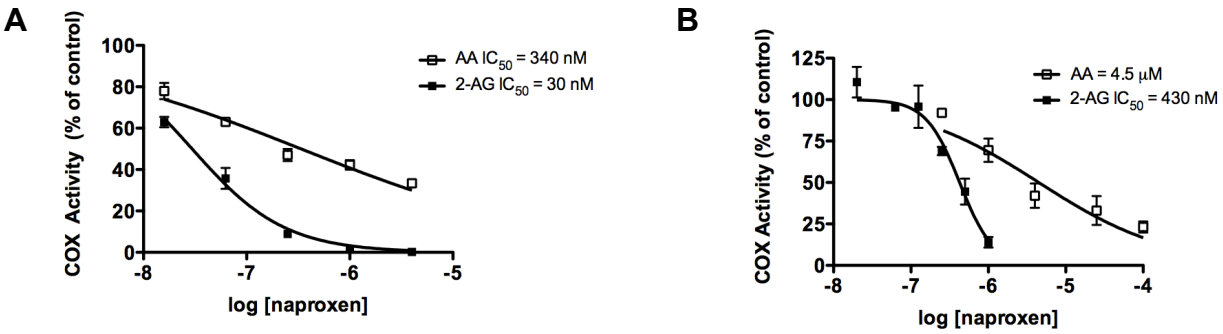

Figure 5. Substrate-selective inhibition of mCOX-2 by naproxen. *A*: Naproxen (15.6 – 4000 nM) was preincubated with 45 nM mCOX-2 for 5 minutes before the addition of 5 μM AA or 2-AG for 30 seconds. Product formation was analyzed using LC-MS/MS as described in Experimental Procedures. *B*: Naproxen (20 nM - 100 μM) was preincubated with 200 nM mCOX-2 for 2 min prior to the addition of 50 μM substrate. Oxygen uptake was monitored for 30 sec to determine the initial rate of the reaction then normalized to DMSO control.

Screening additional molecules. A series of compounds previously classified as rapid, reversible inhibitors or slow, tight binding inhibitors were compared for their ability to inhibit 2-AG or AA oxygenation by COX-2 using the LC-MS/MS assay described above. The results are summarized in Table 1 and are consistent with the initial findings for ibuprofen, mefenamic acid, and indomethacin. Compounds classified as rapid, reversible inhibitors are potent inhibitors of 2-AG oxidation but weaker inhibitors of AA oxidation. In contrast, compounds that are classified as slow, tight-binding inhibitors exhibit potent inhibition of both 2-AG and AA oxidation by COX-2 with comparable IC_{50} values for both substrates. Within inhibitor class, no differences in behavior are observed for compounds that are COX-2-selective inhibitors or non-selective inhibitors of both COX enzymes.

A dramatic example of the differential inhibitory potency of a rapid, reversible inhibitor is provided by lumiracoxib. Lumiracoxib is a COX-2-selective inhibitor of the

arylacetic acid class that exhibits the highest selectivity for COX-2 of all inhibitors in the *ex vivo* human whole blood assay. Previous work from our laboratory established that lumiracoxib is a poor inhibitor of AA oxygenation at saturating concentrations of substrate. This is confirmed in Figure 6 by the near complete absence of inhibition even at high inhibitor concentrations. In contrast, lumiracoxib is an extremely potent inhibitor of 2-AG oxygenation with an IC_{50} of 40 nM. In fact, lumiracoxib is one of the most potent inhibitors of COX-2 oxygenation of 2-AG we have evaluated despite the fact that it was assayed at a saturating concentration of 2-AG (50 μM). The potent inhibitory activity of lumiracoxib against 2-AG oxygenation is especially interesting because the close structural analog, diclofenac, is a potent slow, tight-binding inhibitor of both 2-AG and AA oxygenation (Figure 6). The poor inhibition of AA oxygenation by lumiracoxib is partly a reflection of the fact that it is a competitive inhibitor of AA oxidation, and the assays summarized in Figure 6 were performed at saturating substrate concentrations. When assays are performed at 5 μM, which is close to the K_m value for both substrates, inhibition of AA oxygenation is detectable (IC_{50} = 140 nM). However, even under these conditions, lumiracoxib exhibits considerable selectivity for inhibition of 2-AG oxygenation (IC_{50} = approximately 3 nM).

Table 2. IC_{50} values for the inhibition of COX-2 oxygenation of AA and 2-AG by various COX inhibitors.

	Inhibitor	50 μM AA	50 μM 2-AG
reversible	Ibuprofen*	7 μM	20 nM
	Mefenamic Acid*	180 μM	210 nM
	DM-INDO	> 25 μM	110 nM
	Lumiracoxib	no inhib.	40 nM
	SC-58076	> 4 μM	40 nM
slow, tight binders	Diclofenac	60 nM	50 nM
	Flurbiprofen	130 nM	30 nM
	INDO	180 nM	10 nM
	Celecoxib	80 nM	95 nM
	Rofecoxib	520 nM	85 nM

Enzyme and inhibitor were pre-incubated for 15 minutes prior to the addition of 50 uM substrate for 30 seconds. Reactions were quenched with organic solvent containing deuterated internal standards. Product formation was analyzed by LC-MS/MS using SRM and normalized to DMSO control. *AA oxygenation was measured using an oxygen electrode. Values for ibuprofen and mefenamic acid were taken from (2).

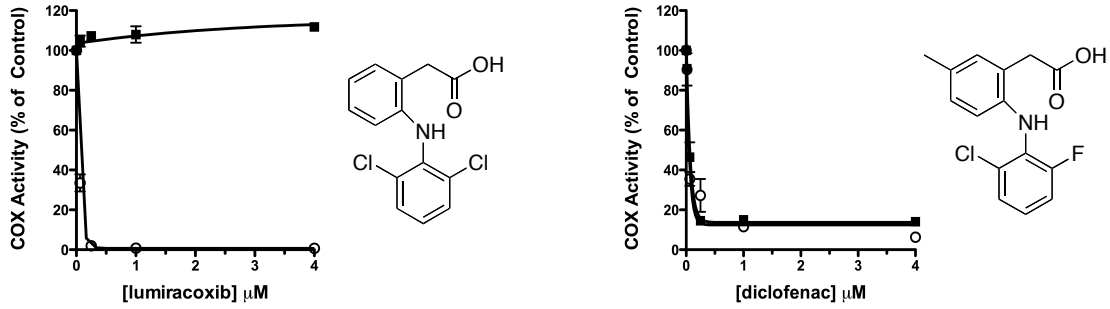

Figure 6. Inhibition of mCOX-2 oxygenation of AA and 2-AG by lumiracoxib and diclofenac. *Panel A:* mCOX-2 and lumiracoxib were pre-incubated for 5 minutes before the addition of 50 μM AA (■) or 2-AG (○) for 30 seconds. *Panel B*: Following a 15 minute incubation of diclofenac and mCOX-2, 50 μM AA (■) or 2-AG (○) was added for 30 seconds. Reactions were quenched with ethyl acetate containing 0.5% acetic acid (v/v) and internal standards. PG or PG-G formation was measured using a selected reaction monitoring LC-MS/MS method.

Discussion

Rome and Lands first demonstrated that some COX inhibitors display rapid, reversible inhibition, whereas others exhibit slow, tight-binding inhibition after the initial rapid, reversible interaction with the enzyme (10). The rapid, reversible inhibitors are often relatively weak inhibitors of AA oxygenation, whereas the slow, tight-binding inhibitors are more potent. The slow, tight-binders exhibit very low dissociation rates so they are poorly reversible even in the presence of saturating concentrations of AA. The validity of the two-step mechanism of inhibition has been demonstrated repeatedly and in some cases extended, as exemplified by certain diarylheterocycles, which demonstrate a second time-dependent step responsible for COX-2-selective inhibition (17-19). Subsequent work has revealed that for several slow, tight-binding inhibitors (e.g., indomethacin, flurbiprofen) association of only a single molecule of inhibitor is sufficient to inhibit the activity of both subunits, and this can be understood by the recent discovery that the two subunits communicate through the dimer interface (3).

Our data suggest that binding of a single molecule of a rapidly reversible or slow, tight-binding inhibitor is sufficient to cause noncompetitive inhibition of 2-AG oxygenation but only slow, tight-binders inhibit AA oxygenation under these conditions. These observations indicate that although all of the inhibitors induce conformational changes in the second subunit following binding in the first subunit, there are differences in the nature of the conformational changes induced as judged by the differential effects on 2-AG and AA binding in the second subunit. In addition, this differential sensitivity to inhibition reveals differences in the binding of 2-AG and AA that are not anticipated by the similarities in the k_{cat}/K_m value for oxygenation of the two substrates (1).

It is intriguing to consider the possibility that the greater potency for inhibition of 2-AG oxygenation exhibited by certain NSAIDs against purified protein has implications for understanding the pharmacological properties of these compounds *in vivo*. The endocannabinoids 2-AG and anandamide are selectively oxygenated by COX-2 to form PG-Gs and prostaglandin-ethanolamides (PG-EAs), respectively (20). Evolving data indicate that these neutral PG derivatives exhibit biological functions distinct from those of AA-derived PGs (21). Endocannabinoids bind and activate the cannabinoid receptors CB1 and CB2 leading to the regulation of a wide range of physiological and behavioral functions including analgesia and anti-inflammatory effects. PG-G and PG-EA formation may be viewed as an inactivation pathway for endocannabinoids and therefore, inhibition of endocannabinoid metabolism by COX-2 inhibitors may be related to the anti-inflammatory and analgesic properties of these drugs.

References

1. Kozak, K. R., Rowlinson, S. W., and Marnett, L. J. (2000) *J. Biol. Chem.* **275**, 33744-33749

2. Prusakiewicz, J. J., Duggan, K. C., Rouzer, C. A., and Marnett, L. J. (2009) *Biochemistry* **48**, 7353-7355

3. Yuan, C., Rieke, C. J., Rimon, G., Wingerd, B. A., and Smith, W. L. (2006) *Proc. Natl. Acad. Sci. U.S.A.* **103**, 6142-6147

4. Rowlinson, S. W., Crews, B. C., Lanzo, C. A., and Marnett, L. J. (1999) *J. Biol. Chem.* **274**, 23305-23310

5. Blobaum, A. L., and Marnett, L. J. (2007) *J. Biol. Chem.* **282**, 16379-16390

6. Prusakiewicz, J. J., Felts, A. S., Mackenzie, B. S., and Marnett, L. J. (2004) *Biochemistry* **43**, 15439-15445

7. Prasit, P., Wang, Z., Brideau, C., Chan, C. C., Charleson, S., Cromlish, W., Ethier, D., Evans, J. F., Ford-Hutchinson, A. W., Gauthier, J. Y., Gordon, R., Guay, J., Gresser, M., Kargman, S., Kennedy, B., Leblanc, Y., Leger, S., Mancini, J., O'Neill, G. P., Ouellet, M., Percival, M. D., Perrier, H., Riendeau, D., Rodger, I., Zamboni, R., and et al. (1999) *Biorg. Med. Chem. Lett.* **9**, 1773-1778

8. Duggan, K. C., Walters, M. J., Musee, J., Harp, J. M., Kiefer, J. R., Oates, J. A., and Marnett, L. J. (2010) *J. Biol. Chem.* **285**, 34950-34959

9. Blobaum, A. L., and Marnett, L. J. (2007) *J. Med. Chem.* **50**, 1425-1441

10. Rome, L. H., and Lands, W. E. (1975) *Proc. Natl. Acad. Sci. U.S.A.* **72**, 4863-4865

11. Kulmacz, R. J., and Lands, W. E. (1985) *J. Biol. Chem.* **260**, 12572-12578

12. Shoichet, B. K. (2006) *J. Med. Chem*. **49**, 7274-7277

13. Kurumbail, R. G., Stevens, A. M., Gierse, J. K., McDonald, J. J., Stegeman, R. A., Pak, J. Y., Gildehaus, D., Miyashiro, J. M., Penning, T. D., Seibert, K., Isakson, P. C., and Stallings, W. C. (1996) *Nature* **384**, 644-648

14. Yuan, C., Sidhu, R. S., Kuklev, D. V., Kado, Y., Wada, M., Song, I., and Smith, W. L. (2009) *J. Biol. Chem.* **284**, 10046-10055

15. Rimon, G., Sidhu, R. S., Lauver, D. A., Lee, J. Y., Sharma, N. P., Yuan, C., Frieler, R. A., Trievel, R. C., Lucchesi, B. R., and Smith, W. L. (2010) *Proc. Nat. Acad. Sci. U.S.A.* **107**, 28-33

16. Gierse, J. K., Koboldt, C. M., Walker, M. C., Seibert, K., and Isakson, P. C. (1999) *Biochem. J.* **339 (Pt 3)**, 607-614

17. Lanzo, C. A., Sutin, J., Rowlinson, S., Talley, J., and Marnett, L. J. (2000) *Biochemistry* **39**, 6228-6234

18. Walker, M. C., Kurumbail, R. G., Kiefer, J. R., Moreland, K. T., Koboldt, C. M., Isakson, P. C., Seibert, K., and Gierse, J. K. (2001) *Biochem J.* **357**, 709-718

19. Copeland, R. A., Williams, J. M., Giannaras, J., Nurnberg, S., Covington, M., Pinto, D., Pick, S., and Trzaskos, J. M. (1994) *Proc. Natl. Acad. Sci. U.S.A.* **91**, 11202-11206

20. Kozak, K. R., Crews, B. C., Morrow, J. D., Wang, L. H., Ma, Y. H., Weinander, R., Jakobsson, P. J., and Marnett, L. J. (2002) *J. Biol. Chem.* **277**, 44877-44885

21. Woodward, D. F., Carling, R. W., Cornell, C. L., Fliri, H. G., Martos, J. L., Pettit, S. N., Liang, Y., and Wang, J. W. (2008) *Pharmacol. Ther.* **120**, 71-80

CHAPTER V

SUBSTRATE-SELECTIVE INHIBITION OF CYCLOOXYGENASE-2 CATALYZED ENDOCANNABINOID OXYGENATION BY (*R*)-PROFENS

Introduction

The endocannabinoids 2-arachidonoylglycerol (2-AG) and arachidonoylethanolamide (AEA), exert analgesic and anti-inflammatory effects through their actions at the cannabinoid receptors CB1 and CB2. As discussed in Chapter I, they are also substrates for fatty acid oxygenases such as lipoxygenases and cyclooxygenases (COXs), which convert them to bioactive oxygenated metabolites. 2-AG and AEA are oxygenated efficiently by COX-2 but not COX-1 to prostaglandin glycerol esters (PG-Gs) and prostaglandin ethanolamides (PG-EAs), respectively, which are potent activators of calcium mobilization in macrophages, trigger miniature inhibitory postsynaptic currents in neurons, induce mechanical allodynia, and stimulate thermal hyperalgesia (1-6). 2-AG and AEA are rapidly hydrolyzed by monoacylglycerol lipase or fatty acid amide hydrolase, respectively, to AA, which terminates endocannabinoid signaling but produces a fatty acid that is converted to leukotrienes and prostaglandins *inter alia*. Thus, 2-AG and AEA are at the nexus of a complex cascade of bioactive lipid production, inactivation, and signaling.

The importance of endocannabinoids as naturally occurring analgesic agents provides a potential mechanism for inhibition of neuropathic pain through the development of agents that prevent endocannabinoid metabolism at sites of neuroinflammation. Since COX-2 is induced at sites of neuroinflammation, non-steroidal

anti-inflammatory drugs (NSAIDs), whether non-selective or selective for COX-2, may contribute to endocannabinoid-sparing by preventing COX-2-mediated oxygenation of 2-AG and AEA. The ability to focus selectively on endocannabinoid-sparing by NSAIDs would appear to be limited by their concomitant inhibition of AA oxygenation, which confers a risk of gastrointestinal and cardiovascular toxicity. However, our laboratory recently reported that NSAIDs that interact with COX-2 in a reversible manner are significantly more potent inhibitors of 2-AG oxygenation than AA oxygenation by purified COX-2 – a phenomenon we dubbed "substrate-selective inhibition" (7). The explanation for this dramatic substrate-selective inhibition is based on the recent discovery that binding of substrate or inhibitor to the first monomer of the COX homodimer is communicated to the second monomer through the extensive dimer interface, effectively transforming the protein into a conformational heterodimer (8,9). We hypothesize that binding of a rapidly reversible inhibitor in a single monomer of the COX homodimer is sufficient to block the productive binding of 2-AG, but not AA, in the partner monomer. To inhibit AA oxygenation, a molecule of inhibitor must be present in both active sites. For slow, tight-binding inhibitors (e.g. flurbiprofen and indomethacin), previous work has shown that a single molecule of inhibitor effectively inhibits AA oxygenation in both subunits of the COX homodimer (8,10). In accordance with these studies, we found that slow, tight-binding inhibitors prevent AA and 2-AG oxygenation with similar IC_{50} values.

These and related findings shed important new insights into the mechanisms of inhibition of COX proteins by NSAIDs and may serve as a model for ligand-binding by other multimeric proteins. Further, development of a truly "substrate-selective" inhibitor

provides a potential mechanism to prevent endocannabinoid oxygenation at the sites of neuroinflammation without affecting AA oxygenation. We report here that (*R*)-enantiomers of 2-arylpropionic acid NSAIDs, which do not effectively inhibit AA oxygenation, are, in fact, able to bind in the COX active site to block COX-2-mediated oxygenation of 2-AG.

Experimental Procedures

Materials. mCOX-2 was expressed and purified as previously described (11). (*R*)-flurbiprofen, 2-AG, PGE_2-d_4, and 5-phenyl-4-pentenyl hydroperoxide (PPHP) were obtained from Cayman Chemical Company (Ann Arbor, MI). (*R*)-naproxen as well as reagents for the synthesis of PGE_2-G-d_5, PGE_2 and glycerol-d_5, were purchased from Sigma-Aldrich (Milwaukee, WI). (*R*)-ibuprofen was purchased from Santa Cruz Biotechnology (Santa Cruz, CA). AA was obtained from Nu-Check Prep, Inc. (Elysian, MN). Crystallization reagents were purchased from Hampton Research (Aliso Viejo, CA).

COX inhibition assay. Hematin-reconstituted mCOX-2 (200 nM) was preincubated with varying concentrations of inhibitor (63 nM to 25 μM) for 15 minutes prior to the addition of 50 μM AA or 2-AG at 37 °C. For 5 μM substrate, the concentration of COX-2 was reduced to 45 nM. Reactions were carried out in 100 mM Tris buffer containing 500 μM phenol, pH 8.0. The reaction was quenched after 30 seconds by the addition of ice-cold quench solution followed by vigorous mixing. The quench solution consisted of ethyl acetate with 0.5% acetic acid (v/v) and deuterated internal standards, PGE_2-d_4, and PGE_2-G-d_5. The organic layer was removed and evaporated to near-dryness under

nitrogen. The residue was reconstituted with 1:1 MeOH:H_20 (v:v), and PGD_2/E_2 and PGD_2/E_2-G production was monitored by liquid chromatography-tandem mass spectrometry (LC-MS/MS). Samples were chromatographed using an isocratic method of 66% 5 mM ammonium acetate, pH 3.5 and 34% acetonitrile (v/v) at a flow rate of 375 mL/min on a 50 Å C18 Luna column (5 x 0.2 cm, 3 micron). To quantitate product formation, a selected reaction monitoring method was utilized to measure the following transitions: PGE_2/D_2 *m/z* 370 → 317, PGE_2/D_2-d_4 *m/z* 374 → 321, PGE_2/D_2 - G *m/z* 444 → 391 and PGE_2/D_2 - G-d_5 *m/z* 449→ 396. The amount of PG products was determined by normalization of the peak area of the analyte to the peak area of internal standard. The percent of COX activity remaining in the presence of inhibitor was determined by normalization to a DMSO control.

Peroxidase activity assay – Assays were performed as described by Markey *et al*. with the following modifications (12). Hematin-reconstitued mCOX-2 (100 nM) in 100 mM Tris-HCl buffer, pH 8, was incubated with inhibitor (100 μM – 5 mM) in the presence of 200 μM phenol at 37 °C for 5 min. The reaction was initiated by the addition of PPHP (100 μM) and terminated after 5 min by the addition of ice cold quench solution (ethyl acetate + 0.5% acetic acid (v/v)) followed by vigorous mixing and centrifugation at 4 °C. The organic layer was removed, evaporated to dryness under nitrogen, and reconstituted in 300 mL of a 1:1 solution of methanol and water. Samples were separated by reverse phase HPLC with UV detection at 254 nM. Samples are chromatographed utilizing a C8 reverse-phase column (Luna C_8 3 μm HPLC column (150 x 2.00 mm)) with a gradient elution beginning at 50% (v/v) methanol/water increasing to 90% methanol (v/v) over 9

minutes and held at 90% methanol (v/v) for 10 additional minutes at a flow rate of 0.20 mL/min. The concentrations of the analytes were estimated from the area of the representative peak. Peroxidase activity was measured by the percent conversion of PPHP to 5-phenyl-4-pentenyl alcohol, PPA, using the equation: [PPA]/([PPA]+[PPHP]).

Crystallography. COX-2 was expressed and purified as previously described. Purified protein was prepared for crystallization, and hanging-drop crystallization experiments were set up according to published methods (13). All diffraction data were collected at 100 K at the beamline 24ID-E located at the Advanced Photon Source, using an ADSC Quantum 315 charge-coupled-device-based detector. Diffraction data were processed with HKL2000 (14). Initial phases were determined by molecular replacement using a search model (PDB 3NT1) with MOLREP (15). A solution having two molecules in the asymmetric unit was obtained. The model was improved with iterative rounds of model building in Coot and refinement in PHENIX (16,17). Data collection and refinement statistics are shown in Table I. Molecular graphics were generated using PyMOL (18).

Inhibition of COX in dorsal root ganglion cells (DRGs). Dorsal root ganglion neurons and glia were harvested from E14 mouse embryos and plated onto collagen coated dishes at 100,000 cells per dish. The cells were cultured in 3 mL of medium consisting of 1.5 mL Lonza's ultraculture and 1.5 mL L-glutamine with Neurobasal, N2, and B27 supplements, with 3% Hyclone fetal bovine serum, 1% penicillin or streptomycin, and 50 ng/ml mouse nerve growth factor), and the medium was replaced every 3-4 days. For the inhibition assay, cells were stimulated overnight with 20 ng/mL of granule macrophage

colony stimulating factor. The following morning, the medium was replaced, and the cells were treated with 100 ng/mL lipopolysaccharide, 20 units/ml mouse interferon γ, and 10 μM 15(S)-HETE. The cells were treated with varying concentrations of inhibitor (or DMSO control) 2 hours after medium replacement, and 2 μM ionomycin 3 hours after medium replacement. The cell medium was collected 3 hours after ionomycin treatment and extracted with two equivalents of ethyl acetate with 1% glacial acetic acid (v/v) spiked with deuterated standards of PGs. The extracts were evaporated under nitrogen and reconstituted in 1:1 methanol and water (v/v). Samples were analyzed by reverse-phase liquid chromatography using an Ascentis C18 5cm x 2.1mm with 3 μm particle size column. The chromatography and SRM methods were as described above for *in vitro* COX inhibition; transition for PG-EAs *m/z* = 413→ 378. Product identities were confirmed by comparing the retention times and collision-induced dissociation spectra to standards.

Results

NSAIDs of the arylpropionic acid class exhibit marked enantiospecificity for inhibition of AA oxygenation by COX enzymes. The (*S*)-enantiomers of ibuprofen, flurbiprofen, and naproxen effectively inhibit COX-1 and COX-2, but the (*R*)-enantiomers are either poor inhibitors or exhibit no observable inhibitory activity. As described in Chapter IV, the (*S*)-enantiomers of the arylpropionic acid class of NSAIDs are also potent inhibitors of COX-2-mediated 2-AG oxidation. To determine whether enantiospecificity is observed with the 2-AG as the substrate as it is for AA, we evaluated the ability of the (*R*)-enantiomers of ibuprofen, naproxen, and flurbiprofen to inhibit 2-AG oxygenation by COX-2. As shown in Figure 1, (*R*)-enantiomers inhibit 2-AG

oxidation, albeit less potently than the (*S*)-enantiomers. Importantly, (*R*)-ibuprofen, (*R*)-naproxen, and (*R*)-flurbiprofen did not inhibit AA oxygenation by COX-2. The experiments summarized in Figure 2 were performed at 50 μM substrate concentrations, so they were repeated at 5 μM substrate (the approximate K_m for both substrates). The IC_{50}'s for inhibition of 2-AG oxygenation decreased ((*R*)-ibuprofen IC_{50} = 10 μM, (*R*)-naproxen IC_{50} = 3.0 μM, (*R*)-flurbiprofen IC_{50} = 0.08 μM) but none of the three compounds inhibited AA oxygenation (data not shown). Thus, the decrease in enantiospecificity for inhibition of 2-AG oxygenation compared to AA oxygenation observed at saturating substrate concentrations was maintained at substrate concentrations near the K_m.

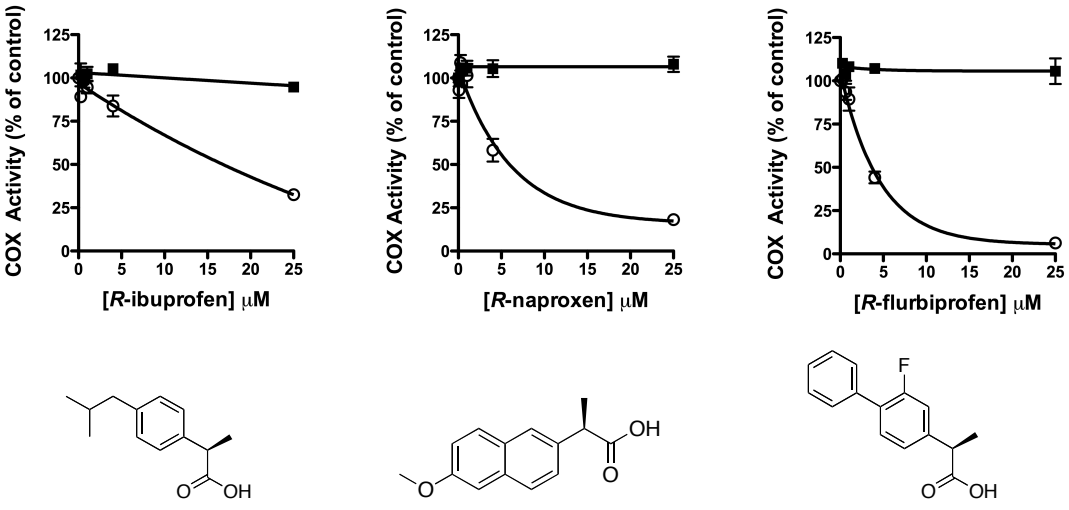

Figure 1. Inhibition of COX-2-mediated AA and 2-AG oxygenation by (*R*)-profens. COX-2 was preincubated with 63 nM – 25 μM (*R*)-ibuprofen, (*R*)-naproxen or (*R*)-flurbiprofen for 15 minutes followed by the addition of 50 μM AA (■) or 2-AG (○) for 30 seconds. PG and PG-G production was measured by LC-MS/MS as described under Experimental Procedures.

These findings suggest that the (*R*)-enantiomers of arylpropionic acids bind in the COX-2 active site and inhibit the oxygenation of 2-AG. This was surprising given prior

results suggesting that steric clashes with active site residues prevent binding of (*R*)-arylpropionic acids (19). To ensure that (*R*)-profens inhibit 2-AG oxygenation by binding in the COX active site and not at the POX active site, we examined the ability of (*R*)-naproxen to inhibit COX-2 POX activity. In these studies, POX activity was measured by monitoring the conversion of the POX hydroperoxide substrate PPHP to the corresponding alcohol, PPA, by HPLC. As shown in Figure 2, no significant inhibition of POX activity was observed at concentrations of (*R*)-naproxen up to 500 μM, suggesting that the inhibitor does not bind at the POX active site. Similar results were obtained with (*R*)-flurbiprofen (data not shown).

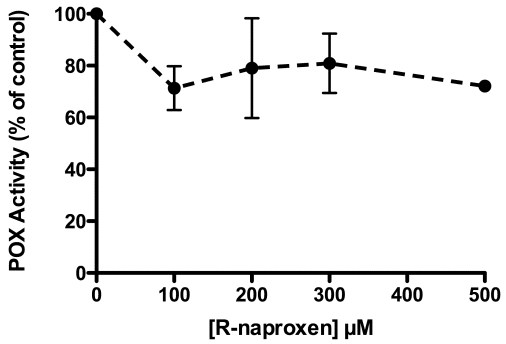

Figure 2. Attempted inhibition of POX activity by (*R*)-naproxen. (*R*)-naproxen (100-500 μM) was preincubated with mCOX-2 for 5 minutes at 37 °C prior to the addition of 100 μM PPHP. The reaction was quenched after 5 minutes by the addition of ethyl acetate with 0.5% acetic acid. Conversion of PPHP to PPA was monitored by HPLC as described under Experimental Procedures.

To determine the orientation of these substrate-selective inhibitors in the active site, attempts were made to crystallize complexes of each of the (*R*)-enantiomers with murine COX-2 utilizing recently described procedures. Diffraction-quality crystals were

Table I. Data collection and refinement statistics.

Data collection	
Space group	I222
Cell dimensions a, b, c (Å) α,β,γ (°)	 122.74, 133.03, 181.04 90.00, 90.00, 90.00
Resolution (Å)	2.4 (2.48-2.40)
R_{merge} (%)	11.7 (43.4)
$I/\sigma I$	15.7 (3.6)
Completeness (%)	99.9
Redundancy	5.7 (5.8)
Refinement	
Resolution (Å)	2.4
No. reflections	55701
R_{work} / R_{free}	17.7 / 23.3
No. of atoms	
Protein	8946
Ligand / Ions	332 / 2
Water	601
B-factors	
Protein	28.6
Ligand / Ions	42.0 / 33.0
Water	31.7
R.m.s. deviations	
Bond lengths (Å)	0.008
Bond angles (°)	1.3

Values in parentheses correspond to the highest resolution shells.
$R_{merge} = \Sigma_{hkl} \Sigma_{j=1,N} \left| \langle I_{hkl} \rangle - I_{hklj} \right| / \Sigma_{hkl} \Sigma_{j=1,N} \left| I_{hklj} \right|$ where the outer sum (hkl) is taken over the unique reflections.
$R_{work} = \Sigma_{hkl} ||F_{o,hkl} - k|F_{c,hkl}||/\Sigma_{hkl}|F_{o,hkl}|$, where $|F_{o,hkl}|$ and $|F_{c,hkl}|$ are the observed and calculated structure factor amplitudes, respectively.
R_{free} is same as for R_{work} for the set of reflections (5% of the total) omitted from the refinement process.
NE-CAT, North Eastern Collaborative Access Team

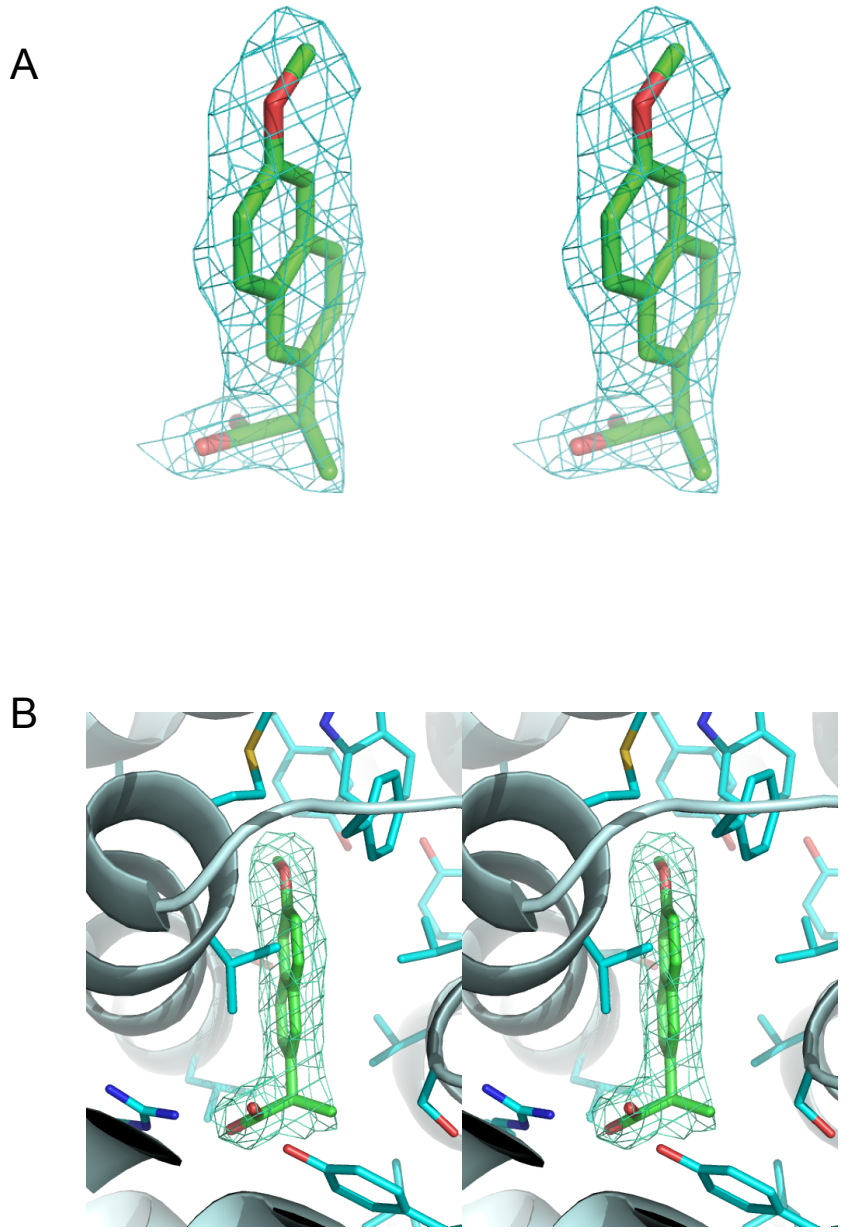

Figure 3. Crystal structure of (R)-naproxen bound in the active site of mCOX-2 at 2.4 Å. *A*. Difference electron density map ($2F_o$-F_c) contoured at 1σ shown in stereoview. *B*. Stereoview of the active site of the (*R*)-naproxen-COX-2 complex. Active site residues are shown as cyan sticks while the (*R*)-naproxen molecule is shown in lime sticks. The carboxylate moiety participates in hydrogen bonding interactions with Arg-120 and Tyr-355. The (*R*)-a-methyl group is adjacent to Tyr-355.

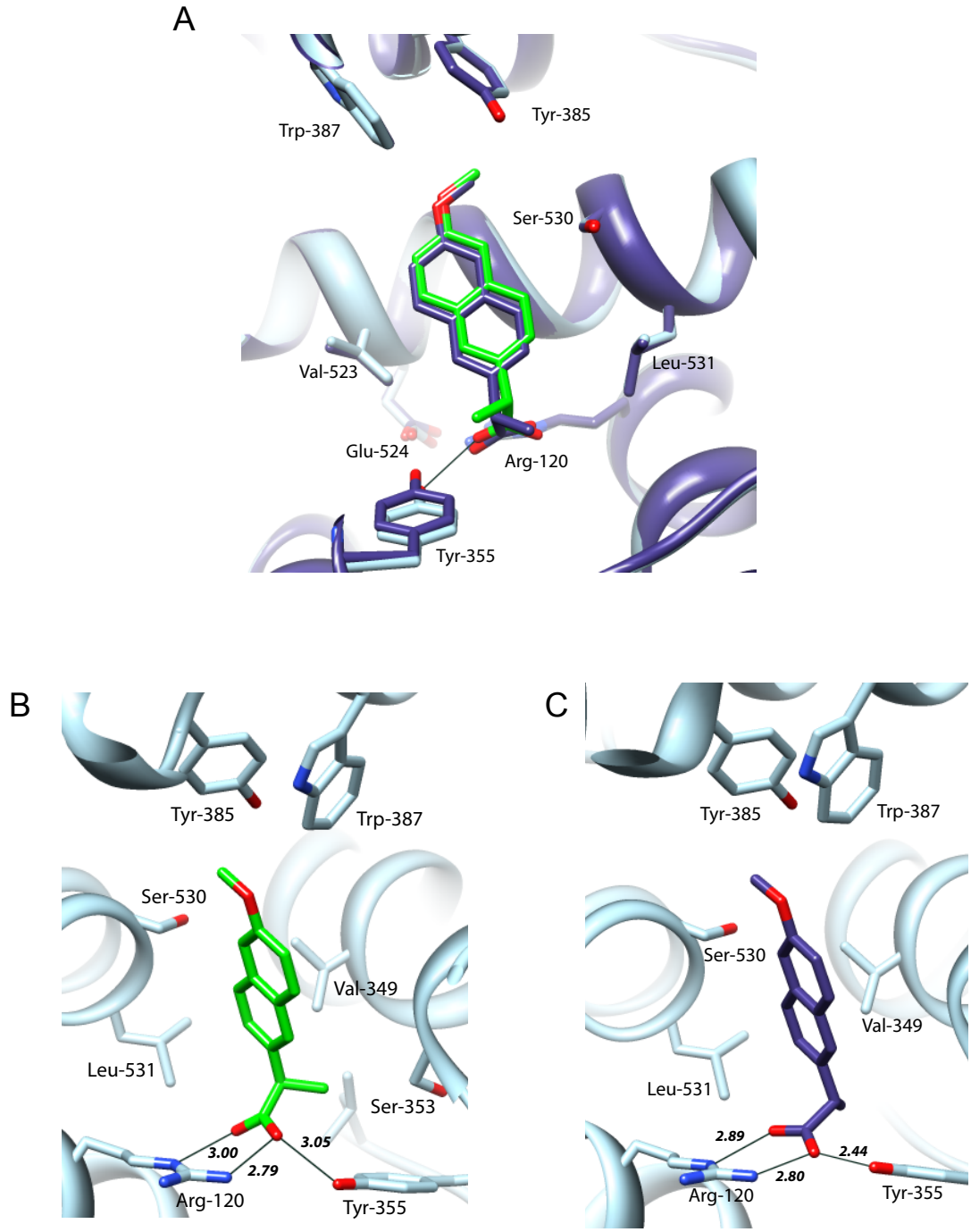

Figure 4. Comparison of the crystal structures of mCOX-2:(*R*)-naproxen and mCOX-2:(*S*)-naproxen. *A*. Overlay of the COX active site of the crystal structures of (R)-naproxen (inhibitor is shown in green, protein in cyan) and (S)-naproxen (purple) bound to mCOX-2. *B*. Crystal structure of (R)-naproxen (green) bound to mCOX-2 (cyan). Hydrogren bonds between the carboxylate of the inhibitor and constriction site residues Arg-120 and Tyr-355 are shown in black lines with the distance (in angstroms) labeled. *C*.(S)-naproxen in the active site of mCOX-2. The inhibitor is shown in purple sticks and protein active site residues are shown in cyan. Black lines represent hydrogen bonds.

obtained with (*R*)-naproxen complexed to COX-2. The electron density map and a stereo drawing of the bound inhibitor in the active site are shown in Figure 3A. The carboxylate of the inhibitor is located near the mouth of the active site coordinated to Arg-120 and the naphthyl ring projects up into the center of the active site. This is typical of the orientation of arylpropionic acids in the COX active site as been reported for (*S*)-ibuprofen complexed to COX-1, (*S*)-naproxen complexed to COX-2, and (*S*)-flurbiprofen complexed to COX-1 or COX-2 (13,20-22). Previous reports based on site-directed mutagenesis and structure-activity relations have suggested that the α-methyl groups of the (*R*)-arylpropionic acids clash with Tyr-355 at the mouth of the active site to prevent stable binding (19). However, as illustrated in Figure 3B, the α-methyl group of (*R*)-naproxen binds adjacent to Tyr-355.

A comparison of the binding of (*R*)-naproxen to (*S*)-naproxen in the COX-2 active site is shown in Figure 4. The 1.7 Å mCOX-2:(*S*)-naproxen crystal structure is described in detail in Chapter III. The general binding modes of the two enantiomers are similar, although the chirality of the two α-methyl groups is reversed. The two naphthyl rings are nearly superimposed; however the naphthyl ring of (*R*)-naproxen appears to be shifted somewhat away from the side of the active site adjacent to the D-helix relative to the naphthyl ring of (*S*)-naproxen. The RMSD for the COX-2 active site residues of the two crystal structures is 0.18 Å, suggesting that the active site has slightly rearranged to accommodate the (*R*)-methyl group. The biggest difference in protein structure between the two complexes is the shift in the position of Tyr-355, which increases the hydrogen bond distance between the donor and acceptor to 3.05 Å in the (*R*)-naproxen:mCOX-2

structure compared to a distance of 2.44 Å for (*S*)-naproxen. This increase in hydrogen-bonding distance may reduce the binding energy of the (*R*)-naproxen-COX-2 complex.

(*R*)-Flurbiprofen exhibits analgesic activity in humans and inhibits neuropathic pain in rodents (6,23). It is not converted to (*S*)-flurbiprofen *in vivo* and does not display gastrointestinal toxicity (24). Further, (*R*)-flurbiprofen has been reported to elevate AEA levels in the dorsal horn of rats surgically treated to induce nerve injury (6). The mode of action of (*R*)-flurbiprofen responsible for analgesia and AEA elevation is currently unknown, although it is a weak inhibitor of fatty acid amide hydrolase (IC_{50} = 1 mM *in vitro*) (6). Another possible explanation for the analgesic activity of (*R*)-flurbiprofen is that it inhibits the COX-2-selective metabolism of endocannabinoids. Support for this hypothesis comes from experiments conducted by Daniel Hermanson in our laboratory. He explored whether substrate-selective inhibition can be detected in intact cells with physiological levels of 2-AG and AEA using primary DRGs. Preliminary results indicated that increasing concentrations of (*R*)-flurbiprofen inhibited the synthesis of all three classes of eicosanoids, but the inhibition of the endocannabinoid-derived eicosanoids, PG-Gs and PG-EAs occurred at much lower concentrations than the inhibition of PGs (Figure 5). It is noteworthy that the stimulation of DRGs results in the generation of PG-EAs. This is the first time that these oxygenated metabolites of AEA have been detected in intact cells stimulated to release endogenous COX-2 substrates. The identity of the PG-EAs was verified by collision-induced dissociation and mass spectrometry of the fragments. It is also noteworthy that the concentration-dependences for inhibition of 2-AG oxygenation and AEA oxygenation are similar.

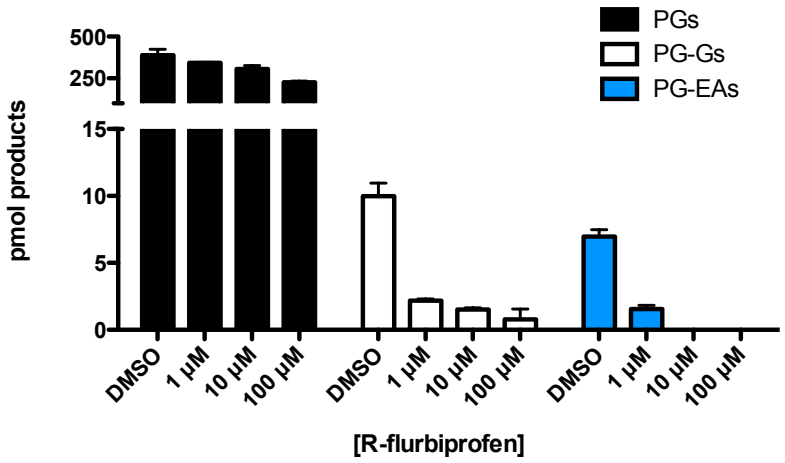

Figure 5. Inhibition of endocannabinoid metabolism in DRGs. DRGs were treated with varying concentrations of R-flurbiprofen for one hour prior to the addition of ionomycin to induce substrate release. The culture medium was harvested after three hours and extracted with ethyl acetate containing 1% acetic acid and deuterated internal standards. The amount of product formation was measured by LC/MS-MS and quantitated by determining the ratio of the peak area of the eicosainoid species to that of the corresponding internal standard. (Experiment designed and performed by D. Hermanson).

Discussion

The results presented here illustrate that (*R*)-enantiomers of arylpropionate inhibitors, which are considered inactive as COX inhibitors because of their inability to inhibit AA oxygenation, actually bind to the enzyme and inhibit endocannabinoid oxygenation. We hypothesize that binding of a single molecule of inhibitor in one monomer of the COX homodimer causes a conformational change in the partner monomer that is sufficient to prevent the productive binding of 2-AG, but not AA. The ability of (*R*)-arylpropionates to inhibit of endocannabinoid oxygenation under conditions where there is no observable inhibition of AA oxygenation is a dramatic illustration of substrate-selective inhibition. Further, the finding that (*R*)-arylpropionates inhibit COX-2-mediated endocannabinoid metabolism raises the possibility that additional small molecules that have been classified as ineffective against COX-2 as measured by

inhibition of PG production may be able to effectively bind COX-2 and prevent the formation PG-Gs and PG-EAs.

Previous studies suggested that (*R*)-arylpropionates could not effectively bind in the COX active site because of unfavorable steric interactions between Tyr-355 and the a-methyl group in the (*R*)-conformation (19). However, crystallographic analysis of (*R*)-naproxen in complex with mCOX-2 indicates that the binding site of (*R*)-arylpropionates is the COX-2 active site. Co-crystallization of mCOX-2 with (*R*)-ibuprofen and (*R*)-flurbiprofen will be important to confirm the binding site of (*R*)-arylpropionates. While (*R*)- and (*S*)- naproxen appear to occupy similar conformations within the COX-2 active site, the differential stereochemistry may lead to different molecular determinants for binding. Therefore, mutagenesis studies will be required to identify the binding determinants of (*R*)-arylpropionates within the COX-2 active site with particular focus on the amino acid residues involved in substrate-selective inhibition. This information will be useful in the design of (*R*)-arylpropionate derivatives with increased potency and/or selectivity against COX-2-mediated 2-AG oxygenation.

These findings provide important new insights into the mechanism of action of NSAIDs and uncover a potential mechanism for the analgesic activity of (*R*)-fluribiprofen. The ability of (*R*)-fluribiprofen to selectively inhibit AEA and 2-AG oxygenation in DRGs correlates to its ability to elevate AEA levels at sites of neuroinflammation in the spinal cord (6). Although fatty acid amide hydrolase and monoacylglycerol lipase are responsible for the basal turnover of endocannabinoids in non-inflammed tissue, induction of inflammation in the peripheral or central nervous system by nerve injury results in high levels of COX-2 in the inflamed tissue, which may

contribute to depletion of AEA and 2-AG. Blockage of this depletion by the endocannabinoid-selective inhibition of COX-2 by (*R*)-flurbiprofen would spare endocannabinoid levels and induce analgesia. Consistent with this mechanism, the analgesic effect of (*R*)-fluribiprofen is prevented by CB1 receptor antagonists despite the fact that (*R*)-fluribiprofen does not activate the CB1 receptor (6). This highlights the importance of maintenance of endocannabinoid tone in the analgesic action of (*R*)-fluribiprofen.

References

1. Yu, M., Ives, D., and Ramesha, C. S. (1997) *J. Biol. Chem.* **272**, 21181-21186

2. Kozak, K. R., Rowlinson, S. W., and Marnett, L. J. (2000) *J. Biol. Chem.* **275**, 33744-33749

3. Kozak, K. R., Prusakiewicz, J. J., and Marnett, L. J. (2004) *Curr. Pharm. Des.* **10**, 659-667

4. Rouzer, C. A., and Marnett, L. J. (2005) *J. Biol. Chem.* **280**, 26690-26700

5. Sang, N., Zhang, J., and Chen, C. (2006) *J. Physiol.* **572**, 735-745

6. Bishay, P., Schmidt, H., Marian, C., Haussler, A., Wijnvoord, N., Ziebell, S., Metzner, J., Koch, M., Myrczek, T., Bechmann, I., Kuner, R., Costigan, M., Dehghani, F., Geisslinger, G., and Tegeder, I. (2010) *PLoS One* **5**, e10628

7. Prusakiewicz, J. J., Duggan, K. C., Rouzer, C. A., and Marnett, L. J. (2009) *Biochemistry* **48**, 7353-7355

8. Yuan, C., Rieke, C. J., Rimon, G., Wingerd, B. A., and Smith, W. L. (2006) *Proc. Natl. Acad. Sci. U.S.A.* **103**, 6142-6147

9. Yuan, C., Sidhu, R. S., Kuklev, D. V., Kado, Y., Wada, M., Song, I., and Smith, W. L. (2009) *J. Biol. Chem.* **284**, 10046-10055

10. Kulmacz, R. J., and Lands, W. E. (1985) *J. Biol. Chem.* **260**, 12572-12578

11. Rowlinson, S. W., Crews, B. C., Lanzo, C. A., and Marnett, L. J. (1999) *J. Biol. Chem.* **274**, 23305-23310

12. Markey, C. M., Alward, A., Weller, P. E., and Marnett, L. J. (1987) *J. Biol. Chem.* **262**, 6266-6279

13. Duggan, K. C., Walters, M. J., Musee, J., Harp, J. M., Kiefer, J. R., Oates, J. A., and Marnett, L. J. (2010) *J. Biol. Chem.* **285**, 34950-34959

14. Otwinowski, Z., and Minor, M. (1997) *Methods. Enzymol.* **276**, 307-326

15. Vagin, A., and Teplyakov, A. (2000) *Acta. Crystallogr. D. Biol. Crystallogr.* **56**, 1622-1624

16. Emsley, P., and Cowtan, K. (2004) *Acta. Crystallogr. D. Biol. Crystallogr.* **60**, 2126-2132

17. Adams, P. D., Grosse-Kunstleve, R. W., Hung, L. W., Ioerger, T. R., McCoy, A. J., Moriarty, N. W., Read, R. J., Sacchettini, J. C., Sauter, N. K., and Terwilliger, T. C. (2002) *Acta. Crystallogr. D. Biol. Crystallogr.* **58**, 1948-1954

18. DeLano, W. L. (2009) *The PyMol Molecular Graphics System.*, DeLano Scientific LLC, Palo Alto, CA

19. Bhattacharyya, D. K., Lecomte, M., Rieke, C. J., Garavito, M., and Smith, W. L. (1996) *J. Biol. Chem.* **271**, 2179-2184

20. Selinsky, B. S., Gupta, K., Sharkey, C. T., and Loll, P. J. (2001) *Biochemistry* **40**, 5172-5180

21. Gupta, K., Selinsky, B. S., and Loll, P. J. (2006) *Acta. Crystallogr. D. Biol. Crystallogr.* **62**, 151-156

22. Kurumbail, R. G., Stevens, A. M., Gierse, J. K., McDonald, J. J., Stegeman, R. A., Pak, J. Y., Gildehaus, D., Miyashiro, J. M., Penning, T. D., Seibert, K., Isakson, P. C., and Stallings, W. C. (1996) *Nature* **384**, 644-648

23. Lotsch, J., Geisslinger, G., Mohammadian, P., Brune, K., and Kobal, G. (1995) *Br. J. Clin. Pharmaco.l* **40**, 339-346

24. Geisslinger, G., Menzel-Soglowek, S., Beck, W. S., and Brune, K. (1993) *Agent Actions Suppl.* **44**, 31-36

CHAPTER VI

SUMMARY

Naproxen has been marketed for the treatment of pain and inflammation for over thirty years. The inhibitor was developed prior to the isolation and purification of COX-1 and long before the discovery of COX-2. Detailed studies of the molecular determinants of naproxen binding to COX had not been performed prior to the initiation of my dissertation project. Naproxen exhibits significant gastrointestinal toxicity but its cardiovascular toxicity appears lower than other drugs in its class. Recently, naproxen was reported to inhibit tumor growth in rodent models of urinary and colon cancers (1). The elucidation of critical interactions between naproxen and COX can be used in the design of more potent or selective naproxen analogs, which may be useful in dissecting the importance of isoform selectivity in cardiovascular toxicity or in the generation of gastrointestinal-sparing chemopreventive agents.

Kinetic studies indicate that naproxen interacts in a slightly different manner with COX-1 compared to COX-2. While there appears to be a time-dependent component to the inhibition of both COX-1 and COX-2, COX-1 is considerably more sensitive to inhibition by naproxen in the absence of a preincubation before the addition of substrate. The hypothesis that naproxen binds differently to COX-1 and COX-2 is supported by previous findings that mutations of COX-2 active site residues to the corresponding amino acid in COX-1 eliminate inhibition by naproxen despite the fact that naproxen is a non-selective inhibitor. The differential binding interactions between naproxen and the

active site of COX-2 and COX-1 could potentially be exploited in the development in selective naproxen analogs. However, our structure-activity studies show that each of the major functional groups of naproxen is required for inhibitory activity, suggesting that generation of active naproxen derivatives may be difficult. Changes in size and/or stereochemistry of either the α-methyl group or the *p*-methoxy group were not tolerated, and esterification of the carboxylic acid rendered naproxen inactive against both COX isoforms. Nevertheless, improved COX-2 selectivity was achieved by substitution of S or CH_2 for the O atom of the *p*-methoxy group. In addition, our examination of the structure-activity relationship for naproxen led to the development of several close structural analogs of naproxen that do not inhibit the oxygenation of AA by COX-1 or COX-2 (e.g. α-ethyl naproxen and α,α-dimethyl naproxen); these compounds may be useful in the examination of the COX-independent effects of naproxen.

We utilized mutagenesis studies and x-ray crystallography to determine the binding mode of naproxen within the active site of COX-2. In addition to being the first structure to be solved by the Marnett laboratory the 1.7 Å mCOX-2:naproxen crystal structure is the highest resolution COX structure published and one of the highest reported for a membrane protein. Our successful development of an X-ray crystallography program will be useful in a variety of ongoing projects in our laboratory including efforts to generate novel COX-2 imaging agents and selective inhibitors of COX-2-mediated endocannabinoid metabolism. The high resolution of the mCOX-2:naproxen structure allowed us to clearly define the conformation of naproxen and COX-2 active site residues and definitively identify solvent and detergent molecules. Although a critical interaction between naproxen and Trp-387 was not predicted by the

co-crystal structure, mutation of this residue to phenylalanine dramatically reduced the potency of naproxen but had no major effects on three other non-selective NSAIDs. Therefore, the interaction with Trp-387 appears to be a binding determinant that is unique to naproxen among NSAIDs. Although, the conformation of the *p*-methylthio-naproxen analog within the COX-2 active site is nearly identical to that of naproxen, the analog shows improved COX-2 selectivity and is not affected by the Trp-387 to phenylalanine mutation. These findings reinforce the concept that individual NSAIDs utilize a unique set of interactions to bind and inhibit the COX enzymes as well as highlight the importance of using crystallographic analyses in combination with mutagenesis and structure-activity studies to obtain a more complete understanding of inhibitor binding.

In addition to evaluating the molecular basis for inhibition of AA metabolism, our laboratory has a growing interest in elucidating the mechanism of inhibition of COX-2 mediated oxygenation of the endocannabinoids, 2-AG and AEA, by NSAIDs. My research was focused on investigating the molecular determinants of "substrate-selective" inhibition as a follow-up to studies that showed two relatively weak, competitive inhibitors of AA metabolism, ibuprofen and mefenamic acid, were potent, non-competitive inhibitors of 2-AG oxygenation by COX-2. I was able to expand upon these findings, and show that reversible COX inhibitors, regardless of structure or isoform selectivity, are significantly more potent inhibitors of 2-AG oxygenation than AA oxygenation. I also demonstrated that slow, tight-binders inhibit AA and 2-AG metabolism by COX-2 with comparable IC_{50} values.

These findings can be explained in light the recent discovery that COX monomers do not act independently of one another but rather exhibit cooperativity within the COX

homodimer. It appears that binding of a rapidly reversible inhibitor in one active site causes a conformational change in the partner monomer that prevents the oxygenation of 2-AG but not AA. A second molecule of inhibitor must bind in the other monomer of the COX homodimer to block AA oxygenation. In contrast, if given an appropriate amount of time, binding of a molecule of a slow, tight-binding inhibitor in a single monomer of the COX-2 homodimer is sufficient to inhibit the metabolism of both AA and 2-AG. This hypothesis is consistent with previous studies that revealed that the stoichiometry of maximal inhibition by the slow, tight -binders, flurbiprofen and indomethacin, is one molecule of inhibitor per COX homodimer (2). Our laboratory and others are attempting to identify the amino acid determinants of substrate-selective COX inhibition as well as visualize putative conformational changes, both in the active site and at the dimer interface.

Regulating endocannabinoid levels may have important therapeutic benefits as these compounds have been shown to be mediators of analgesia and inflammation. The inhibition of 2-AG oxygenation may be partially responsible for the beneficial effects of NSAIDs *in vivo*. However, inhibition of traditional prostaglandin biosynthesis by NSAIDs is associated with gastrointestinal and cardiovascular toxicity and so, I sought to identify a truly selective inhibitor of COX-2 that could raise endocannabinoid levels without affecting AA. I was able to illustrate that (*R*)-enantiomers of the arylpropionate family of NSAIDs, which were previously thought to be inactive against COX enzymes, are effective inhibitors of 2-AG oxygenation by COX-2. Consistent with previous studies, virtually no inhibition of COX-2 mediated AA metabolism under identical conditions was observed. In agreement with these findings, this laboratory has observed

selective inhibition of PG-G and PG-EA formation by (*R*)-flurbiprofen in DRGs and macrophages. My crystallographic studies demonstrated that (*R*)-naproxen binds in the COX-2 active site, which contradicts earlier speculation that (*R*)-arylpropionates can not be accommodated in the COX active site because of unfavorable interactions between the α-methyl group and the constriction site residue, Tyr-355. The presence of (*R*)-naproxen only in the COX active site indicates that inhibition of 2-AG oxygenation does not result from binding in a separate, allosteric site.

(*R*)-Arylpropionates represent the first examples of compounds that *exclusively* inhibit COX-2 mediated endocannabinoid oxygenation, albeit with moderate potency. Currently, this laboratory is attempting to generate (*R*)-arylpropionate derivatives with increased potency against 2-AG and AEA metabolism, as these would be useful probes in the examination of the physiological roles of PG-Gs or PG-EAs. Furthermore, compounds that act to raise endocannabinoid levels may have therapeutic potential in a variety of disease states, and therefore experiments are being conducted to confirm the hypothesis that selective inhibition of endocannabinoid oxygenation by COX-2 will effectively raise the levels of 2-AG and AEA, but not AA, *in vivo.* At present, the major focus of pharmacological endocannabinoid modulation has been on developing inhibitors of hydrolyzing enzymes (e.g. FAAH and MAGL), While these enzymes play a major role in the regulation of AEA and 2-AG, they also appear to act on additional substrates so that the pharmacological effects of their inhibitors may be broader than those mediated by endocannabinoids alone.

The use of COX inhibitors in the treatment of pain and inflammation dates back over three thousand years, and investigators in the COX field are still working to

understand their precise mechanism of action. The research described herein resulted in a more complete understanding of the molecular basis for the action of one of the oldest and most widely used NSAIDs, naproxen. In addition, I have generated support for the hypothesis that the action of NSAIDs *in vivo* is not exclusively dependent on inhibition of prostaglandin biosynthesis but is also related to modulation of the endocannabinoid system. In the future, the identification of a substrate-selective COX-2 inhibitor may serve as the foundation for the development of novel therapeutic agents in the treatment of pain and/or inflammation.

References

1. Steele, V. E., Rao, C. V., Zhang, Y., Patlolla, J., Boring, D., Kopelovich, L., Juliana, M. M., Grubbs, C. J., and Lubet, R. A. (2009) *Cancer. Prev. Res. (Phila Pa)* **2**, 951-956

2. Kulmacz, R. J., and Lands, W. E. (1985) *J. Biol. Chem.* **260**, 12572-12578